THE EFFECTS OF NUCLEOSOME CORE PARTICLE PACKAGING ON DNA

CHARGE TRANSPORT

By

CHAD CHRISTOPHER BJORKLUND

A dissertation submitted in partial fulfillment of
the requirements for the degree of

DOCTOR OF PHILOSOPHY

WASHINGTON STATE UNIVERSITY
School of Molecular Biosciences

DECEMBER 2006

To the Faculty of Washington State University

      The members of the Committee appointed to examine the thesis of CHAD

CHRISTOPHER BJORKLUND find it satisfactory and recommend that it be accepted.

_____

Chair

_____

_____

_____

ACKNOWLEDGMENTS

school, but Nicole did, so I thought I would just work and support her through her studies. However, Nicole and Henry basically 'strong-armed' me into applying. Nicole and I were grateful enough to be accepted into the same school, here at Washington State University (WSU). I really want to extend gratitude to Henry, for believing that I could succeed at this level, even when my grades were not the best. Had it not been for him, my passion for research would not be what it is today.

Here at WSU I had the fortune of joining the same lab that I was originally very excited about during my recruitment weekend. I knew I wanted to work with DNA, and the P.I. seemed like a perfect fit. He even liked most of my crappy music, which is always a plus. I want to thank my Ph.D advisor, William B. Davis for instilling in me the desire to learn, and to further my passion for scientific research. Bill has also shown me what it takes to be a top notch scientific writer. Something that I know I will continue to work on for the rest of my career. Bill has been there for me, not only professionally but personally as well and I don't think that I would have prospered nor survived if I had ventured into another lab.

I also want to acknowledge my thesis committee, Dr. Lisa Gloss, Dr. Chulhee Kang, and Dr. Jim Schenk. They have all been such a core source of support both on the professional and personal level as well. I really struggled the first couple of years during my research and yet I don't think that I ever felt a time of despair, mainly due in part to their generous support.

I want to extend thanks to all my fellow students and friends that I have gained here at WSU. Our 'inner circle' has been more than friends; they have become family in more ways than one. I hope that they know that there will always be a place for them in

our home, and yes, I will cook. I especially want to thank Joey Nichols. Joey has not only been the best co-worker and friend a guy could ask for, he has really become a brother of mine, and an uncle to my boys.

I must also make sure that I thank Mom and Dad. They have been the foundation and driving force behind all of my success. From kindergarten until now, both emotionally and financially, they have always been there for me. This doctoral degree is not just for me, in some ways it is more for them. I've just wanted to make them proud, and I hope I have done that.

Lastly, I want to thank my family, especially my wonderful wife Nicole. She has always been my partner in crime and my closest friend. Without her, I wouldn't be where I am today, nor would I have the desire to be anything more than average. Her encouragement and undying support for me have been the keys to my happiness and my sanity. Not to mention, the two wonderful sons, Wyatt and Aidan, that she has given me. Without Nicole and the boys, none of this would have ever been possible.

Thank you everyone. This is for all of those who believed in me.

THE EFFECTS OF NUCLEOSOME CORE PARTICLE PACKAGING ON DNA

CHARGE TRANSPORT

Abstract

By Chad Christopher Bjorklund, Ph.D.
Washington State University
December 2006

Chair: William B. Davis

Consequences of DNA oxidation can be critical to the healthy maintenance of genomic integrity. When left undetected or unrepaired, DNA oxidative lesions can contribute to various adverse health conditions including cancer, heart disease, and neuronal deterioration. Most DNA oxidative lesions are localized on guanine (G) residues due to the low ionization potential as compared to the other nucleotides found in DNA. One electron oxidation of G results in the formation of a guanine radical cation ($G^{\bullet+}$), or an electron deficient hole, which then has several fates available to it. One fate is that it may react with a molecule in solvent (O_2, H_2O, $O_2^{\bullet-}$) to form an irreversible oxidative lesion. Another option for the $G^{\bullet+}$ is a nearly isoenergetic exchange with another G within a DNA base stack, thereby mobilizing the electron hole to a site other than where it originated. This mobile electron hole may then migrate over long distances on DNA (>200Å) before becoming irreversibly trapped. While this phenomenon has been extensively studied in B-form DNA systems, little has been done to explore the potential and/or consequences of these events in biological settings. I have taken the nucleosome core particle (NCP) as a biological model to investigate the dynamics of DNA charge transport (CT). Here I report the results of using an Anthraquinone (AQ) photooxidant to initiate DNA CT in NCPs using highly thermodynamic NCP positioning

sequences (TG-motif and 601). My studies show that there are significant qualitative and

quantitative differences in G damage distributions in both free DNA and reconstituted

NCPs. I have also identified a unique DNA protein crosslink as a result of DNA CT.

Additionally, I have observed a previously undiscovered phenomenon called protein

mediated DNA CT. The results and interpretations of the data presented here will have

profound impacts on future studies of DNA CT in biological systems.

TABLE OF CONTENTS

LIST OF TABLES

CHAPTER II.

LIST OF FIGURES

CHAPTER III

CHAPTER IV

CHAPTER V

CHAPTER I

INTRODUCTION

1. Cellular Oxidative Stress

Many age-related degenerative diseases have been associated with the functional deterioration of somatic cell systems over time. These ailments include cancer[1, 2], immunodeficiency[2, 3], neurodegeneration[4], and diabetes[5]. Oxidative damage to cellular components are considered to be a major cause for the breakdown of fundamental cellular processes affiliated with these disease states. Additionally, it has been proposed that the appearance of these age-related degenerations in mammals may be directly linked to metabolic rate and oxidative stress.[6] An increase in metabolic activity may indicate an increase in endogenous cellular oxidants, thus causing an increase in the amount of intracellular oxidative damage. Additionally, it has been shown that the activity of inherent antioxidant defense mechanisms not only decline with age, but they may become supersaturated due to a steady accumulation of oxidants.[7] While oxidative stress is by no means the single culprit responsible for both the aging process and those diseases associated with aging, it is nonetheless a significant contributing factor.

Harmful cellular oxidants can evolve from a variety of both endogenous and exogenous sources. Exogenous sources like ionizing radiation[8] (IR) and ultraviolet radiation[9] (UR) can give rise to free radicals and other damaging reagents. Other exogenous sources can include environmental factors[10], self-imposed toxins (i.e. smoking)[10], or even certain pharmaceuticals used for treating diseases such as cancer (i.e. anthracyclines)[11]. Endogenous generation of harmful oxidative species usually results from a disruption of the homeostatic balance between active redox species and the innate oxidative defense mechanisms within the cell. Domestic cellular oxidants typically originate from four basic cellular processes. 1) Cellular respiration and the electron

transport chain conclude with the reduction of O_2 to H_2O, which is the primary source of some reactive oxygen species (ROS) including hydroxyl radicals ($OH^{\bullet}$), superoxide ($O_2^{\bullet-}$), and hydrogen peroxide (H_2O_2).[3, 7-9] 2) Phagocytes and neutrophils destroy bacteria and virus infected cells by producing nitrogen reactive species such as nitric oxide (NO) and hyperchlorous acid (HOCl).[6] 3) Peroxisomes produce H_2O_2 during degradation of lipids and other macromolecules.[12] 4) The by-products of detoxification enzymes such as cytochrome P450s also result in the production of ROS.[13] It is clear that both endogenous and exogenous sources of oxidative stress can generate a variety of potentially damaging reagents.

The targets of oxidative stress include the entire constituency of a cellular system. Oxidation of lipids may lead to compromised membrane systems which can ultimately affect whole cell or organelle function.[14] Proteins can be oxidized, which may alter an enzymatic activity, or result in dysfunction of receptors, transporters, or structural components (i.e. actin proteins of the cytoskeleton).[15] Within the nucleus, nucleic acids are also a common target of cellular oxidation[16], which may eventually lead to mutations and the induction or enhancement of a disease state. There are also important antioxidant defense mechanisms that are responsible for suppressing damaging redox reagents. Peroxisomes serves as protection by isolating and degrading enzymes that produce destructive oxidants.[12] Enzymatic defense systems like superoxide dismutase and catalase convert superoxide into hydrogen peroxide and eventually water and oxygen.[15] Protein chelation of free iron or copper ions reduces Fenton-like chemistry reactions that can produce hydroxyl radicals.[17] In addition to these endogenous defense mechanisms, dietary supplementation of fat soluble antioxidants like tocopherol and carotenoids are

also very effective at scavenging dangerous redox species and free radicals.[18] However,

when these defense mechanisms fail or become overwhelmed, the cell becomes

vulnerable to an oxidative assault.

1.1. DNA Oxidative Damage

Direct damage to one of the four nucleotides of DNA, Guanine (G), Adenine (A),

Cytosine (C), or Thymine (T) (Figure 1.1) can occur as a result of a variety of processes.

Damage may occur by enzyme modification, chemical modification, photoexcitation of

the nucleobase pi-systems, or by oxidation. These DNA lesions can manifest themselves

as single or double-stranded breaks, abasic sites, cyclobutane pyrimidine dimers, DNA-

protein crosslinks, or stable nucleobase modifications. DNA damage due to oxidation is

most commonly found localized on G residues. From thermodynamics, this is consistent

with the low oxidation potential of G ($\sim$1.3 V vs. NHE)[19] as compared to the other

nucleobases (A $\sim$1.4 V, C $\sim$1.7 V, and T $\sim$1.8 V; all vs. NHE)[19] or the sugar phosphate

backbone. Oxidized forms of A can also be observed, and to a minimal extent C[20] and

T[21]. Fortunately, cellular defense mechanisms responsible for detecting and eliminating

these DNA lesions have evolved in order to combat the potential of their deleterious

effects.[22-24]

There are two major pathways of G oxidation, Type I and Type II reactions

(Figure 1.2). Type I G oxidation refers to a one-electron oxidation of G to form a

Guanine radical cation ($G^{\bullet+}$) that can then undergo subsequent chemistry (Figures 1.2 and

1.3) to form stable G lesions. Type II G oxidation involves the attack of singlet oxygen

($^1O_2$) to generate an endoperoxide intermediate that eventually forms G lesions, some of

4

which are identical to those of the Type I pathway (Figure 1.2). One such lesion is 8-oxoguanine (8OG) (Figures 1.2 and 1.3), a lesion commonly used as a biomarker for oxidative stress in disease states such as cancer[25], diabetes[26], and brain dysfunction[27]. The formation of 8OG results in a species that has a lower oxidation potential than that of G.[28] This means that the oxidative lesion is even more vulnerable to oxidative attack than its original counterpart. The consequences of sequential G oxidation can result in lesions that may or may not be as stable as 8OG, but may also be as dangerous to the cell.[29, 30]

G oxidative lesions are capable of generating point mutations within a DNA sequence.[29, 31] Generally, these lesions are detected and repaired back to their original undamaged form by cellular repair machinery, such as the Base Excision Repair (BER) pathway.[22-24] However, if these lesions are not detected or improperly repaired they may become a seed for mutagenesis. For example, generation of 8OG results in a new hydrogen bond donor and a new hydrogen bond acceptor on the Hoogstein face of the purine (Figure 1.4). During a cellular replication event, 8OG may undergo a conformational flip about its glycosidic bond from *anti*- to *syn*- conformation.[32] In this configuration, a DNA polymerase will recognize the Hoogstein face as that of a T, and insert an A opposite in the counter-strand.[31] Assuming this lesion is still not repaired, and following an additional DNA replication event, a T will be placed opposite the A to complete a G:C to T:A transversion mutation (Figure 1.4). Depending on the mutational frequency or the exact position of this cellular event, this may result in permanent damage to the genome. For instance, mutations may lead to the activation of protooncogenes and/or inactivation of tumor suppressor genes, resulting in direct participation of DNA oxidative damage in progression to a cancerous cellular state.

2. Mechanisms of DNA Charge Transport

The first step in Type I G oxidation is the formation of a $G^{\bullet+}$, or an electron deficient "hole". The $G^{\bullet+}$ may be trapped by reaction with reagents in the aqueous medium to form a G lesion, or an additional oxidation event can occur between the $G^{\bullet+}$ and another G within the DNA duplex (Figure 1.5).[33-37] Consider this simple model where a $G^{\bullet+}$ has been generated in a DNA base stack and the electron hole "hops" to another G within the duplex:

$$G^{\bullet+}\left(\frac{A}{T}\right)_n G\left(\frac{A}{T}\right)_n G\left(\frac{A}{T}\right)_n \xleftrightarrow{Hop\,1} G\left(\frac{A}{T}\right)_n G^{\bullet+}\left(\frac{A}{T}\right)_n G\left(\frac{A}{T}\right)_n \cdots$$

$$\cdots \xleftrightarrow{Hop\,2} G\left(\frac{A}{T}\right)_n G\left(\frac{A}{T}\right)_n G^{\bullet+}\left(\frac{A}{T}\right)_n \tag{1}$$
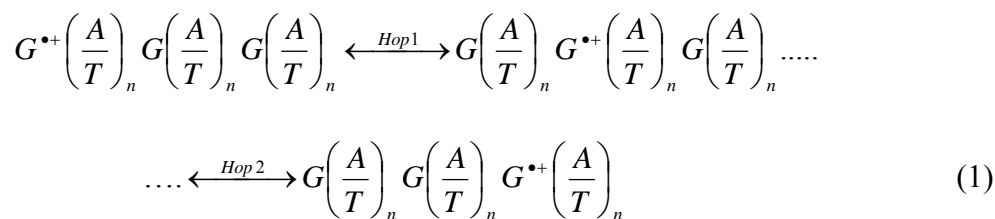
The radical cation transfer occurs over short, intervening A:T or T:A (where n = 1, 2, or 3) stretches that exist as a "bridge" in between the electron deficient site ($G^{\bullet+}$). Movement of the hole over short distances (a single bridge) is currently defined as DNA charge *transfer*, while movement over long distances (multiple bridges) is referred to as DNA charge *transport* (CT).[36, 45] Thermodynamically, the transfer is facilitated by the nearly identical oxidation potentials between the $G^{\bullet+}$ and the G, making the energetics of this electron transfer favorable. Hole transfer typically occurs between intra-strand G's, but it can also move via inter-strand migration within the duplex DNA structure.[37] Hole transfer continues until the electron deficient site is irreversibly trapped. The overall transport distance is ultimately determined by a competition between the rates of i) hole transfer, and ii) the trapping reactions (Figure 1.5).

The competition between these rates can also be influenced by the fact that not all G's are created equal. Multiple G stacks, like double GG and triple GGG regions are considered to be even better hole acceptors than a single G.[38, 39] Within G stacks hole trapping primarily occurs on the 5'-G of GG and the central G of GGG. Theoretical predictions using semi-empirical and *ab initio* calculations show that the majority of the highest occupied molecular orbital (HOMO) of a GG stack lies on the 5'-G.[40] These studies attribute this stabilization of the radical cation hole at the 5'-G by the overlap of the N7 nitrogen and the O6 oxygen of the 3'-G (Figure 1.1). The increased stability allows time for the radical cation to deprotonate to either solvent or the base paired C to form the neutral G radical ($G^{\bullet}(-H^+)$). The $G^{\bullet}(-H^+)$ is a much poorer G oxidant than the $G^{\bullet+}$ and is subsequently thought to be the species required for the initial trapping chemistry (Figure 1.3).[41, 42] In optimized systems, the migration of a $G^{\bullet+}$ has been shown to travel very long distances (>200 Å) in naked DNA complexes.[43, 44]

2.1 Experimental DNA CT Systems and Measured CT Rates

Since the initial observation of DNA CT, chemists and biochemists have rushed to answer some of the most basic questions; how and why does it occur, and what can we learn from it. For nearly two and a half decades, many different approaches have been utilized to probe the dynamics of DNA CT. Unfortunately, this variation in experimental approaches may have contributed to our incomplete understanding of the underlying mechanisms of DNA CT. Here I will briefly lay out some of the experimental DNA CT systems and experimentally derived kinetic properties of DNA CT.

The majority of DNA CT dynamics have been probed using either

electrochemistry or photoinducible DNA CT chemistry. Photochemical oxidation studies

with duplex DNA are perhaps the most effective method of studying DNA CT. These

types of techniques allow one to probe various aspects of DNA CT including specific CT

rates, CT efficiencies, identification of CT intermediates, and chemically trapped end-

products (G lesions). Many durable photooxidants have been used to induce DNA CT

including rhodium and ruthenium metallointercalators[44], anthraquinone derivatives[51],

ethidium bromide with methyl viologen[52], napthalamides[44], riboflavins[44], stilbenes[53], and

enol ether radicals[35]. Studies have been carried out with these various photooxidants

either free in solution or covalently attached to a DNA duplex end (either 5' or 3')[43], the

deoxyribose sugar[54], peptide nucleic acids (PNA)[55], or DNA hairpins[53]. In solution, most

of these compounds will associate with DNA through either binding in the major or

minor groove, or by intercalation between adjacent nucleobases of duplex DNA. These

systems are activated by photoexcitation (visible (600 nm) to near-UV (300 nm)) to form

an excited state. These excited photooxidant states then have high enough oxidation

potentials to oxidize nearby nucleobases within their respective DNA constructs. Other

photoinduced systems, like the enol ether radical utilize a modified deoxyribose (C4' *t*-

butyl aldehyde) that initially forms the electron deficient hole on the sugar moiety

following absorption of UV-A radiation.[35]

Kinetic schemes of DNA CT can be simple or complex depending upon the

system used to probe such rates. Most measurements have come from the measurement

of single charge transfer steps from a donor to an acceptor. In some cases, both the donor

and the acceptor are photosystems, or a combination of photooxidants and G steps or

other modified nucleobases. Single step hole transfers have been measured between

10^{12}-10^8 s^{-1} for 0-4 A:T intervening bp using a small DNA hairpin end-capped on both ends by a stilbene donor and acceptor system.[53] Quenching of photoexcited acridine dyes covalently attached to DNA found CT rates at 10^{11} s^{-1}, for nearest neighbor transfer and 10^8-10^7 s^{-1} for one intervening base pair.[56] Rate measurements utilizing the enol ether radical cation as a charge injector into DNA found rates at 10^9-10^6 s^{-1} for a 0-3 A:T bridge length.[57] In summary, it is apparent that there are distinct observations for rates over small distances depending upon the type of DNA CT induction system employed. The discordance between the short bridge transfer systems is thought to be due to the inherent variabilities of the DNA structures, differences in localized energetic potentials, and the photosystems in general. While the absolute rates may be debated, it is generally agreed that transfer of an electron deficient hole through small bridges is on extremely fast time scales of hundreds of microseconds to picoseconds. In contrast to these hole transfer rates, the rates of the trapping reactions with H_2O or O_2 are thought to be on a much slower time scale (~10^3 for H_2O).[35] This explains why these transfer processes are able to occur over long distances in the presence of short hopping steps. These studies also show the lack of exponential decay (β value) at these small transfer distances, and that some of these processes are much faster than predicted by theory.

2.2 Marcus Theory and Electron Transfer

The thermodynamics of electron transfer from a donor (D) molecule to an acceptor (A) molecule is determined by the overall free energy change (ΔG^o) of the charge separation. This is a direct function of the differences in reduction-oxidation (redox) potentials of the reactants.   For a single step electron transfer:

$$D + A \rightarrow D^{\bullet+} + A^{\bullet-} \tag{2}$$

the net reaction potential (ΔE°) is given by:

$$\Delta E^0 = E_A - E_D \tag{3}$$

and the overall free energy change is:

$$\Delta G^0 = -nF\Delta E^0 \tag{4}$$

where n is the number of electrons transferred, F is the Faraday constant, and spontaneous reactions typically occur when $\Delta G^{\circ} < 0$. A driving force of $\Delta E^{\circ} > 0.3$ V is usually required to observe redox reactions under ground state conditions.

Electron transfer theory is most notably attributed to the seminal work of Rudolph Marcus in 1956.[46] Semi-classical Marcus theory predicts that the first-order rate constant of electron transfer from D to A is dependent upon ΔG°, temperature (T), the electronic coupling element (H_{DA}) that describes electronic overlap of the D and A, and the reorganization energy (λ) which is related to the amount of nuclear motion necessary to reach the transition state. λ reflects the changes about the molecular structure and the solvent surrounding the transition state that must occur upon movement of the electron from D to A . Marcus theory assumes that electron transfer is non-adiabatic, where the electronic interaction between D and A is weak (small H_{DA}). The key equation of Marcus theory is:

$$k_{ET} = \sqrt{\frac{4\pi^3}{h^2 \lambda k_B T}} H_{DA}^2 \exp\left(-\frac{(\Delta G^{\circ} + \lambda)^2}{4\lambda k_B T}\right) \tag{5}$$

and that k_{ET} is maximal when $-\Delta G^0 = \lambda$ so that:

$$k_{ET} = \sqrt{\frac{4\pi^3}{h^2 \lambda k_B T}} H_{DA}^2 \qquad (6)$$

Consider the equilibrium of hole transfer between two G's within a DNA strand separated by some $(A:T)_n$ bridge:

$$G^{\bullet+}\left(\frac{A}{T}\right)_n G \Leftrightarrow G\left(\frac{A}{T}\right)_n G^{\bullet+} \qquad (7)$$

the rate of electron transfer between them is most often going to be governed by the nonadiabatic limit of electron transfer rates. This emphasizes the dependence of the rate on the electronic coupling element (H_{DA}), since the two G's are well separated in space. With an increasing bridge length, the direct distance between the D (G) and the A ($G^{\bullet+}$) become increasingly further, thus making their interaction weaker (smaller H_{DA}). In order for DNA CT to proceed at these longer distances, theory would suggest that electron tunneling through this large barrier would be the most direct path of exchange. This model would then predict that the rate of electron transfer would decay exponentially with increasing distance between the D (G) and the A ($G^{\bullet+}$). The Marcus-Levich-Jortner equation indicates that:

$$k_{ET} \propto e^{-\beta R_{DA}} \qquad (8)$$

where the decay constant, β, is a reflection of the barrier height, and R_{DA} represents the spatial distance between the D and the A. In DNA CT, one would expect the barrier to be lower and the tunneling to be faster the smaller the A:T bridge is in between successive

11

G's. Conversely, the longer the A:T bridge is, the slower the tunneling rate should be, which in turn decreases the efficiency of long-range DNA CT.

2.3 Superexchange vs. Thermally-Induced Hopping

Thermodynamic and kinetic considerations of DNA CT have all been derived from experimental observations. However, theoretical interpretations of these observations are still evolving. The predominant theoretical model of long-range DNA CT involves a combination of superexchange and thermally-induced hopping mechanisms. In simple terms, this describes the transfer of a $G^{\bullet+}$ to another G through a short $(A:T)_n$ ($n \leq 4$) bridge through a superexchange electron tunneling mechanism, coupled with a thermally-induced hopping mechanism over long bridges ($n > 4$) (Figure 1.6a and 1.6b).[33, 35, 36] That is, the exothermic barrier over short bridges is not large enough to require localization of the electron deficient hole on the bridge itself (assumedly on A because of the lower oxidation potential than T). On longer bridges, the endothermic penalty for the electron deficient site to localize on an adjacent A is small in comparison to the length of the exothermic barrier over the long bridge. In other words, the rates of hole localization on the bridge is much faster than the slow tunneling rate. The thermal activation of the hole to localize on the A:T bridge can result in a very fast transport over the entire length of the A:T bridge to the low energy site of the nearest G. This explanation must be based upon a couple of assumptions. First, the lifetime of a $G^{\bullet+}$ must be long enough to overcome the endothermic barrier to transiently oxidize the nearby A. Second, the rates of chemical trapping of an oxidized adenine must be much slower than the rate of transport over the A:T tract. There are several pieces of

experimental evidence that support this combination of theoretical mechanisms to describe DNA CT, however one major alternative theory has been proposed.

2.4 Polaron Theory as an Alternative to the Superexchange/Hopping Model

The polaron model for migration of an electron deficient hole down a DNA duplex describes DNA CT in a manner that differs slightly from the superexchange /hopping theory (Figure 1.6c).[37, 49, 50] This theory compares DNA CT to the polaron theory of solid-state semi-conductors that describes the coupling interaction between vibrational and electronic modes that result in a structural distortion of the local environment. In an analogous manner, this would describe the delocalization of the electron deficient hole over a stretch of nucleobases through structural deformation of the DNA helix. In this scenario, the rate for electron tunneling through the exothermic activation barrier would be much slower than the endothermic occupation of a delocalized charge on a stack of A:T base pairs.

2.5. The Anthraquinone Photooxidant System

Despite the fact that there are many robust photooxidant systems, the only one employed within the studies reported here is an anthraquinone 2-carboxylic acid derivative (AQ; Figure 1.7a). An AQ photooxidant can either be used as a random DNA intercalator where binding is not controlled nor are the sites of DNA oxidation[51], or it can be covalently attached to either the 5'-end via phosphoramidite chemistry[43] or to the 2'-oxygen of a ribose sugar[54]. In all experiments reported here, the AQ phosphoramidite was synthesized in-house and attached to the 5'-end of oligonucleotides during solid

phase synthesis. Attachment of AQ to the 5'-end of DNA duplexes serves several important functions. 1) Ab initio calculations, molecular modeling[54], and NMR structures of similar dyes[58] predict that the planar hydrophobic AQ will end-cap onto a DNA duplex essentially behaving as an additional base pair. This not only increases the stability of the DNA duplex (higher T_m), but also decreases unwanted interactions of the AQ with any other sections of the DNA or proteins used in these studies. 2) The covalent attachment gives us absolute control over the sites of $G^{\bullet+}$ injection and allows for efficient monitoring of DNA CT. 3) Additionally, some photooxidants like the Rh and Ru metallointercalators have shown a propensity to cause structurally uncharacterized aggregates in higher order DNA structures[59], whereas the AQ has not. This allows for structurally sound DNA systems with well-behaved properties that do not complicate the results or interpretations of the observed data.

Under ground state conditions, the oxidation potential of AQ (-0.6 V vs. NHE)[60] is much too low to spontaneously oxidize G (+1.3 V vs. NHE)[19] within a DNA duplex in aqueous solution. The driving force of electron transfer from G to AQ is governed by the overall free energy change (ΔG^o) of the reaction as described in section 2.2. Applying the oxidation potentials of G and AQ to Eq.4, it is apparent that the ground state interaction ($\Delta G^o = +183$ kJ/mol) will not result in a spontaneous electron transfer. AQ has two major absorption bands at ~330 nm and ~260 nm. The 330 nm peak is ideal because this region does not overlap with any absorption spectra of the aromatic DNA nucleobases (peak at 260 nm), thereby avoiding any unwanted reactions that could result from nucleobase excitation. UV irradiation of AQ at 350 nm results in photon absorption and the promotion of an electron from the highest occupied molecular orbital (HOMO) to

the lowest unoccupied molecular orbital (LUMO) (Figure 1.7b). The first excited AQ

population is the singlet state (^{1}AQ*), which is energetically capable of oxidizing a G

within a duplex. However the electron transfer from G to ^{1}AQ* is thought to be much

too slow compared to the extremely fast back electron transfer process (Figure 1.7b).[37]

Formation of ^{1}AQ* also results in rapid intersystem crossing to the excited AQ triplet

state (^{3}AQ*). Due to spin conservation rules, the ^{3}AQ* is much longer lived and

predicted to be the predominant species responsible for G photoinduced oxidation.

Promotion of an electron to the singlet and eventually the triplet state results in a vacancy

in the HOMO, which is low enough in energy for transfer of an electron from a

neighboring G residue, eventually forming the charge separated state, AQ$^{\bullet -}$ - G$^{\bullet +}$ (Figure

1.7b). In thermodynamic terms, photoexcitation of AQ adds an additional variable (E^o_{0-0})

to account for the energy added to the system upon photon absorption by using the

Rehm-Weller Equation:

$$\Delta G^0 = 96.48(E_D - E_A - \Delta E^0_{0-0}) \qquad \text{Eq.9}$$

The ΔE^o_{0-0} of the lowest energy triplet state of AQ is +2.68 V.[60] Substitution of this into

Eq.9 gives a ΔG^o = -75 kJ/mol, which is indicative of an energetically favorable oxidative

process under photoexcitation conditions.

Formation of the charge separated state (AQ$^{\bullet -}$ - G$^{\bullet +}$) leads to a competition of

rates between charge recombination (ground state reformation AQ-G) and liberation of

the excess electron on AQ$^{\bullet -}$ via oxygen to generate O$_2$$^{\bullet -}$. If electron liberation of the AQ$^{\bullet -}$

occurs before charge recombination, the photoreaction then becomes irreversible due to

the formation of the AQ - G$^{\bullet +}$ state. The fate of the G radical cation then lies down two

distinct pathways. 1) The G$^{\bullet +}$ may deprotonate to either solvent or the base pairing

cytosine to form the G neutral radical (G$^{\bullet}$(-H)) which is both a very poor oxidant of G

and is thought to be responsible for most of the G lesion chemistry (Figure 1.3). 2) The

G$^{\bullet+}$ may oxidize a neighboring guanine within a duplex stack, thus transferring the

electron deficient site to a region that is distal from its point of origin (Figure 1.5), and

initiating long-range DNA CT. Radical cation hole migration will continue until it is

trapped by reaction with solvent to generate a stable G lesion. These lesions can then be

detected using one of the cleavage techniques described in the next section and quantified

using DNA sequencing gels and autoradiography. This brief introduction to AQ

photoinducible oxidation of G should serve as the background for a general

understanding of the data presented in the subsequent chapters of this thesis.

2.6 Detection of DNA CT by Cleavage Reactions

Oxidation of G, directly or via CT, leads to the formation of G lesions that often

differ dramatically in chemical structure to that of the native G (Figure 1.3). The

alteration in the chemical properties of this nucleobase renders it susceptible to alkali

lability or susceptible to Schiff base formation by primary or secondary amines.[61] Abasic

sites are extremely alkali labile (Figure 1.8a). After the formation of an abasic site and

resonance rearrangement to form the sugar C1' keto group, the C2' hydrogen becomes

highly acidic (Figure 1.8a). In the presence of high heat and extreme alkaline conditions,

this species is pushed to a phosphate β-elimination. Additionally, due to the acidity the

C4' hydrogen, a second δ-elimination can occur to leave three products: 1) the 5'

phosphorylated end as a product of the initial elimination reaction, 2) a 3' phosphorylated

end as a product of the second elimination reaction, and 3) the deoxyribose fragmented

into a keto aldehyde. Under alkaline conditions, primary or secondary amines can act as a catalyst for the elimination reactions due to Schiff base formation on the sugar C1'. Destabilization of the imidizole ring on an oxidized G (Figure 1.8a and 1.8b) results in the loss of electron density within the heterocycle and can promote abasic site formation through a nucleophilic attack at C1', thus forming a Schiff base. The destabilization makes the modified nucleobase a better leaving group. Modifications of the G imidizole ring can occur via alkylation (i.e. Maxam-Gilbert DMS reaction) or by oxidative ring-opened products (i.e. imidazolone and oxazolone). The most common detection method of an oxidative G lesion utilizing both alkali lability and Schiff base formation is by piperidine cleavage, a technique originally developed by Maxam and Gilbert[62] to sequence DNA. Piperidine is a heterocyclic secondary amine with a pKa > 11.[61] Incubation at high heat (90ºC) for 30 min in the presence of 1 M piperidine is sufficient to cleave most oxidized G's (inefficiently cleaves 8OG due to lack of imidizole destabilization) within a ^{32}P-labeled DNA strand. The sites of oxidative damage can then be visualized by autoradiography and denaturing gel electrophoresis.

An additional form of oxidative G lesion detection is by enzymatic cleavage of the damaged base. A commercially available enzyme called foramidopyrmidino-glycosylase (Fpg) is an *E.coli* enzyme capable of detecting and excising damaged G nucleobases.[63] The mechanism for cleavage includes glycosylase activity (cleavage of the glycosidic bond), lyase activity (β-elimination), and δ-elimination to completely excise the damaged lesion from the DNA strand (Figure 1.8b).[64] Fpg is capable of detecting and revealing a wide range of oxidized G nucleobases including 8OG. However, there are some lesions that are not detected and cleaved as efficiently as others.

This property becomes essential for some of the data interpretations within this thesis (see Chapter 3). Thorough comparison of different G lesion cleavage mechanisms (piperidine vs. Fpg) can give us insight into the types of lesions occurring at specific sites within the DNA complexes during a DNA CT experiment. Through identification of the yields of specific lesions at specific structural positions within a biological model, we can explore the potential for specific lesion repair pathways that may be required in vivo.

3. DNA CT and Biology

Experimental evidence of DNA CT has been extensively explored using finite systems to measure the complex characteristics that govern this phenomenon. There are two major disciplines that have served as the driving force behind this quest for knowledge. 1) The potential applications of DNA CT for molecular electronic devices, and 2) the impact of DNA CT upon biological systems. Unfortunately, only preliminary studies have begun to address how DNA CT might be influenced in biological systems, and what significant consequences may result from those processes.

3.1 DNA CT in Biological Models

There have been relatively few biological models employed to study DNA CT in a more physiologically relevant context. Most of them have relied upon the interactions of protein recognition sequences and their respective DNA-binding proteins. DNA-binding proteins have been shown to have both large and small effects on DNA CT. The TATA-Box binding protein (TBP) binds a recognition sequence and introduces a 90° kink in the DNA backbone.[65] The gross disruption of the pi-stack nearly shuts down

DNA CT through the DNA sequence.[66] The restriction endonuclease *BamHI* attenuates DNA CT even though there is no structural disruption of the base pair stack.[67, 68] This attenuation was predicted to be due to an electrostatic effect contributed by an arginine residue inserted into the major groove of the helix. In contrast, other DNA-binding proteins have been shown to increase DNA CT efficiency upon binding, which has been interpreted as an increase in duplex rigidity and thus a restriction on conformational dynamics that would influence base stacking.[66, 69] Another biological model utilized spermine and spermidine DNA-condensates to mimic the compaction of DNA inside a eukaryotic nucleus.[74] They found that through this compaction there was an overall decrease in G oxidative damage, indicating that these highly-compacted complexes may serve as protection against DNA CT and G lesion formation. Obviously, there is no definitive data that would enable us to predict the consequences of DNA CT in vivo.

3.2 Chromatin and Nucleosome Core Particles (NCPs)

Since most current studies of DNA CT use short pieces of DNA, they do not serve as accurate models of the structure or environment of DNA within a eukaryotic cell. In fact, extremely long pieces of DNA are subjected to many levels of compaction within a eukaryotic nucleus that are facilitated by an array of proteins. Nucleosome core particles (NCPs) form the first level of nuclear DNA compaction. Briefly, 147 base pairs of DNA is wrapped 1.65 turns around a core of eight histone proteins to form a two-fold pseudo-symmetrical dyad axis (Figure 1.9).[70, 71] This octamer of proteins consists of four different histones (H2A, H2B, H3, H4), with two of each making up the core. Histones are generally basic (pI~11), especially the N-terminal tails that consist mainly of positive

charged residues (i.e. Arg & Lys) that create electrostatic interactions with the extremely negative DNA phosphate backbone. During chromatin remodeling events (i.e., replication, transcription) that require greater DNA duplex access, these electrostatic interactions can be tuned through various chemical modifications like acetylation and phosphorylation of the N-terminal tails.[70] Contacts between the phosphate backbone and the surface of the histone octamer occur roughly every ten base pairs due to the helical twist of B-form DNA.[70,72] Furthermore, nucleosomal DNA does not display the typical structural configuration as that of B-form DNA. At the entrance/exit of the NCP, DNA is overwound with a helical repeat of 10 bp per turn compared to 10.5 bp/turn in free DNA, and is underwound with approximately 10.7 bp/turn at the dyad axis.[72] The non-uniform structure of the DNA on the NCP suggests that not all regions are equally susceptible to damage. Intuitively, one might expect that the nucleosomal DNA structure at the underwound regions has greater accessibility to damaging oxidative agents, whereas the overwound portions are less accessible. The rotational setting of the DNA is another consideration for how the NCP may impact DNA damage. Residues that face inward towards the protein structure are theoretically less prone to oxidative attack than the residues facing outward, even though the sugar-phosphate backbone is still vulnerable to attack.

Through the study of the effects of NCP packaging on DNA CT we might be able to predict what types of biological consequences may occur in vivo. One report that has investigated the role of charge transport on reconstituted NCPs has indicated that NCPs did not protect the duplex DNA from long-range oxidative damage through the base pair stack.[73] However, the photoinjection system employed in these studies (rhodium

metallointercalators) has since been placed under much scrutiny due to its propensity to aggregate highly ordered DNA structures (Holliday Junctions).[59] These results make room for questioning the validity of some of the conclusions formed from the use of the rhodium metallointercalator system. Other systems, like the use of covalently attached AQ found no such aggregation, implicating the AQ system as a better defined system for studying DNA CT in biological models.

The specific intentions of this work were to explore the effects of lower order chromatin structure on both DNA oxidation, and DNA CT. Through the use of an AQ photooxidant and the NCP as the biological model, I have begun to address these priority questions: 1) does NCP compaction affect the distributions of oxidative DNA damage, and if so, 2) will this assist us in understanding how complex cellular machinery finds and repairs these lesions, 3) can DNA CT occur in a biological system like the NCP, and if so 4) what biological consequences may manifest themselves directly due to this physical event, or if DNA CT does not occur, 5) does chromatin packaging serve as a protective barrier to DNA oxidative damage? These fundamental questions are imperative due to the lack of understanding at the molecular level of these cellular events (particularly DNA damage from oxidative stress) that are known to contribute to severe pathological consequences. The studies I am reporting here not only begin to answer some of the questions described above, but have generated a mountain of new and provocative ones. In addition, I have identified two unique events completely unanticipated in the undertaking of this research which may have profound implications in not only the field of DNA damage and repair, but also in DNA CT. The conclusions of this research should not only deepen the understanding of some poorly understood

concepts, but the discovery of unique and potentially seminal observations could greatly

impact the way the scientific community approaches this subject in the future.

Figure 1.1

Guanine (G) Adenine (A)

Cytosine (C) Thymine (T)
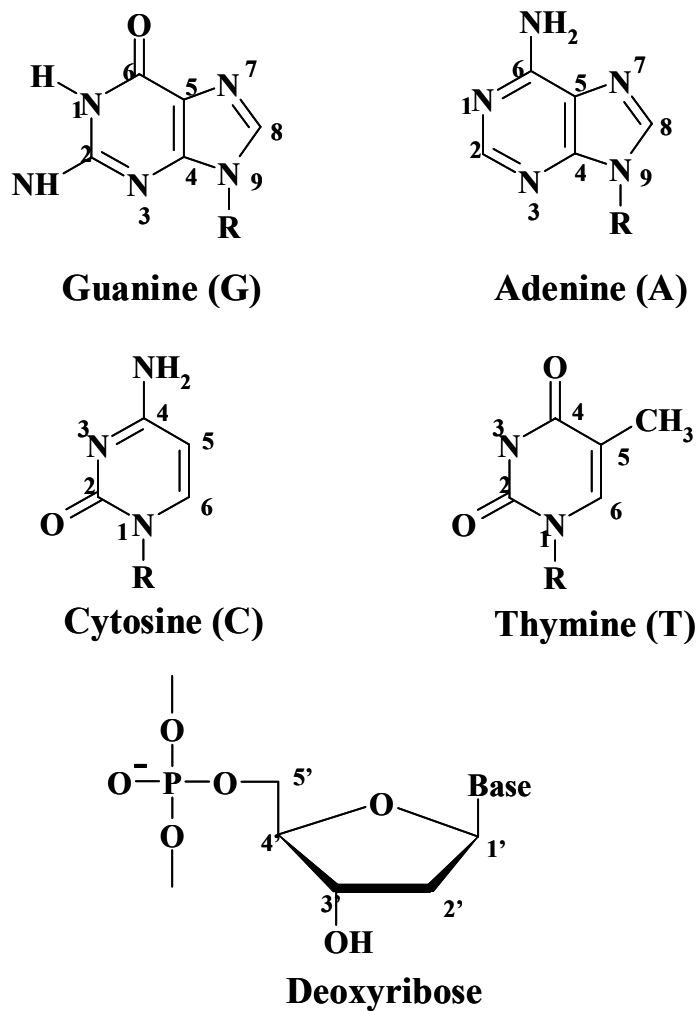
Deoxyribose

Figure 1.1: Chemical structures of the four nucleobases and the deoxyribose sugar of that form the basis of a DNA polymer. The numbering system for each structure is indicated.

Figure 1.2
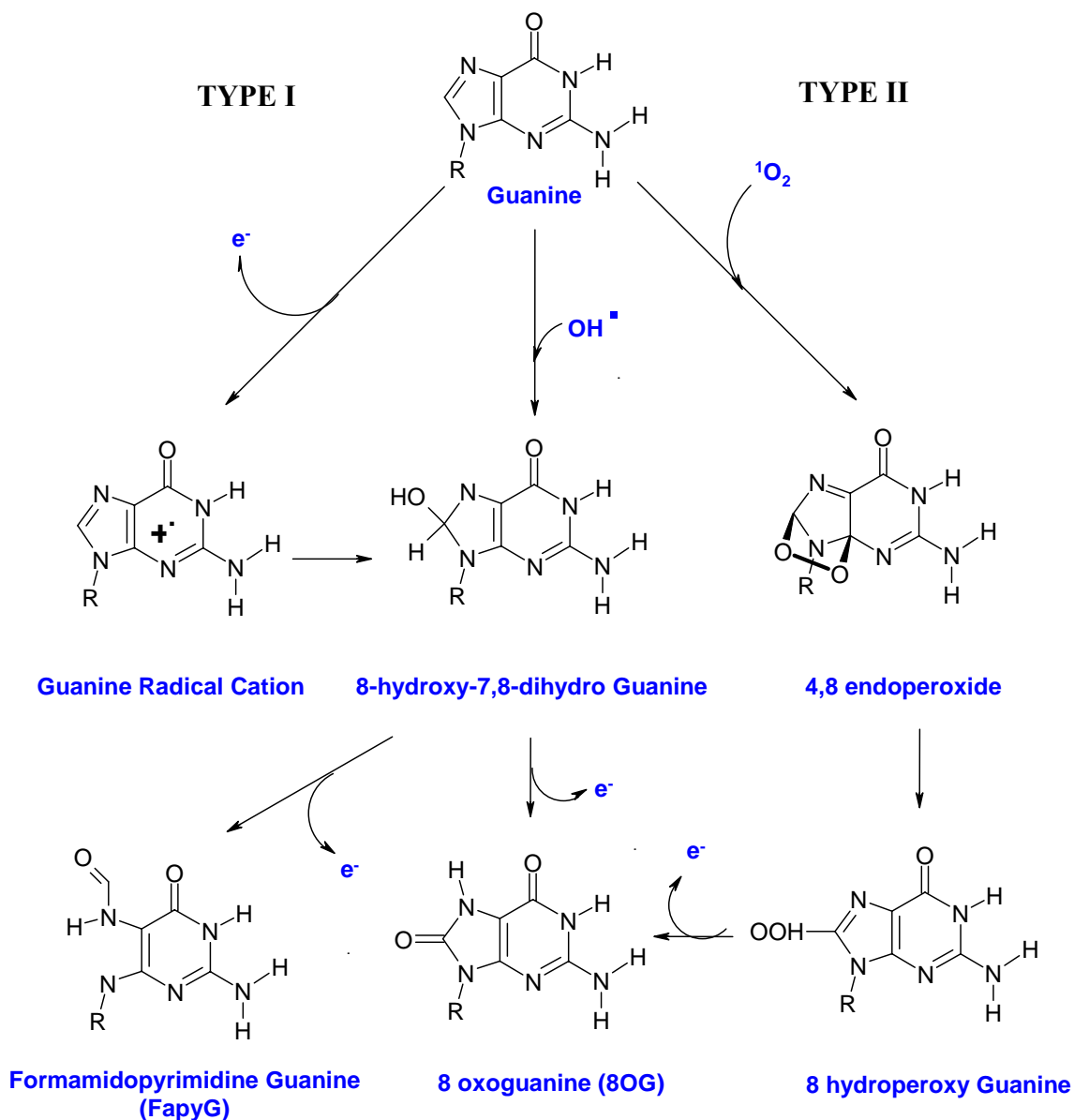
Figure 1.2: Oxidation of Guanine (G) by either the Type I or Type II pathway. Type I involves an initial one electron oxidation of G to form the Guanine radial cation ($G^{\bullet+}$). The $G^{\bullet+}$ can then become hydrated and become oxidized to form 8OG. Type II G oxidation involves attack by singlet oxygen ($^1O_2$) to form an endoperoxide intermediate, that can also form 8OG by a separate pathway.

24
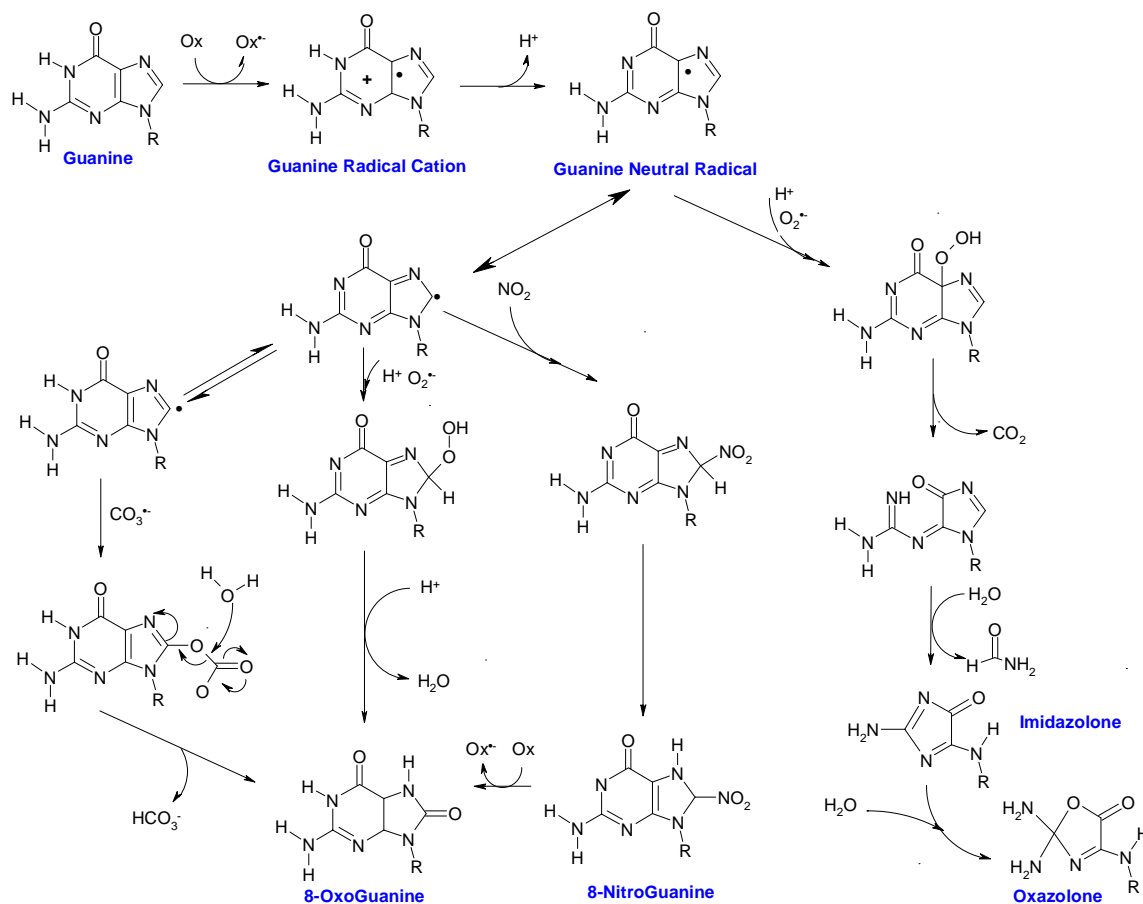
Figure 1.3

Figure 1.3: Chemical trapping pathways for a one-electron oxidation of G. Formation of the $G^{\bullet+}$ results in a species that deprotonates either to solvent or the base pairing cytosine to form the Guanine neutral radical ($G^{\bullet}(-H)$). The $G^{\bullet}(-H)$ is thought to be the G oxidation state responsible for the trapping chemistries associated with the formation of 8OG, imidazolone (Iz), oxazolone (Oz), and formamidopyrimidine (FAPY). These lesions can be detected either by piperidine or Fpg cleavage on a DNA sequencing gel.

Figure 1.4:
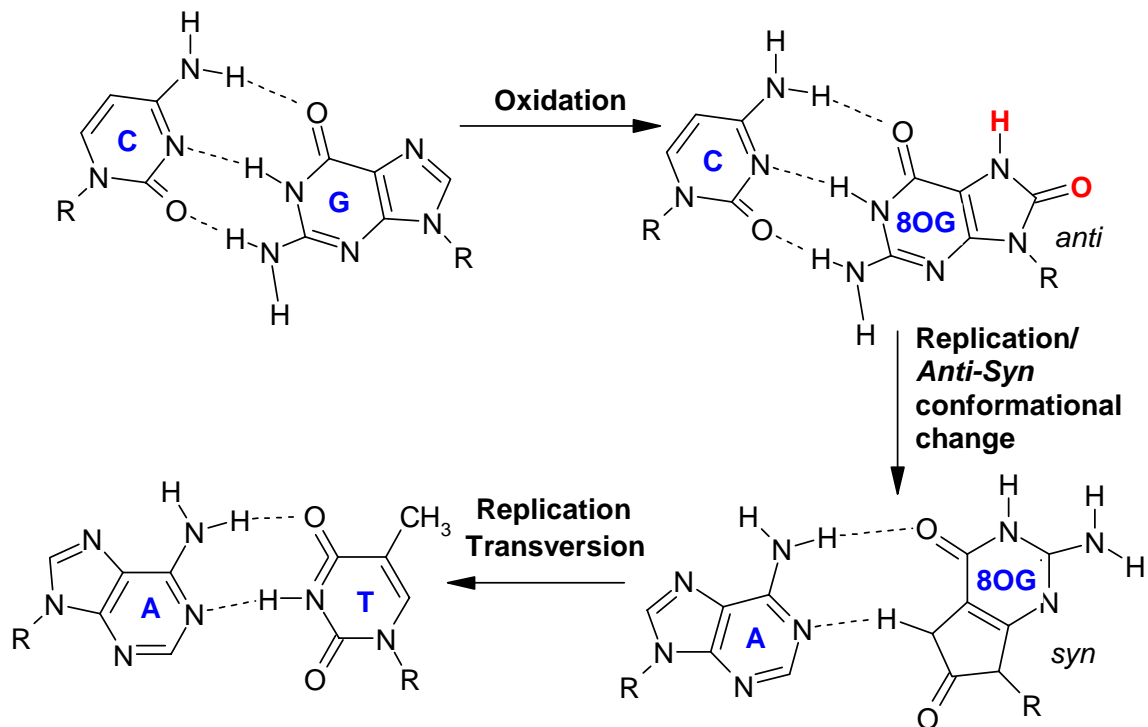
Figure 1.4: One-electron oxidation of G can lead to the formation of an oxidative G lesion like 8OG. In vivo consequences of 8OG formation are the potential to be mutagenic and possibly carcinogenic. Following formation of 8OG, a new hydrogen bond donor (N7) and hydrogen bond acceptor (C8) have been formed. During cellular replication, there is a conformational flip about the glycosidic bond from an anti- to syn-conformation. A DNA polymerase will recognize the Hoogstein face of 8OG as properly base pairing to adenine (A). Another round of DNA replication will result in a complete G:C to T:A transversion mutation.

Figure 1.5:
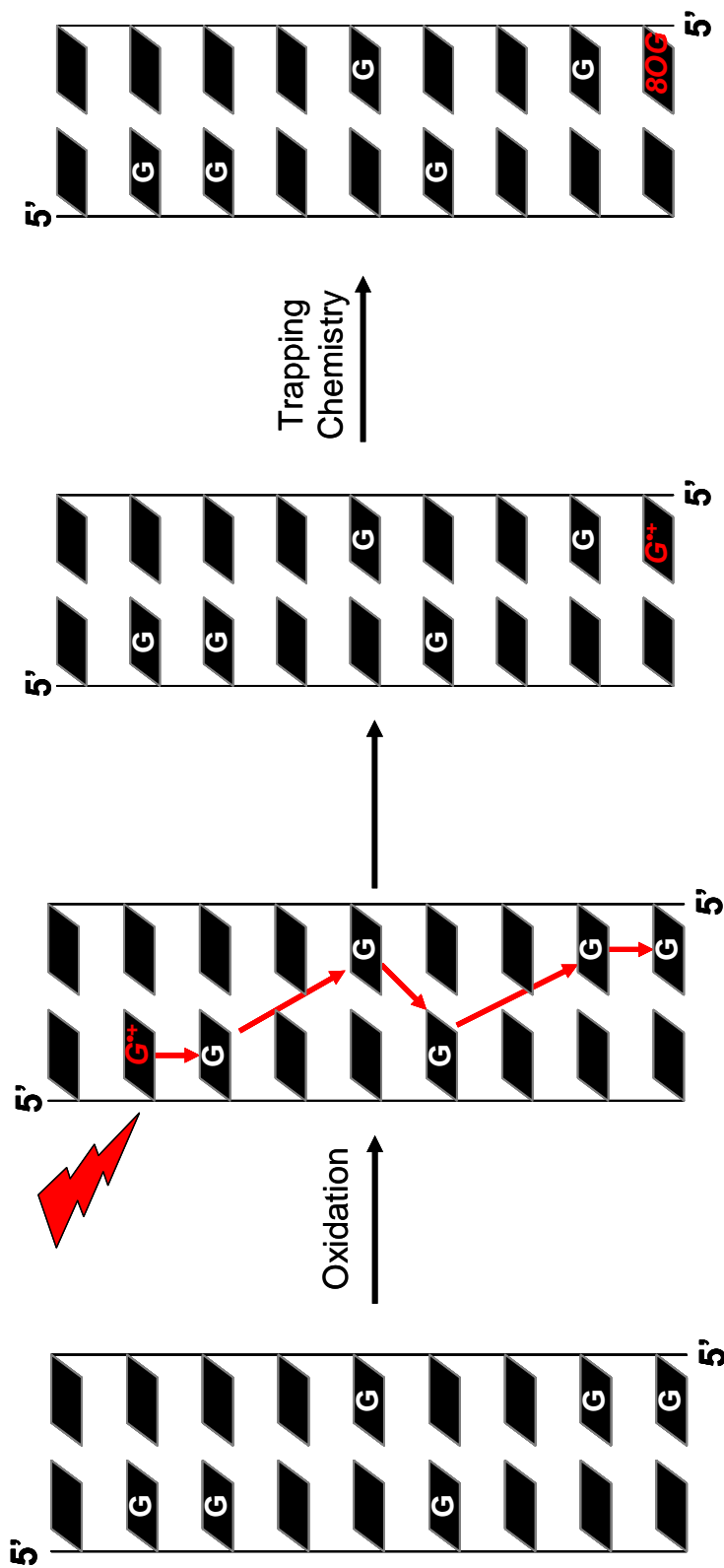
Figure 1.5: DNA Charge Transport (CT). Following one-electron oxidation of G to form the G$^{•+}$, a nearly isoenergetic exchange with another G within the bp stack results in the migration of the G$^{•+}$ to a distal G before it is preferentially trapped out. This results in the formation of a potentially mutagenic lesion at a site that is distal to the oxidative origin.

27
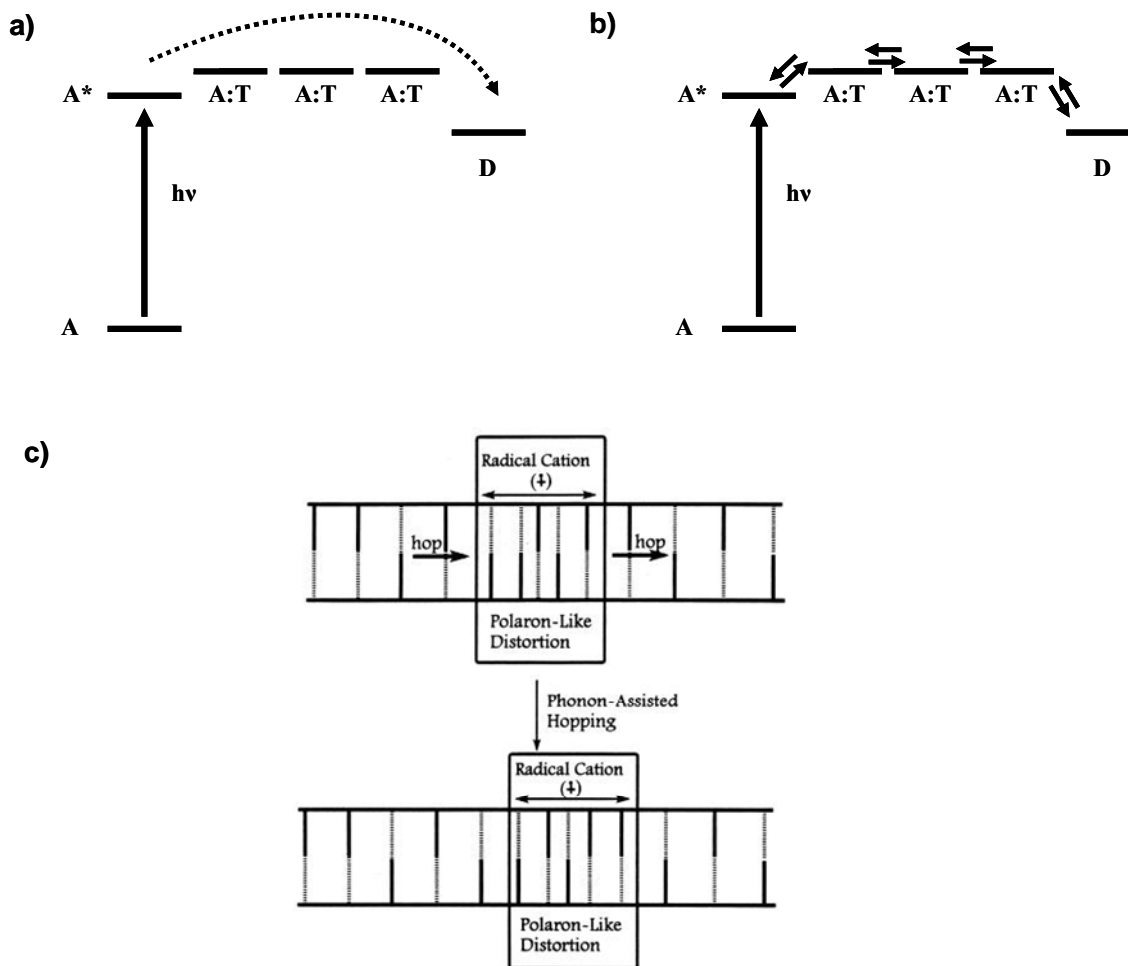
Figure 1.6:

Figure 1.6: Theoretical models for DNA CT. Photoexcitation of an A molecule results in an excited state can then oxidize a G by superexchange (a) over an A:T bridge of 4 or less and thermally-induced hole hopping (b) over a bridge of 4 or more. (c) Polaron theory of DNA CT. Hole transfer over long A:T bridges results in the structural distortion of the local matrix allowing the delocalized charge to migrate down the DNA duplex. Model in (b) is reproduced by Henderson et.al[43].

Figure 1.7:

a)
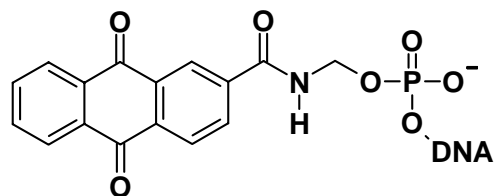
Anthraquinone (AQ)

b)
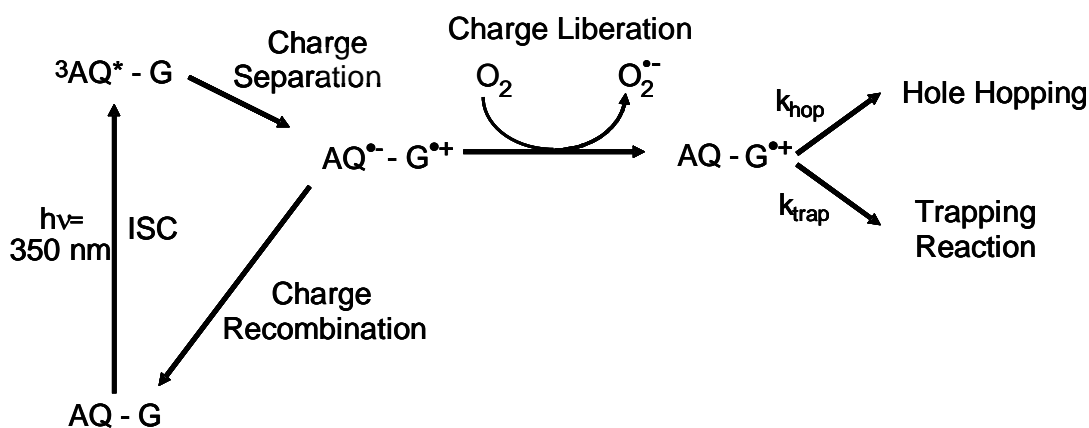
Figure 1.7: (a) Chemical structure of the Anthraquinone (AQ) photooxidant linked to the 5'-end of a DNA strand. (b) Scheme of photoinduced DNA oxidation by AQ. Irradiation of AQ results in an excited singlet state that quickly intersystem crosses (ISC) to form the excited triplet state (^{3}AQ*). Next is a charge separated state between the AQ and the nearest G within the DNA stack. By avoiding charge recombination the excess AQ$^{\bullet-}$ electron is liberated by oxygen to irreversibly form of a G$^{\bullet+}$. The G$^{\bullet+}$ can either migrate down the DNA duplex or be chemically trapped by reaction with solvent. These two fates are governed by, k_{hop} and k_{trap}.

Figure 1.8
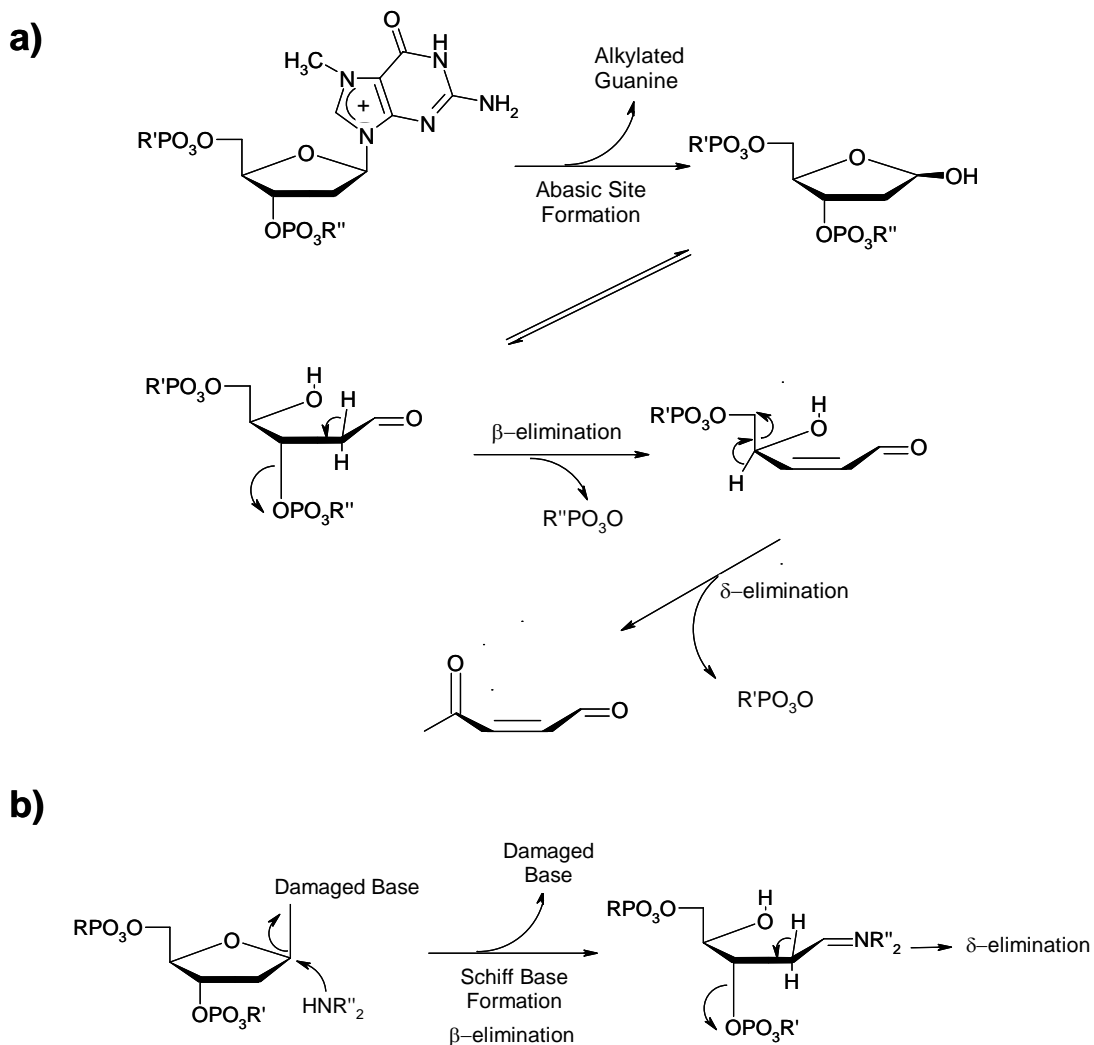
Figure 1.8: Cleavage mechanisms of oxidized G nucleobases. (a) Cleavage reaction under alkaline conditions of an N7 alkylguanine. Following abasic site formation, there is a rearrangement to form the C1' keto group. This is followed by two elimination reactions to completely excise the damage nucleotide. (b) Cleavage reaction facilitated by a secondary amine (as for piperidine or Fpg) that results in Schiff base formation followed by elimination reactions similar to those in (a).

Figure 1.9:
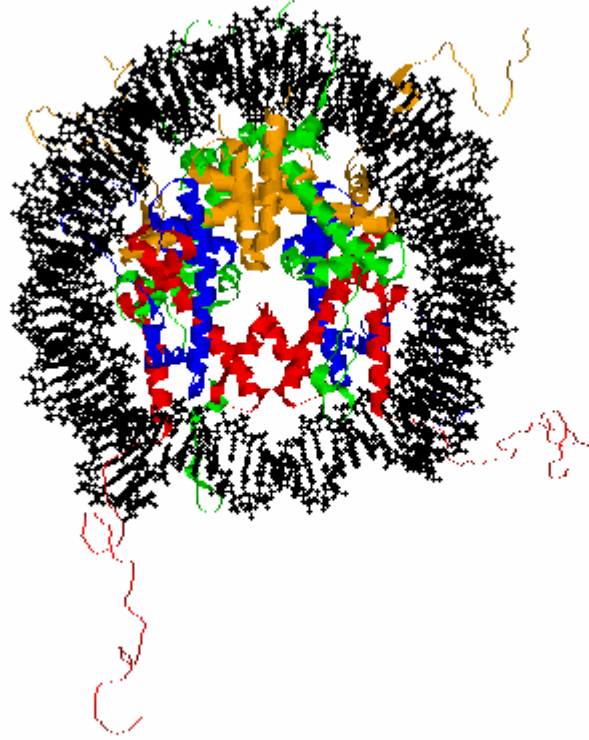
Figure 1.9: Crystal structure of the Nucleosome Core Particle (NCP; PDB#1kx5) rendered using RasMol (http://www.openrasmol.org/). Shown are 147 base pairs of DNA (black) wrapped 1.65 turns around the histone octamer. The histone octamer is consists of two copies each of histones H2A (orange), H2B (green), H3 (red), and H4 (blue).

References:

1. Fearon, E. R. *Science* **1997,** 278, 1043-1050.

2. Olinski, R.; Gackowski, D.; Foksinski, M.; Rozalski, R.; Roszkowski, K.; Jaruga, P. *Free Radic. Biol. Med.* **2002,** 33, 192-200.

3. Singh, U.; Jialal, I. *Pathophys.* **2006,** 13, 129-142.

4. Loh, K. P.; Huang, S. H.; De Silva, R.; Tan, B. K. H.; Zhu, Y. Z. *Current Alzheimer Research* **2006,** 3, 327-337.

5. Simmons, R. A. *Free Radical Bio. Med.* **2006,** 40, 917-922.

6. Ames, B. N.; Shigenaga, M. K.; Hagen, T. M. *Proc. Natl. Acad. Sci. USA* **1993,** 90, 7915-7922.

7. Wei, Y.-H.; Lee, H.-C. *Experimental Biology and Medicine* **2002,** 227, 671-682.

8. Miura, Y. *J. Rad. Res.* **2004,** 45, 357-372.

9. Renzing, J.; Hansen, S.; Lane, D. P. *J. Cell Science* **1996,** 109, 1105-1112.

10. Irie, M.; Tamae, K.; Iwamoto-Tanaka, N.; Kasai, H. *Cancer Science* **2005,** 96, 600-606.

11. Joshi, G.; Sultana, R.; Tangpong, J.; Cole, M. P.; St. Clair, D. K.; Vore, M.; Estus, S.; Butterfield, D. A. *Free Radical Res.* **2005,** 39, 1147-1154.

12. Kasai, H.; Okada, Y.; Nishimura, S.; Rao, M. S.; Reddy, J. K. *Cancer Res.* **1989,** 49, 2603-5.

13. Park, J.-Y. K.; Shigenaga, M. K.; Ames, B. N. *Proc. Natl. Acad. Sci. USA* **1996,** 93, 2322-7.

14. Niki, E.; Yamamoto, Y.; Komuro, E.; Sato, K. *Am. J. Clin. Nutr.* **1991,** 53, (1, suppl.), 201S-205S.

15.   Davies, K. J. A. *IUBMB Life* **2000,** 50, 279-289.

16.   Evans, M. D.; Cooke, M. S. *BioEssays* **2004,** 26, 533-542.

17.   Biemond, P.; van Eijk, H. G.; Swaak, A. J.; Koster, J. F. *J. Clin. Invest.* **1984,** 73, 1576-9.

18.   Di Mascio, P.; Murphy, M. E.; Sies, H. *Am. J. Clin. Nutr.* **1991,** 53, (1 Suppl), 194S-200S.

19.   Steenken, S. *Chem. Rev.* **1989,** 89, 503-520.

20.   Shao, F. W.; Augustyn, K.; Barton, J. K. *J. Am. Chem. Soc.* **2005,** 127, 17445-17452.

21.   Joy, A.; Ghosh, A. K.; Schuster, G. B. *J. Am. Chem. Soc.* **2006,** 128, (16), 5346-5347.

22.   Boiteux, S.; Radicella, J. P. *Biocheimie* **1999,** 81, 59-67.

23.   Chen, L. W.; Haushalter, K. A.; Lieber, C. M.; Verdine, G. L. *Chem. Biol.* **2002,** 9, 345-350.

24.   Fromme, J. C.; Bruner, S. D.; Verdine, G. L. *Nat. Structural Biol* **2003,** 10, 204-211.

25.   Loft, S.; Svoboda, P.; Kasai, H.; Tjoenneland, A.; Vogel, U.; Moeller, P.; Overvad, K.; Raaschou-Nielsen, O. *Carcinogenesis* **2006,** 27, 1245-1250.

26.   Shin, C. S.; Moon, B. S.; Park, K. S.; Kim, S. Y.; Park, S. J.; Chung, M. H.; Lee, H. K. *Diabetes Care* **2001,** 24, 733-737.

27.   Wang, J.; Xiong, S.; Xie, C.; Markesbery, W. R.; Lovell, M. A. *J. Neurochem.* **2005,** 93, 953-962.

28.   Yanagawa, H.; Ogawa, Y.; Ueno, M. *J. Biol. Chem.* **1992,** 267, 13320-6.

29.   Duarte, V.; Muller, J. G.; Burrows, C. J. *Nucleic Acids Res.* **1999,** 27, 496-502.

30.   Henderson, P. T.; Delaney, J. C.; Gu, F.; Tannenbaum, S. R.; Essigmann, J. M.
       Biochemistry **2002,** 41, 914-921.

31.   Avkin, S.; Livneh, Z. *Mut. Res.* **2002,** 510, 81-90.

32.   Kamiya, H. *Nucleic Acids Res.* **2003,** 31, 517-531.

33.   Berlin, Y. A.; Burin, A. L.; Ratner, M. A. *J. Am. Chem. Soc.* **2001,** 123, 260-268.

34.   Boon, E. M.; Barton, J. K. *Curr. Opin. Struc. Biol.* **2002,** 12, 320-329.

35.   Giese, B. *Annu. Rev. Biochem.* **2002,** 71, 51-70.

36.   Jortner, J.; Bixon, M.; Langenbacher, T.; Michel-Beyerle, M. E. *Proc. Natl. Acad.
       Sci. USA* **1998,** 95, 12759-12765.

37.   Liu, C.-S.; Hernandez, R.; Schuster, G. B. *J. Am. Chem. Soc.* **2004,** 126, 2877-
       2884.

38.   Davis, W. B.; Naydenova, I.; Haselsberger, R.; Ogrodnik, A.; Giese, B.; Michel-
       Beyerle, M. E. *Angew. Chemie Int. Ed.* **2000,** 39, 3649-3652.

39.   Saito, I.; Nakamura, T.; Nakatani, K.; Yoshioka, Y.; Yamaguchi, K.; Sugiyama,
       H. *J. Am. Chem. Soc.* **1998,** 120, 12686-12687.

40.   Voityuk, A. A.; Jortner, J.; Bixon, M.; Rosch, N. *Chem. Phys. Lett.* **2000,** 324,
       430-434.

41.   Langmaier, J.; Samec, Z.; Samcova, E.; Hobza, P.; Reha, D. *J. Phys. Chem. B*
       2004, 108, 15896-15899.

42.   Neeley, W. L.; Essigmann, J. M. *Chem. Res. Toxicol.* **2006,** 19, 491-505.

43.   Henderson, P. T.; Jones, D.; Hampikian, G.; Kan, Y.; Schuster, G. B. *Proc. Natl.
       Acad. Sci. USA* **1999,** 96, 8353-8358.

44. Nunez, M.; Hall, D. B.; Barton, J. B. *Chem. Biol.* **1999,** 6, 85-97.

45. Giese, B. *Acc. Chem. Res.* **2000,** 33, 631-636.

46. Marcus, R. A. *J. Chem. Phys.* **1956,** 24, 966-78.

47. Brauns, E. B.; Madaras, M. L.; Coleman, R. S.; Murphy, C. J.; Berg, M. A. *J. Am. Chem. Soc.* **1999,** 121, 11644-11649.

48. Gueron, M.; Leroy, J. L. *Nucleic Acids and Molecular Biology* **1992,** 6, 1-22.

49. Conwell, E. M.; Rakhmanova, S. V. *Proc. Natl. Acad. Sci. USA* **2000,** 97, 4556-4560.

50. Zheng, B.; Wu, J.; Sun, W.; Liu, C. *Chem. Phys. Lett.* **2006,** 425, 123-127.

51. Armitage, B.; Schuster, G. B. *Photochem. Photobiol.* **1997,** 66, 164-170.

52. Hall, D. B.; Holmlin, R. E.; Barton, J. K. *Nature* **1996,** 382, (6593), 731-735.

53. Senthilkumar, K.; Grozema, F. C.; Guerra, C. F.; Bickelhaupt, F. M.; Lewis, F. D.; Berlin, Y. A.; Ratner, M. A.; Siebbeles, L. D. A. *J. Am. Chem. Soc.* **2005,** 127, 14894-14903.

54. Gasper, S. M.; Schuster, G. B. *J. Am. Chem. Soc.* **1997,** 119, 12762-12771.

55. Armitage, B.; Koch, T.; Frydenlund, H.; Orum, H.; Schuster, G. B. *Nucleic Acids Res.* **1998,** 26, 715-720.

56. Hess, S.; Gotz, M.; Davis, W. B.; Michel-Beyerle, M. E. *J. Am. Chem. Soc.* **2001,** 123, 10046-10055.

57. Giese, B.; Biland, A. *Chem. Comm.* **2002**, 667-672.

58. Norman, D. G.; Grainger, R. J.; Uhrin, D.; Lilley, D. M. J. *Biochemistry* **2000,** 39, 6317-6324.

59.   Fahlman, R. P.; Sharma, R. D.; Sen, D. *J. Am. Chem. Soc.* **2002,** 124, 12477-12485.

60.   Ma, J. h.; Lin, W. z.; Wang, W. f.; Han, Z. h.; Yao, S. d.; Lin, N. y. *J. Photochem. Photobiol. B* **2000,** 57, 76-81.

61.   Burrows, C. J.; Muller, J. G. *Chem. Rev.* **1998,** 98, 1109-1151.

62.   Maxam, A. M.; Gilbert, W. *Proc. Natl. Acad. Sci. USA* **1977,** 74, (2), 560-4.

63.   Pereira de Jesus, K.; Serre, L.; Zelwer, C.; Castaing, B. *Nucleic Acids Res.* **2005,** 33, (18), 5936-5944.

64.   Fromme, J. C.; Verdine, G. L. *J. Biol. Chem.* **2003,** 278, (51), 51543-51548.

65.   Kim, Y.; Geiger, J. H.; Hahn, S.; Sigler, P. B. *Nature* **1993,** 365, 512-20.

66.   Rajski, S. R.; Barton, J. K. *Biochemistry* **2001,** 40, 5556-5564.

67.   Nakatani, K.; Dohno, C.; Ogawa, A.; Saito, I. *Chem. Biol.* **2002,** 9, 361-366.

68.   Newman, M.; Strzelecka, T.; Domer, L. F.; Schildkraut, I.; Aggarwal, A. K. *Science* **1995,** 269, 656-663.

69.   Rajski, S. R.; Kumar, S.; Roberts, R. J.; Barton, J. K. *J. Am. Chem. Soc.* **1999,** 121, 5615-5616.

70.   Kornberg, R. D.; Lorch, Y. *Cell* **1999,** 98, 285-294.

71.   Richmond, T. J.; Davey, C. A. *Nature* **2003,** 423, 145-150.

72.   Hayes, J. J.; Tullius, T. D.; Wolffe, A. P. *Proc. Natl. Acad. Sci. USA* **1990,** 87, 7405-7409.

73.   Nunez, M. E.; Noyes, K. T.; Barton, J. B. *Chem. Biol.* **2002,** 9, 403-415.

74.   Das, P.; Schuster, G. B. *Proc. Natl. Acad. Sci. USA* **2005**, 102, 14227-14231.

CHAPTER II

ATTENUATION OF DNA CHARGE TRANSPORT BY COMPACTION INTO A

NUCLEOSOME CORE PARTICLE

ABBREVIATIONS

AQ, anthraquinone; TG, TG-motif; bp, base pairs; CT, charge transport; EMSA, electrophoretic mobility shift assay; ExoIII, Exonuclease III; G, guanine; $G^{\bullet+}$, guanine radical cation; NCP, nucleosome core particle; $OH^{\bullet}$, hydroxyl radical; rNCP, reconstituted nucleosome core particle; Arg, arginine

SUMMARY

The Nucleosome Core Particle (NCP) is the fundamental building block of chromatin which compacts ~146 base pairs of DNA around a core histone protein octamer. The effects of NCP packaging on long-range DNA charge transport reactions have not been adequately assessed to date. Here we study DNA hole transport reactions in a 157 base pair DNA duplex (AQ-157TG) incorporating multiple repeats of the DNA TG-motif, a strong NCP positioning sequence, and a covalently attached Anthraquinone photooxidant. Following a thorough biophysical characterization of the structure of AQ-157TG NCPs by Exonuclease III and hydroxyl radical footprinting, we compared the dynamics of DNA charge transport in UV-irradiated free and NCP-incorporated AQ-157TG. Compaction into a NCP changes the charge transport dynamics in AQ-157TG drastically. Not only is the overall yield of oxidative lesions decreased in the NCPs, but the preferred sites of oxidative damage change as well. This NCP-dependent attenuation of DNA charge transport is attributed to DNA-protein interactions involving the folded histone core since removal of the histone tails did not perturb the charge transport dynamics in AQ-157TG NCPs.

INTRODUCTION

Genomic DNA is under constant oxidative stress arising from agents like endogenous and exogenous free radicals, and γ- and x-ray irradiation. This challenge leads to DNA damage ranging from oxidized nucleobase products to single and double strand breaks.[1] Understanding the origins of DNA oxidative damage is critical since increased levels of oxidative lesions have been implicated in the pathologies of adverse health conditions including cancer, atherosclerosis, and diabetes.[2-4] An analysis of the effects of oxidative stress on genomic DNA is complicated by the fact that DNA can act as an efficient carrier of excess charges. In other words, an excess electron or electron hole generated at a specific location in duplex DNA may not stay localized, but instead possess the ability to migrate long distances away from the initial damage site. Evidence for this electronic property of DNA comes primarily from in vitro experiments where the DNA nucleobases are either oxidized[5-8] or reduced[9, 10] by a variety of exogenous agents. When DNA is oxidized, the resulting hole usually will localize at guanine to form a guanine radical cation ($G^{\bullet+}$), since the oxidation potential of this nucleobase is lower than those of A, T, C, and the sugar phosphate backbone.[11] Once formed, a $G^{\bullet+}$ has several fates available to it. First, it can simply recombine with the removed electron to return the system back to ground state. Second, $G^{\bullet+}$ can react with agents such as water to yield mutagenic guanine oxidative lesions.[12] Third, the initially formed $G^{\bullet+}$ can undergo a hole hop, or a nearly isoenergetic electron exchange reaction with a nearby guanine,[13, 14] moving the electron deficient site over 200 Å away from the site of initial oxidation.[15, 16]

While long-range DNA hole transport has been definitively established in vitro, the importance of this process in the eukaryotic nucleus has not. The primary reason for

40

the lack of understanding of DNA hole migration in vivo arises from an incomplete picture of how chromatin structure impacts these reactions. The majority of the previous studies on DNA hole transport dynamics have been carried out using DNA substrates which were present naked in solution, and therefore free of any bound proteins. The reversible formation of a compact DNA-protein complex known as chromatin is a critical structural feature of the eukaryotic nucleus since 2 meters of genomic DNA must fit into a ~10 μm diameter human cell nucleus. The initial level of DNA compaction in chromatin is carried out by the formation of a Nucleosome Core Particle (NCP). NCPs have been well characterized structurally through X-ray crystallography[17] and various additional thermodynamic and biophysical methodologies[18, 19]. A NCP consists of 146-147 bp of DNA wrapped 1.75 turns around an octamer built from two copies each of histones H2A, H2B, H3, and H4.[17-19] Between each NCP on a chromosome lies a linker region of DNA between 20 and 100 bp in length. The structure of the DNA packaged into a NCP is not the same as the Watson-Crick, B-form DNA found predominantly in naked DNA under intercellular conditions.[17-19] For example, the DNA at the entrance and exit of the nucleosome is overwound and has a pitch of 10.0 bp/turn instead of the B-form 10.5 bp/turn. To help alleviate the strain placed upon the duplex in the overwound regions, the DNA near the pseudo-symmetry axis of the NCP is underwound and possesses a pitch of 10.7 bp/turn.

The effects of the changes in the DNA structure and/or local DNA environment associated with NCP formation on DNA hole transport reactions are of primary concern in the studies reported here. In the previous literature, the binding of proteins to DNA has been shown to have a variety of effects on the dynamics of DNA charge transport.

Rajski et al. studied the effects of three different DNA binding proteins—restriction endonuclease *PvuII*, transcription factor ANTP, and TATA-box binding protein (TBP)—on hole transport dynamics in DNA duplexes modified by a Rh-metallorganic photooxidant.[20] Binding of *PvuII* and ANTP increased hole transport, whereas the binding of TBP decreased hole transport through the TBP-binding site. The authors attributed the different effects of these proteins to the extent of base stack structural perturbation in the DNA-protein complex. Consistent with their hypothesis that changes in DNA base stacking are responsible for the observed hole transport dynamics in DNA-protein complexes, Nunez et al. recently found that hole transport dynamics in a reconstituted NCP were nearly identical to those in the same DNA free in solution.[21] This picture of base pair continuity being the primary factor controlling DNA hole transport in protein-DNA complexes is challenged by a report from Nakatani et al[22]. Here hole transport between two guanine oxidation sites flanking a *BamHI* binding site was greatly reduced by DNA-protein interactions, even though previous X-ray crystal structures indicated that *BamHI* does not perturb the integrity of the DNA base pair stacking upon binding.[23] The authors attributed the attenuation of hole transport in the DNA-*BamHI* complex to the presence of a charged arginine residue making hydrogen bonding interactions with one of the guanine bases in the DNA major groove. Taken together, these studies indicate that an understanding of the effects of DNA-protein interactions on the dynamics of DNA hole transport is still in its infancy.

Even though Nunez et al. have studied DNA hole transport in the setting of a NCP, questions surrounding the effects of nucleosome formation on these long-range hole transport reactions are far from settled. For starters, NCPs form on a wide variety of

genomic DNA sequences. This fact is reinforced by the observation that in the published X-ray structures, electrostatic interactions are largely responsible for the stabilization of NCPs since there are no specific hydrogen bonds between the histone amino acid residues and the DNA nucleobases.[17] Even though the histone octamer does not utilize a direct readout of DNA sequences, the thermodynamic stability of a NCP is directly related to the sequence of the bound DNA.[18, 19, 24, 25] With this large in vivo distribution of NCP thermodynamic stability in mind, we are initiating a strategic assessment of the hole transport dynamics in NCPs of varying DNA sequence in order to assess global trends. Our first efforts towards this endeavor are communicated in this paper for an artificial DNA sequence known as the TG-motif,[26, 27] a sequence which leads to the formation of structurally well-defined NCPs. For the selective initiation of oxidative damage, we utilize DNA duplexes covalently-modified by an Anthraquinone photooxidant (Figure 2.1A) at one 5'-terminus. We show in this communication that NCP formation does in fact lead to drastic changes in both i) the overall yield of DNA oxidative lesions and ii) the observed distribution of oxidative damage sites in TG-motif NCPs. The results of this study are expected to contribute to our understanding of how DNA-protein interactions impact the dynamics of DNA-mediated charge transport reactions, as well as the impact of oxidative stress-induced DNA charge migration on global genomic integrity in eukaryotes.

MATERIALS AND METHODS

Reagents and Chemicals

Monobasic sodium phosphate, phenylmethylsulfonic fluoride (PMSF), thiourea, and

43

sodium L-ascorbate were purchased from Sigma-Aldrich. Urea, phenol/chloroform, and
H_2O_2 were obtained from Fisher Scientific. Stock 40% acrylamide solutions were
supplied by BioRad. T4 Polynucleotide Kinase (PNK), T4 DNA Ligase (T4 Lig), and
Exonuclease III (ExoIII) were purchased from New England Biolabs. [γ-^{32}P]ATP (5
mCi/mL, 3000 Ci/mmol specific activity) was supplied by Perkin Elmer. 3500 MWCO
Mini Slide-a-Lyzer Dialysis units were from Pierce. All phenol/chloroform based
separations of DNA and protein were performed using 0.5 mL Eppendorf Gel Phase Lock
tubes. G-50 ProbeQuant micro spin columns were purchased from Amersham
Biosciences.

Construction of DNA Duplex AQ-TG157

AQ-157TG, a 157-bp DNA duplex covalently modified by AQ at one 5'-terminus and
built around the strong NCP positioning TG DNA motif, was constructed in the following
modular fashion. Six oligonucleotides **AQ-A** AQ-d(AAA TGC CGG TGA GGT CGG
TGT TAG TGC CTG TAA CTC GGT GTT AGA GCC TGT AAC TCG G), **B** d(GTT
ACA GGC ACT AAC ACC GAG TTA CAG GCA CTA ACA CCG ACC TCA CCG
GCA TTT), **C** d(TGT TAG AGC CTG TAA CAC TCT CAG CCT TTG GC), **D** d(GAG
TGC CAA AGG CTG AGA GTG TTA CAG GCT CTA ACA CCG A), **E** d(ACT CTC
GGT GTT AGA GCC TGT AAC TCG GTG TTA GAG CCT GTA ACT CGG TGT
TAG AGC CTG TAA CGA TA), and **F** d(TAT CGT TAC AGG CTC TAA CAC CGA
GTT ACA GGC TCT AAC ACC GAG TTA CAG GCT CTA ACA GCG A) were
synthesized by standard solid phase synthesis on an ABI Applied Biosystems 380B DNA
synthesizer. Strand **AQ-A** was modified at its 5'-terminus by an AQ-phosphoramidite

reagent generated using a previously reported synthetic scheme.[28] Oligonucleotides **B-F** were synthesized Trityl-On, and all six strands were individually deprotected by heating them for 16 hours at 55°C in concentrated ammonium hydroxide. After deprotection, the oligonucleotides were purified by HPLC on a Waters 2690 system equipped with a Waters 996 Photodiode Array Detector and a Nucleosil C18 RP column (Hichrom). Following purification, oligonucleotides **B-F** were lyophilized, de-tritylated by treatment with 80% acetic acid for 30 minutes, and ethanol precipitated. Strand **AQ-A** was lyophilized, resuspended in H_2O and ethanol precipitated. Oligonucleotide purity was ascertained using 20% PAGE electrophoresis, and the product yield determined by A_{260} measurements on a Cary 100 Bio spectrophotometer (Varian).

After purification, the 5'-termini of strands **B**, **C**, **D**, and **E** (2 nmol each) were phosphorylated by incubation with 20 units of PNK and 10 mM ATP at 37°C for 45-60 min. The three duplexes **AQ-AB**, **CD**, and **EF** were individually hybridized in a buffer composed of 100 mM NaCl, 10 mM Tris, and 1 mM EDTA. Briefly, equimolar amounts of complementary oligonucleotides were mixed and placed in a temperature controlled spectrophotometer (Cary Bio 100), the samples heated to 90°C over 10 minutes, and the mixtures cooled at a rate of 0.5°C / min to 10°C. After hybridization, each duplex was ethanol precipitated. Next, the full length AQ-157TG duplex was produced by a step-wise DNA ligation protocol. First, duplexes **CD** and **EF** were ligated together in a reaction mixture containing 120 U of T4 Lig, 10 mM ATP, and 2 μM total DNA incubated at 16°C overnight. After verification of successful ligation (≥ 50% product yield) by electrophoresis on a 3% agarose gel, an equal concentration of duplex **AQ-AB** was added in situ, the ligation mixture supplemented with additional T4 Lig, and the

reaction incubated overnight at 16°C. The desired 157-bp DNA product was purified by preparative (20 cm x 20 cm) 10% denaturing (7 M urea) PAGE, re-hybridized by the same protocol described previously for the individual duplexes, and precipitated by ethanol treatment. Following purification, the yield of AQ-157TG was calculated using A_{260} measurement. Before reconstitution, the 5'-terminus of strand **BDF** (counter to the AQ-labeled strand) was labeled with ^{32}P by incubation of AQ-157TG with 20 units of T4 polynucleotide kinase and 2 μL (20μCi) [γ-^{32}P]ATP. Labeled samples were then extracted with phenol/chloroform, the excess [γ-^{32}P]ATP removed using a G-50 ProbeQuant size exclusion column, and the DNA precipitated using ethanol.

Preparation of Reconstituted Nucleosome Core Particles

Chicken erythrocyte nucleosome core particles (NCPs) stripped of linker histones H1 and H5[29] were a gift from the laboratory of Dr. Michael J. Smerdon (Washington State University). The integrity of the core histone proteins was verified by 18% SDS-PAGE analysis on a routine basis. Reconstitution of the AQ-157TG DNA duplex onto NCPs was performed using the method of Moyer et al.[30] The ^{32}P-labeled duplex (~100 nM, ~100k cpm) was combined with NCPs (0.6 mg/mL) at a 1:50 molar ratio in 60 μL of a 1 M NaCl, 10 mM sodium phosphate buffer (pH 7.0). Salt exchange dialysis was performed in 3500 MWCO Mini Slide-a-Lyzer Dialysis units at 4°C. Immediately prior to dialysis at each salt concentration, PMSF was added to the dialysis buffer to 0.2 mM final concentration. Initial dialysis was against buffered 1M NaCl for 45 min., followed by buffered 600 mM NaCl for 60 min., buffered 300 mM NaCl for 60 min., and finally 10 mM sodium phosphate (pH = 7.0) for 60 min. Evaluation of the reconstitution

efficiency was performed by EMSA on 6% native acrylamide gels ran at 100 V and ~ 0 W. The gels were dried, exposed to a Phosphorscreen (Amersham Biosciences), and visualized on a 445 SI Phosphorimager (Molecular Dynamics). All gel analysis was performed using ImageQuant software (Molecular Dynamics).

Footprinting of reconstituted nucleosome core particles

The translational setting of AQ-157TG rNCPs was assessed by ExoIII digestion. Briefly, separate samples of reconstituted nucleosomes and free AQ-157TG were digested by 1U of ExoIII for 3 min at 37°C. The reaction was quenched by rapid phenol/chloroform extraction of the ExoIII from the mixture, followed by DNA ethanol precipitation. The DNA pellets were then resuspended in formamide loading buffer and run on an 8% (7 M Urea) sequencing gel at 60 W for 120 min. To examine the rotational positioning of the DNA on the reconstituted NCPs, hydroxyl radical (OH$^{\bullet}$) footprinting was employed.[31] Redox reactions between Fe(II)-EDTA (20 μM), H_2O_2 (0.3% v/v), and sodium L-ascorbate (1mM) were used to generate OH$^{\bullet}$ in situ. After 1 min. at room temperature for free AQ-157TG, or 10 min at room temperature for rNCPs, the reactions were quenched by the addition of EDTA (40 mM) and thiourea (7 mM). The DNA was then treated by phenol/chloroform extraction and ethanol precipitation was carried out in the presence of glycogen. The DNA was resuspended in formamide loading buffer and was then analyzed by application to a 7 M urea PAGE (6-8%) sequencing gel, followed by autoradiography.

UV-Irradiation and Assessment of DNA Charge Transport Reactions

Irradiation of free AQ-157TG (~100 nM) and rNCPs were separately performed

in a Luzchem photoreactor (Luzchem Research) with 6 UV-A lamps (~0.3 mW/cm^2 per

lamp) centered at 350 nm for 30-60 minutes at 25˚C. After irradiation, the AQ-157TG

duplex was dissociated from the core histones by heating the samples at 90˚C for 5 min.

The DNA was then immediately subjected to a phenol/chloroform extraction and ethanol

precipitation with 2 μL glycogen (20 mg/mL) as a carrier. Both irradiated and non-

irradiated DNA were treated with hot 10% piperidine (90˚C) for 30 minutes, followed by

lyophilization and two washes with 30 μL ddH$_2$O. The dried DNA pellets were

resuspended in formamide loading buffer and samples (~10k cpm) were loaded and ran

on 7 M urea, 8% acrylamide sequencing gels at 60 W constant power for 2 hours. The

gels were dried, exposed to a Phosphorscreen (Amersham Biosciences), and visualized

on a 445 SI Phosphorimager (Molecular Dynamics). All gel analysis was performed

using ImageQuant software (Molecular Dynamics).

RESULTS

Design and Construction of AQ-157TG DNA

N-alkyl-Anthraquinone-2-amide (AQ; Figure 2.1A) is a well characterized

photooxidant used in many previous studies to initiate DNA charge transport (CT)

reactions.[7, 32, 33] A reaction scheme for AQ-initiated DNA hole transport is shown in

Figure 2.1B. Briefly, irradiation of AQ at ~350 nm generates the lowest singlet excited

state of AQ (^{1}AQ*) which quickly undergoes intersystem crossing (ISC; Figure 2.1B) to

the lowest triplet state (^{3}AQ*).[7] ^{3}AQ* oxidizes a nearby G base, thus forming the AQ

radical anion (AQ$^{\bullet-}$) and guanine radical cation (G$^{\bullet+}$). To liberate the electron hole in the

DNA base pair stack, O_2 acts as a scavenger to remove the excess electron from $AQ^{\bullet-}$.[7] Once liberated, the hole is free to move between guanines in the DNA duplex. The interplay of hole hopping rates (k_{hop}) between guanine sites and site-dependent charge trapping rates by agents like water, O_2[34], and $O_2^{\bullet-}$ [35] (k_{trap}) leads to a final steady state distribution of piperidine-labile oxidized guanine products.

In order to study DNA CT reactions in NCPs possessing a well-defined structure, we chose to utilize DNA duplexes containing multiple repeats of the non-natural TG-motif NCP binding sequence d(TCGGTGTTAGAGCCTGTAAC).[27] The phasing of the alternating G/C and A/T rich blocks (underlined above) was designed to ensure that DNA duplexes built around the TG-motif will possess only one structural conformation upon reconstitution to form a NCP.[27] Our 157 bp synthetic oligonucleotide duplex, AQ-157TG (Figure 2.1C), incorporates a total of six TG motifs. The AQ photooxidant was covalently attached at one 5' end of the duplex, while the other 5'-end was labeled by ^{32}P for the quantitation of DNA oxidative damage products using autoradiography. Previous NMR structures[36] of 5'-covalent DNA modifications, and molecular modeling of AQ-DNA complexes[28], lead to the expectation that in an aqueous environment the AQ photooxidant will preferentially end-cap, or stack onto the base pairs at the end of the DNA duplex. However, we initially had uncertainties about whether the AQ would end-cap onto the DNA duplex in a reconstituted NCP (rNCP), as intended, or instead associate with hydrophobic regions on the core histone proteins. We therefore designed AQ-157TG such that the AQ would be placed at the end of 10 bp of linker DNA, and thus one full duplex turn away from the expected entrance of a rNCP. Additionally, the sequence d(AAATGCC) was placed proximal to the AQ in order to ensure that DNA

oxidative damage yields would not be limited by charge injection efficiency in these studies.[37]

The production of AQ-157TG utilized a modular system involving the solid phase synthesis of six oligonucleotides, labeled **AQ-A** through **F**, through standard phosphoramidite chemistry. Following reverse phase purification by HPLC, oligonucleotides **B**, **C**, **D**, and **E** were phosphorylated at their 5'-termini. Duplexes **AQ-AB**, **CD**, and **EF** were individually hybridized, then ligated together in a stepwise, one-pot ligation reaction. The results of a typical multistep ligation are shown in Figure 2.2A. AQ-157TG was purified from the ligation reaction by electrophoresis on a 10% denaturing PAGE gel. The AQ-157TG single strands were then extracted from the appropriate acrylamide fragments, rehybridized, and the yield of AQ-157TG calculated from A_{260} measurements. This methodology does not produce high yields of full length AQ-157TG (< 10%); however it does result in a very pure (>95%) single parent band when labeled with ^{32}P and electrophoresed on a DNA sequencing gel. In particular, we note that there are little to no extra non-ligated DNA fragments present in any of the experiments reported here.

Reconstitution of AQ-157TG Nucleosome Core Particles and Footprinting

The incorporation of AQ-157TG into nucleosome core particles (NCPs) was carried out by process known as reconstitution.[19] NCP reconstitution is initiated by mixing, in the presence of 1 M NaCl, native NCPs with DNA that forms thermodynamically stable NCPs. The high salt concentration will disrupt the electrostatic interactions between the negatively charged genomic DNA and the basic histones.

Lowering the ionic strength of the solution by stepwise dialysis leads to the formation of NCPs, only now the exogenous DNA duplex out-competes some of the endogenous DNA to yield reconstituted nucleosome core particles (rNCPs).[29] Reconstitution was initiated by mixing a ~ 1:50 molar ratio of ^{32}P labeled either NH$_2$-157TG or AQ-157TG and chicken erythrocyte NCPs in a 1 M NaCl, 10 mM NaP$_i$, pH 7.0 buffer, followed by slow dialysis down to 10 mM NaP$_i$. The reconstitution products were analyzed by an electrophoretic mobility shift assay (EMSA) (Figure 2.2B). This EMSA shows that; 1) from autoradiography, the reconstitution efficiency of AQ-157TG was >95%, 2) AQ-157TG reconstitutes onto NCPs to form predominantly mononucleosomes since there is only i) one slow migrating band and ii) no evidence of higher order DNA-protein aggregates in the gel (Figure 2.2B), and 3) the presence of the 5'-AQ label does not perturb the reconstitution of AQ-157TG onto NCPs since this EMSA is identical to an EMSA of NCPs formed via the reconstitution of a 157TG duplex with a 5'-aminopropyl linker in place of the AQ chromophore (data not shown).

In order to characterize the conformational structure of the AQ-157TG reconstituted NCPs (rNCPs), DNA footprinting experiments were performed. These experiments allow a full characterization of both the rotational and the translational settings of a DNA duplex on the surface of a NCP. To investigate the perturbation of DNA CT by NCP formation, ideally a homogeneous mixture of rNCPs containing only one DNA rotational and one DNA translational setting would be used. When a NCP possesses a single translational setting, there is no sliding of the DNA on the protein surface and there are defined nucleobases at the entrance and exit to the core particle.[38] Exonuclease III (ExoIII) is a 3'-5' DNA exonuclease whose activity is retarded by the

presence of DNA-protein contacts.[39] Hence, a limited ExoIII digestion can determine if

there is a single, well-defined, nucleobase at the entrance of a rNCP. Figure 2.3A shows

the results of ExoIII digestion of both free and rNCP AQ-157TG DNA. Free AQ-157TG

is easily digested along its entire length by ExoIII, with some regions of preferred cutting

apparent. After reconstitution onto NCPs, AQ-157TG is vigorously digested in the ~10

bp region next to the AQ photooxidant, whereas the rest of the DNA is highly protected

from ExoIII cutting. These experiments indicate that (i) the extended 10 base pair

overhang with the AQ cap is outside of the NCP, (ii) AQ does not interact with the

histone proteins since we observe ExoIII activity on the surrounding nucleobases, and

(iii) there appears to be only one major translational setting of AQ-157TG on the

nucleosome surface since only the ~10 bp of DNA proximal to the AQ-label are digested.

The term rotational setting refers to how the minor groove of the DNA duplex at

each individual base pair is oriented with respect to the histone octamer.[31] On a rNCP

with only one rotational setting, there are specific regions where the minor groove rotates

inward to face the histone protein core interspersed with regions where the minor groove

rotates outward towards solution. Hydroxyl radical (OH$^{\bullet}$) footprinting is a very sensitive

method to probe the DNA rotational setting in rNCPs.[31] Generation of OH$^{\bullet}$ in the

presence of DNA results in the induction of DNA strand breaks in regions where the

phosphodiester backbone, and hence DNA minor groove, is exposed to solvent. The

results of OH$^{\bullet}$ footprinting experiments on free and rNCP AQ-157TG are shown in

Figure 2.3B. When free in solution, there is nearly equal intensity of strand breaks at

every base as ascertained by autoradiography (Figure 2.3C). Conversely, AQ-157TG

rNCPs show the expected periodical phasing of damaged/protected regions associated with a single DNA rotational setting (Figure 2.3C).

Taken together, the footprinting experiments and EMSAs indicate that there is one predominant structure of AQ-157TG in an rNCP and that any measurements of DNA CT come from a nearly homogenous source.

DNA Charge Transport in free AQ-157TG and rNCPs

Irradiation of both free and rNCP AQ-157TG was achieved by placing the samples in the rotating carrousel of a Luzchem photoreactor. The photoreactor was equipped with six UV-A lamps whose emission was centered at 350 nm and cutoff at 300 nm in order to selectively irradiate the AQ-photooxidant but not the DNA nucleobases or aromatic amino acid side chains of the histones. After irradiation at room temperature, the oxidative lesions arising from $G^{\bullet+}$ trapping reactions were treated with hot piperidine and the ensuing strand cleavage products visualized by autoradiography of a 8% PAGE/ 7 M Urea DNA sequencing gel. Separate time courses for both free and rNCP AQ-157TG DNA were conducted to ensure that single hit conditions, as defined by the relative ratios of the oxidized guanine nucleobases remaining unchanged, were fulfilled in both samples (data not shown).

In the AQ-157TG sequence chosen for study, there are three guanine-containing steps in the first 28 bp of the 5'-^{32}P labeled counterstrand (**BDF**). In order of increasing distance from AQ, these sites are labeled GG_1, G_1, and GG_2 (Figure 2.1C). In free AQ-157TG DNA CT is observed over 95 Å (28 bp) to the 5'-Guanine of the GG_2 step (Figure 2.4A, Lane 5). The yield of CT to the next single G in strand **BDF** (G_2; 34 bp, 116Å

from AQ) is not significantly above background. In addition, Figure 2.4A also displays the results using non-irradiated, piperidine treated AQ-157TG (Lane 4) indicating i) the minimal background inherent in these experiments, and ii) the lack of piperidine-labile lesions in the absence of AQ photooxidation. Using autoradiography, the ratios of the strand break yields at each guanine step (GG_1/G_1, G_1/GG_2, and GG_1/GG_2) in free AQ-157TG were determined (Table 1, Figure 2.4B). These ratios give an approximate steady state snapshot of the guanine damage distribution resulting from the interplay between k_{hop} and k_{trap} (Figure 2.1B). Additionally, the overall yield of guanine oxidative damage (Y_{dam}, Table 1) was obtained by calculating the ratio of total piperidine-sensitive guanine oxidative damage to the intensity of all bands in that lane.

The rNCP samples were irradiated and treated with piperidine in exactly the same manner as the free AQ-157TG. A typical DNA sequencing gel resulting from these reactions is shown in Figure 2.4A. Once again, the non-irradiated samples (Lane 6) show the lack of piperidine-labile nucleobase oxidation products in the absence of photoinduced charge injection. A minor shift of the piperidine cleavage bands and the 157 bp parent band in the rNCP samples was repeatedly observed on the DNA sequencing gels. This shift was attributed to a rNCP-related gel artifact, and it does not interfere with the analysis of the oxidative damage product ratios or Y_{dam}. A cursory examination of the sequencing gel in Figure 2.4A indicates that while the damage spectrum in free AQ-157TG (Lane 5) and rNCPs (Lane 7) is similar, there is an attenuation of the total yield of piperidine-labile guanine oxidation products in the rNCPs. This qualitative observation was quantified by autoradiography and it was found that the value of Y_{dam} decreases by ~60% in the rNCPs (Table 1).

Not only is the overall yield of oxidative damage decreased in a nucleosome core particle, but the distribution of oxidative damage is also perturbed by packaging DNA into chromatin structures (Table 1, Figure 2.4B). The site damage ratio GG_1/G_1 does not differ significantly between the free AQ-157TG and the rNCPs, however significant increases in the ratios G_1/GG_2 (46% increase), and GG_1/GG_2 (59% increase) were reproducibly observed in the rNCPs.

As a control reaction, we mixed free AQ-157TG with chicken erythrocyte NCPs at a 1:50 molar ratio in a 10 mM sodium phosphate buffer without performing a reconstitution and performed similar analyses as those carried out on the AQ-157TG rNCPs. An EMSA showed that incubation of AQ-157TG and native NCPs at low salt results in the formation of aggregates (Figure 2.5) of uncharacterized structure. Irradiation of these aggregates followed by piperidine treatment resulted in a 30% reduction in Y_{dam} as compared to free AQ-157TG, but no changes in the damage ratios G_1/GG_2 and GG_1/GG_2 (data not shown).

Effect of histone tail removal on DNA Charge Transport in rNCPs

From X-ray crystallography and biophysical investigations, it is known that there are two distinct features of the core histones in a NCP. The first are the α-helical regions which form the histone surface which DNA wraps around.[17] The second are the largely unstructured histone N-terminal and C-terminal tails which contain the majority of sites involved in generating the "histone code" arising from posttranslational modifications such as acetylation and methylation.[40] The histone tails are basic in nature, but do not make contact with the DNA wrapped around the NCP. However, there are reports

indicating that the histone tails do make contact with the DNA linker regions between two NCPs in chromatin, regions similar to the AQ-labeled 10 bp overhang.[41] Therefore, we investigated if the histone tails in the AQ-157TG rNCPs are responsible for the observed changes in the DNA CT dynamics by removing the N-terminal tails of native NCPs via a limited trypsin digestion prior to reconstitution (Figure 2.6A). OH[•] footprinting verifed no change in the rotational setting in the tailless AQ-157TG rNCPs (Figures 2.6B and 2.6C). Irradiation of the tailless rNCPs yielded DNA CT results indistinguishable from those of the native rNCPs (Figure 2.4). We infer from this observation that the histone tails play no role in regulating the dynamics of CT in mononucleosomes.

DISCUSSION

Progress in the field of DNA CT has been strongly driven by the possibility of novel applications of this phenomenon in materials science and biosensors.[42] However, consideration of the consequences of efficient, long range DNA CT on fundamental processes in biology has lagged behind. In this paper we have chosen to interrogate the feasibility of intracellular DNA CT by modeling these reactions in a NCP, the fundamental building block of chromatin. The NCP presents a dramatically different DNA structure and environment compared to the typical Watson-Crick B-form structure.[43] For starters, in the regions of the NCP where we observe CT the DNA is overwound and possesses an average 10.0 bp/turn rise instead of the typical 10.5 bp/turn. Also, the accessibility of the DNA grooves is perturbed by NCP formation. For instance, there are alternating regions where the DNA backbone, and hence minor groove, is facing

away from the histone core surface and accessible from bulk solvent, interspersed with regions where the minor groove is rotated inwards towards the histone protein surface. The effects of these structural changes and solvent accessibility on DNA CT reactions are just starting to receive the attention they deserve.[44, 45]

The DNA CT reactions reported here come from protein-DNA complexes whose molecular structure is well-characterized. Neither the extra 10 bp of DNA beyond the 147 in direct contact with the histone octamer nor the covalently-tethered AQ photooxidant perturbed the ability of the TG-motif to generate stable rNCPs.[27] From the EMSAs, AQ-157TG associates with the core histones to form mononucleosomes in >95% yield, without the formation of higher order protein-DNA aggregates. The OH$^\bullet$ experiments indicate that AQ-157TG possesses only one rotational setting on the surface of a NCP. Structurally, this implies that there are specific contact points between the DNA backbone and the core histone proteins which do not vary from NCP to NCP. The ExoIII footprinting reactions show that AQ-157TG has only one translational setting in a NCP. This means that as counted from the 5'-AQ label, base pair 11 always resides near the entrance to the NCP, and there is no evidence for sliding of the DNA along the protein surface. In addition, the AQ-label and the proximal ~10 bp of the duplex are out in solution and not associated with the histone octamer.

A comparison of the oxidative damage yields and distributions between AQ-157TG free and in rNCPs shows that there are several significant effects of chromatin packaging on DNA CT. The first effect is an overall decrease in piperidine-labile guanine oxidation products in the rNCPs when both free and rNCP samples are irradiated and subsequently treated under similar conditions. The decrease in Y_{dam} in the rNCPs

(Table 1) arises solely from interactions between AQ-157TG and the folded histone core since the removal of the histone tails by trypsin digestion had no effect on the rNCP CT reactions. From the reaction scheme illustrated in Figure 1B we can propose and discuss three hypotheses which could account for the observed attenuation of oxidative damage in the rNCPs. Hypothesis 1: the yield of charge injection into the NCP is decreased because AQ preferentially associates with the histone proteins. This hypothesis can be ruled out because i) full activity of both ExoIII and OH$^\bullet$ in the DNA proximal to AQ means AQ is not associating with the folded histone core, and ii) similar CT dynamics in both the native and tailless AQ-157TG rNCPs implies that AQ is not associating with the histone tails. Hypothesis 2: charge liberation is inefficient because O$_2$ is restricted from oxidizing AQ$^{\bullet-}$. We reject this hypothesis because the DNA near the AQ is accessible to OH$^\bullet$ generated in solution, and it is difficult to envision a scenario where OH$^\bullet$ and O$_2$ accessibility would differ so dramatically. Hypothesis 3: the rates of charge trapping at G$^{\bullet+}$ to form piperidine-labile lesions (k$_{trap}$) and/or the rates of hole transport between neighboring guanines (k$_{hop}$) are different between the rNCP and free DNA environments. The perturbation of either k$_{trap}$ or k$_{hop}$ by the formation of a rNCP is plausible for two reasons. First, k$_{hop}$ may decrease because the DNA in the entrance to the nucleosome is overwound, and thus the bases are stacked closer together and have a slightly larger helical twist angle as compared to B-form DNA. From quantum chemical calculations,[46, 47] changes in either of these DNA structural features can perturb the relative energetics of the GG and G oxidation sites in AQ-157TG. According to Marcus theory, these changes in energetics could lead directly to changes in k$_{hop}$.[48] Additionally, the change in the energetics of G$^{\bullet+}$ could also perturb k$_{trap}$.[49] A second possibility would be changes in k$_{trap}$

58

in the rNCPs arising from DNA-protein contacts restricting the accessibility of trapping reagents to $G^{\bullet+}$.

With just the Y_{dam} values, we would be unable to ascertain whether the changes in structure or solvent accessibility were responsible for the changes in CT dynamics in the rNCPs. However, the differences in the site-specific relative yields of piperidine-labile damage in AQ-157TG rNCPs allow us to propose a clearer picture of how DNA packaging perturbs DNA CT in AQ-157TG. In the non-AQ counterstrand of AQ-157TG (**BDF**), the three sites of guanine oxidation are labeled GG_1 (7 bp from AQ), G_1 (16 bp from AQ), and GG_2 (28 bp from AQ) (Figure 2.1C). While the damage ratio GG_1/G_1 is insensitive to DNA compaction, there are significant increases in the ratios GG_1/GG_2 and G_1/GG_2 when AQ-157TG is incorporated into a NCP (Table 2.1, Figure 2.4B). These results imply that there might be something specific occurring to GG_2 in the rNCP which changes the relative k_{hop} and/or k_{trap} values associated with this site, but not sites GG_1 or G_1. Coupling together the ExoIII and $OH^{\bullet}$ footprinting data in this paper with the previously reported high resolution crystal structure of a core particle,[17] we can map out the structural environment of GG_1, G_1, and GG_2 in AQ-157TG rNCPs (Figure 2.7). First GG_1 is located in a DNA region resembling naked DNA since it does not associate with the histone proteins in the rNCPs. While both G_1 and GG_2 lie within the DNA region compacted into the NCP structure, both oxidation sites are located in regions where the DNA major groove is rotated out towards bulk solvent (Figure 2.7B). Since the solvent accessibility of G_1 and GG_2 appear to be so similar, we contend that changes in k_{trap} due to nucleobase accessibility plays a relatively minor role in the differences in the site damage yields observed between free and rNCP AQ-157TG.

There is a specific DNA-protein interaction in the AQ-157TG rNCPs which could be a possible explanation for the decrease in CT to site GG_2. In NCP crystal structures, the histone H2A Arg77 guanidinium side chain is inserted into the DNA minor groove and causes a local kink in the DNA structure by making hydrogen bonds with phosphate groups from the base pairs 16 and 19 nucleotides away from the NCP entrance.[17] Mapping AQ-157TG onto the NCP crystal structure shows that GG_2 lays dead center of this region, occupying base pairs 17 and 18 from the entrance of the NCP. This local structural change in the DNA near GG_2 could perturb the energetics of this oxidation site and thus perturb either k_{hop} or k_{trap}. While the charge transfer attenuation here is not as dramatic as the Arg-induced diminution of DNA CT in the BamHI experiments of Saito et al.,[22] it suggests that protein-DNA interactions can play subtle, but significant roles in controlling the observed distribution of DNA oxidative damage in protein-DNA complexes. Clearly, additional experimental and theoretical research is needed to address these structural effects further.

There is only one other report of photoinduced DNA CT reactions in the setting of a nucleosome core particle.[21] In contrast to the results obtained here, Nunez et al. found that there was little to no difference in DNA CT dynamics in a rNCP vs. naked DNA. There are several critical differences between these two studies which should be noted. First, the photooxidant used in each experiment is different in nature. Nunez et al. utilized an intercalating Rh-photoinjection system, whereas we have used the smaller end-capping AQ. We note that the absence of reported DNA footprinting experiments on the Rh-labeled rNCPs raises the possibility that their large organometallic photooxidant may have led to changes in rNCP structure, e.g. changes related to DNA aggregation

phenomena known to arise from Rh-labeled DNA.[32, 50] A second difference is that the DNA sequences used in both studies are not the same. The prior report utilized the palindromic DNA sequence from the crystal structures of Luger et al.[51] whereas we have used DNA duplexes built around the TG motif. It may be that the differences between their studies and ours are due to differences in the thermodynamic stability and DNA rotational and/or translational freedom inherent in the two different DNA sequences utilized. If true, this would imply that the effects of NCP formation on DNA CT may vary between different genomic regions based upon the thermodynamic stability of the NCPs present. We are currently investigating this hypothesis by performing DNA CT studies on rNCPs formed from DNA sequences of varying thermodynamic stability and sequence. We also note that our observation of decreased DNA damage in both the AQ-157TG-NCP aggregates and the AQ-157TG rNCPs is similar to the results in a recent report by Das and Schuster[52] on DNA CT reactions in DNA-spermidine condensates. The similarities between these two studies indicates that one of the constant effects of in vivo DNA packaging, in all of its guises, may be to decrease DNA oxidative damage arising from long-range CT reactions.

The observation that the nucleosome core particle can attenuate DNA CT is important from a biological standpoint because it indicates that chromatin may act as a protective barrier against long-range charge migration in genomic DNA sequences. In addition, it implies that oxidative damage may not occur randomly in genomic DNA during times of oxidative stress, but that it might arise from preferential trapping at guanines located in inter-nucleosomal linker regions and near the entrance to the nucleosome.[53] This scenario would have important implications for DNA repair

processes like Base Excision Repair (BER) which must find and repair nucleobase-derived oxidative lesions buried in the vast sea of chromatin in the eukaryotic nucleus. If oxidative damage occurs preferentially in the DNA linker regions, these sites may be easily repaired since they only make contact with the relatively unstructured tail regions of the core histones.[41] Also, oxidative lesions in the first turns of the NCP may be easily repaired as well. Recent FRET measurements on reconstituted NCPs have shown that there is a periodic unwinding of the first couple of turns of DNA near the entrance of a nucleosome.[53, 54] This limited dissociation of the DNA-histone complex may be adequate to allow repair proteins access to any damage sites which are present in the entrance region of the nucleosome. Contrast these scenarios to the case of oxidative damage in the DNA more tightly associated with the histone octamer. Recent experiments by Beard et al.[55] on the efficiency of the removal of uracil residues in nucleosomal DNA by the BER repair protein Uracil deglycosylase have shown a 10 fold decrease in repair efficiency when a uracil is packaged into a rNCP. Therefore, keeping charge migration from leading to oxidative lesions deep in a nucleosome core particle might be advantageous to the cell, since BER repair processes appear to be hindered by nucleosome packaging.

In conclusion, we have found significant differences in the dynamics of DNA-mediated hole transport in the presence and absence of packaging into a nucleosome core particle. The NCPs utilized in this work are structurally well-characterized and this has allowed us to strongly correlate many of the changes in the guanine oxidative damage yields in the rNCP with the observed changes in DNA structure and environment arising from interaction with the core histone proteins. CT attenuation arises solely from interactions between the DNA and the folded core of the histone octamer since removal

of the histone tails has no effect on DNA CT reactions in rNCPs. Clearly, future

experimental and theoretical work will need to focus upon the origin of these changes in

DNA hole transport dynamics, as well as focus upon the effects of higher order

chromatin structure, such as the formation of the 30 nm fiber, on intracellular DNA hole

transport reactions.

Table 2.1

DNA Sample	Y_{dam}	GG_1/G_1	G_1/GG_2	GG_1/GG_2
Free AQ-157TG	0.64	2.6	1.2	3.2
AQ-157TG rNCP	0.21	2.6	2.0	5.2

Table 2.1: Quantitative values for the site damage distribution ratios GG_1/G_1, G_1/GG_2, and GG_1/GG_2 for free AQ157-TG and rNCPs. Y_{dam} values for AQ157-TG and the AQ-157TG rNCPs were determined by normalizing for total damage in a single lane, i.e., Y_{dam}=1-(parent band/total lane counts). All values are averages over five independent experiments.

Figure 2.1
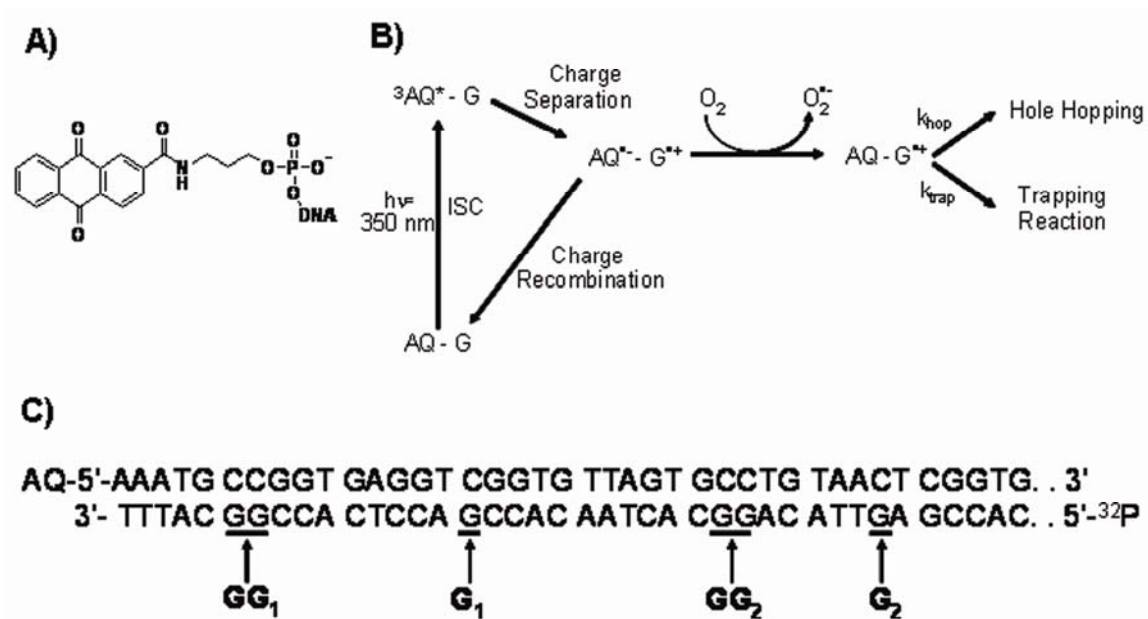
Figure 2.1: A) Chemical structure of the AQ Photooxidant. **B)** Reaction mechanism of photoinduced DNA oxidation in AQ-labeled DNA. Details of each reaction step are provided in the Results Section. **C)** Sequence of the AQ-157TG duplex proximal to the AQ photooxidant. The full DNA sequence can be found in the Materials and Methods.

Figure 2.2
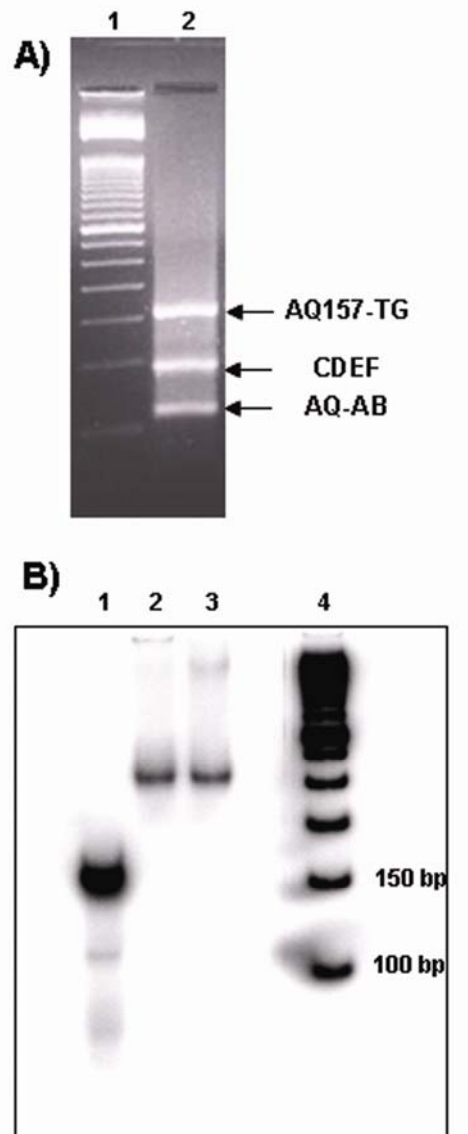
Figure 2.2: A) Ethidium-stained, 3% Agarose gel showing the results of a typical ligation reaction used to produce AQ-157TG. Lane 1) is a 50 bp DNA ladder, and Lane 2) contains the ligation mixture. Assignment of the bands in Lane 2) is indicated on the Figure. **B)** A native 6% acrylamide electrophoretic mobility shift assay (EMSA) showing the reconstitution efficiency of AQ-157TG. Lanes: 1) Free AQ-157TG, 2) and 3) separate rNCP preparations, and 4) 50 bp DNA ladder.

Figure 2.3
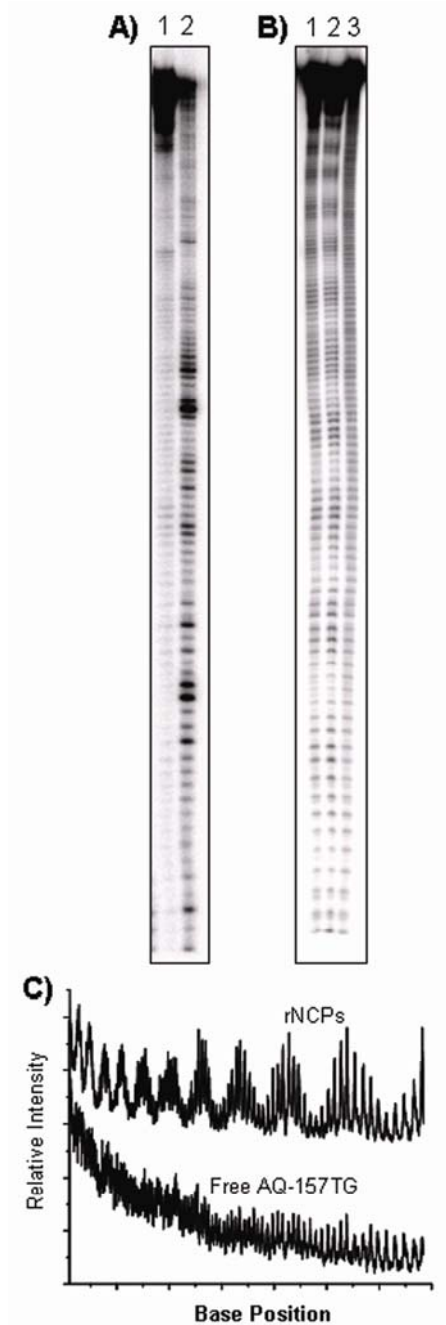
Figure 2.3: Structural characterization of AQ-157TG rNCPs. **A)** Exonuclease III footprinting of AQ-157TG rNCPs (lane 1) and free AQ-157TG (lane 2). The restriction of ExoIII activity to the ~10 bp proximal to AQ in the AQ-157TG rNCPs is evident. **B)** Autoradiogram of hydroxyl radical footprinting on AQ-157TG rNCPs (lanes 1 and 2) and free AQ-157TG (lane 3). **C)** Partial scan of the footprint in Part **B)** of both free AQ-157TG (bottom) and AQ-157TG rNCPs (top). The 10 bp periodic cutting in the rNCPs is apparent.

Figure 2.4

Figure 2.4: Visualization of DNA charge transport products in free AQ-157TG, rNCPs, and tailless rNCPs as a function of 60 minutes of UV-A irradiation and hot piperidine treatment. Lanes: 1) Maxam-Gilbert G ladder, 2) Maxam-Gilbert G+A ladder, 3) 10 bp DNA ladder, 4) free AQ-157TG, 5) free AQ-157TG, 6) AQ-157TG rNCPs, 7) AQ-157TG rNCPs, 8) tailless AQ-157TG rNCPs. **B)** Graphical representation of the damage ratios GG_1/G_1, G_1/GG_2, and GG_1/GG_2 from Table 1.

68
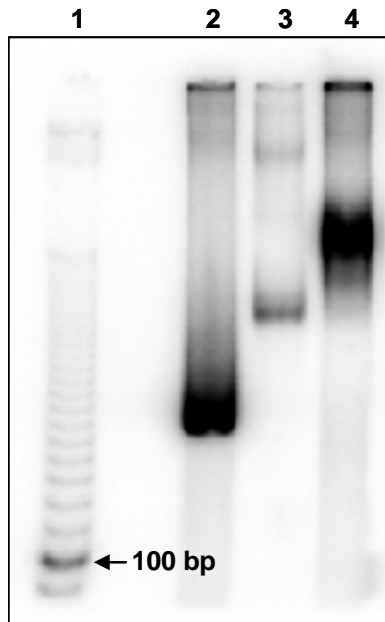
Figure 2.5

Figure 2.5: Analysis of non-reconstituted NCPs mixed with AQ-157TG duplex. Irradiation control experiments with free AQ-157TG with non-reconstituted NCPs showed a slight decrease in overall damage and damage distribution although not as significant when compared to rNCPs. However these results cannot be considered due to the fact that non-reconstituted NCPs and the AQ-157TG duplex form higher order aggregates upon incubation at room temperature for 60 min. Conversely, when AQ-157TG is reconstituted onto the NCPs, no similar higher order aggregates are formed. This EMSA shows the gel shifts resulting from AQ-157TG reconstituted NCPs versus non-reconstituted NCP mixtures at the same DNA and NCP concentrations used in the irradiation experiments. Lane 1: 10 bp ladder. Lane 2: Free AQ-157TG. Lane 3: reconstituted NCP. Lane 4: non-reconstituted NCP aggregate.

Figure 2.6
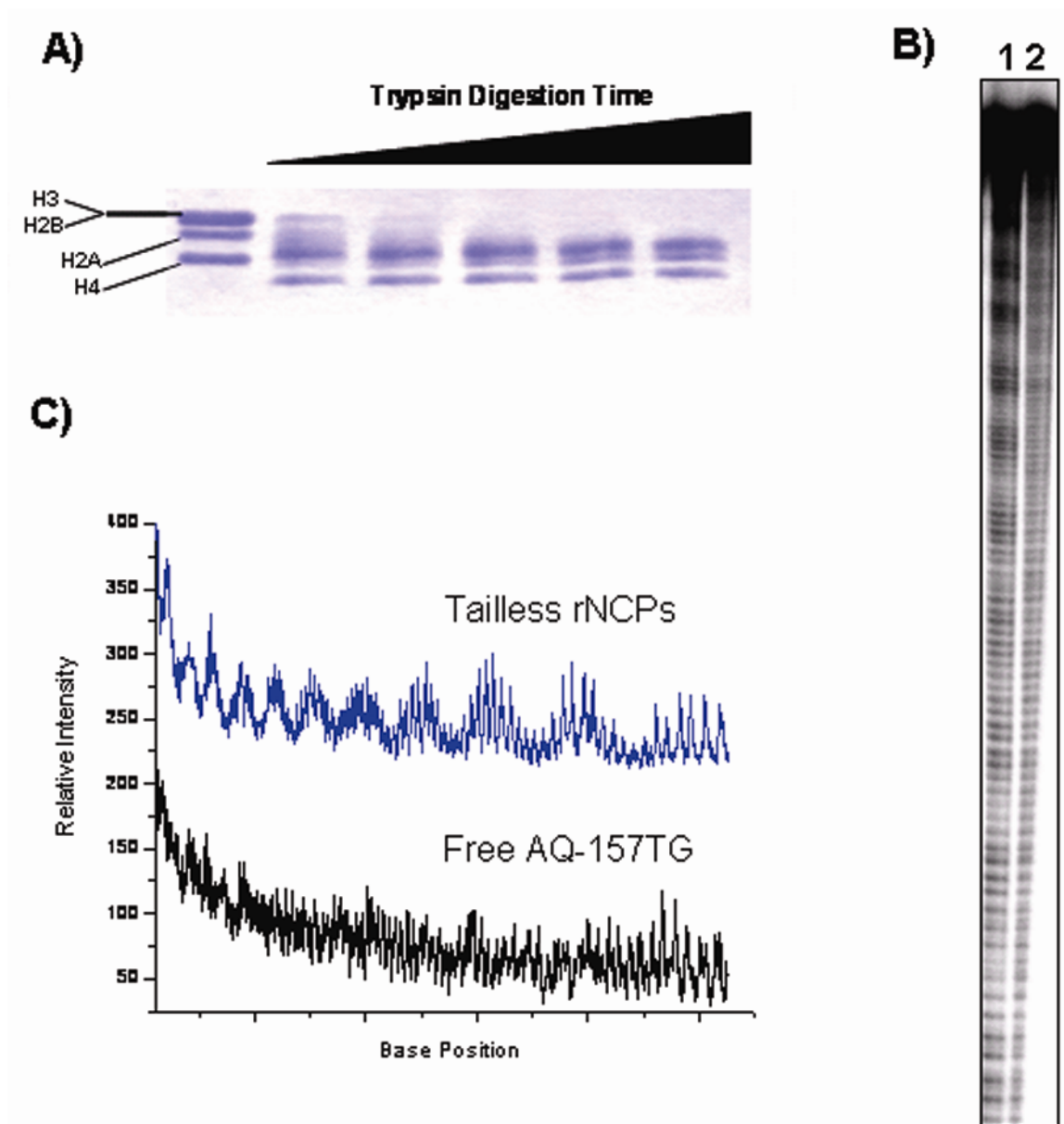
Figure 2.6: Structural analysis of limited trypsin digestion of AQ-157TG rNCPs. **A)** 18% SDS PAGE showing undigested histones (left lane) with increasing trypsin digestion time from left to right. **B)** Autoradiogram of hydroxyl radical footprinting on tailless AQ-157TG rNCPs (lanes 1) and free AQ-157TG (lane 2). **C)** Partial scan of the footprint in Part **B)** of both free AQ-157TG (bottom) and tailless AQ-157TG rNCPs (top). The 10 bp periodic cutting in the tailless rNCPs is apparent.
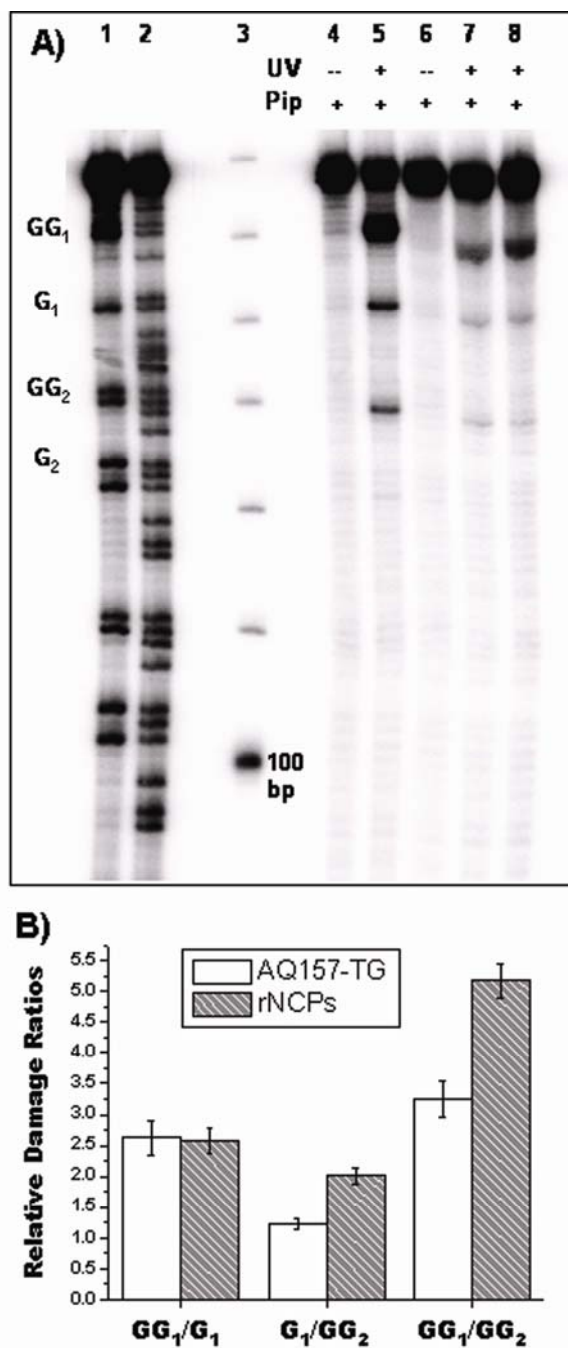
Figure 2.7
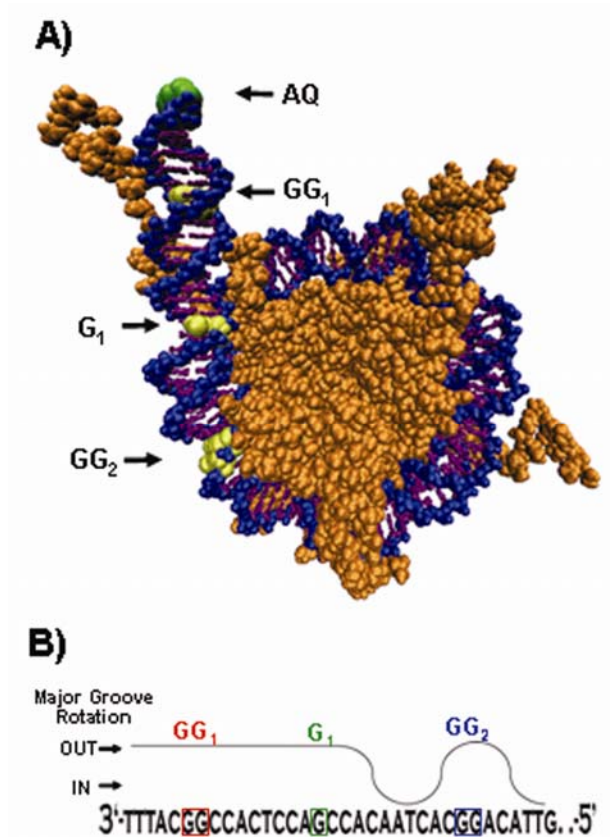
Figure 2.7: **A)** Crystal structure of the nucleosome core particle (Protein Data Bank Accession # 1KX5) with 147 base pairs of DNA (nucleobases = purple, sugar-phosphate backbone = blue) modified to include a 10 base pair extension and a covalently attached AQ (green) end-capped onto the DNA. The histone octamer is in orange. The relative positions of the guanine oxidation sites GG_1, G_1, and GG_2 of AQ-157TG are highlighted in yellow. **B)** Illustration of the rotational position of the DNA major groove in the AQ-157TG rNCPs as deduced from Part **A)**. The relative position of damage sites GG_1, G_1, and GG_2 with respect to the histone protein surface is indicated.

References:

1.   Halliwell, B.; Gutteridge, J. M. C., In *Free Radicals in Biology and Medicine*, 3rd ed.; Oxford University Press: Oxford, 1999; 86-95.

2.   Ames, B. N.; Shigenaga, M. K.; Hagen, T. M. *Proc. Natl. Acad. Sci. USA* **1993,** 90, 7915-7922.

3.   Feig, D. I.; Reid, T. M.; Loeb, L. A. *Cancer Res. Suppl.* **1994,** 54, 1890-1894.

4.   Olinski, R.; Gackowski, D.; Foksinski, M.; Rozalski, R.; Roszkowski, K.; Jaruga, P. *Free Radic. Biol. Med.* **2002,** 33, 192-200.

5.   Boon, E. M.; Barton, J. K. *Curr. Opin. Struc. Biol.* **2002,** 12, 320-329.

6.   Giese, B. *Annu. Rev. Biochem.* **2002,** 71, 51-70.

7.   Joy, A.; Schuster, G. B. *Chem. Comm.* **2005**, 2778-2784.

8.   Lewis, F. D.; Letsinger, R. L.; Wasielewski, M. R. *Acc. Chem. Res.* **2001,** 34, 159-170.

9.   Behrens, C.; Cichon, M. K.; Grolle, F.; Hennecke, U.; Carell, T. *Topics Curr. Chem.* **2004,** 236, (Long-Range Charge Transfer in DNA I), 187-204.

10.   Ito, T.; Rokita, S. E. *J. Am. Chem. Soc.* **2004,** 126, 15552-15559.

11.   Steenken, S.; Jovanovic, S. V. *J. Am. Chem. Soc.* **1997,** 119, 617-618.

12.   Shukla, L. I.; Adhikary, A.; Pazdro, R.; Becker, D.; Sevilla, M. D. *Nucleic Acids Res.* **2004,** 32, 6565-6574.

13.   Jortner, J.; Bixon, M.; Langenbacher, T.; Michel-Beyerle, M. E. *Proc. Natl. Acad. Sci. USA* **1998,** 95, 12759-12765.

14.   Liu, C.-S.; Hernandez, R.; Schuster, G. B. *J. Am. Chem. Soc.* **2004,** 126, 2877-2884.

15. Henderson, P. T.; Jones, D.; Hampikian, G.; Kan, Y.; Schuster, G. B. *Proc. Natl. Acad. Sci. USA* **1999,** 96, 8353-8358.

16. Nunez, M.; Hall, D. B.; Barton, J. B. *Chem. Biol.* **1999,** 6, 85-97.

17. Davey, C. A.; Sargent, D. F.; Luger, K.; Maeder, A. W.; Richmond, T. J. *J. Mol. Biol.* **2002,** 319, 1097.

18. Widom, J. *Proc. Natl. Acad. Sci. USA* **1992,** 89,1095-1099.

19. Wolffe, A. P., *Chromatin Structure and Function.* ed.; Academic Press, Inc.: San Diego, 1992;

20. Rajski, S. R.; Barton, J. K. *Biochemistry* **2001,** 40, 5556-5564.

21. Nunez, M. E.; Noyes, K. T.; Barton, J. K. *Chem. Biol.* **2002,** 9, 403-415.

22. Nakatani, K.; Dohno, C.; Ogawa, A.; Saito, I. *Chem. Biol.* **2002,** 9, 361-366.

23. Newman, M.; Strzelecka, T.; Domer, L. F.; Schildkraut, I.; Aggarwal, A. K. *Science* **1995,** 269, 656-663.

24. Thastrom, A.; Bingham, L. M.; Widom, J. *J. Mol. Biol.* **2004,** 338, 695-709.

25. Widom, J. *Annu. Rev. Biophys. Biomol. Struct.* **1998,** 27, 285-327.

26. Lowary, P. T.; Widom, J. *J. Mol. Biol.* **1998,** 276, 19-42.

27. Shrader, T. E.; Crothers, D. M. *Proc. Natl. Acad. Sci. USA* **1989,** 86, 7418-22.

28. Gasper, S. M.; Schuster, G. B. *J. Am. Chem. Soc.* **1997,** 119, 12762-12771.

29. Libertini, L. J.; Small, E. W. *Nucleic Acids Res.* **1980,** 8, 3517-3534.

30. Moyer, R.; Marien, K.; van Holde, K.; Bailey, G. *J. Biol. Chem.* **1989,** 264,12226-31.

31. Tullius, T. D.; Dombroski, B. A.; Churchill, M. E.; Kam, L. *Methods Enzymol.* **1987,** 155, 537-558.

32.	Fahlman, R. P.; Sharma, R. D.; Sen, D. *J. Am. Chem. Soc.* **2002,** 124, 12477-12485.

33.	Williams, T. T.; Dohno, C.; Stemp, E. D. A.; Barton, J. K. *J. Am. Chem. Soc.* **2004,** 126, 8148-8158.

34.	Kasai, H.; Yamaizumi, Z.; Berger, M.; Cadet, J. *J. Am. Chem. Soc.* **1992,** 114, 9692-9694.

35.	Misiaszek, R.; Uvaydov, Y.; Crean, C.; Geacintov, N. E.; Shafirovich, V. *J. Biol. Chem.* **2005,** 280, 6293-6300.

36.	Norman, D. G.; Grainger, R. J.; Uhrin, D.; Lilley, D. M. J. *Biochemistry* **2000,** 39, 6317-6324.

37.	Sanii, L.; Schuster, G. B. *J. Am. Chem. Soc.* **2000,** 122, 11545-11546.

38.	Negri, R.; Buttinelli, M.; Panetta, G.; De Arcangelis, V.; Di Mauro, E.; Travers, A. *J. Mol. Biol.* **2001,** 307, 987-999.

39.	Neubauer, B.; Horz, W. *Methods Enzymol.* **1989,** 170, 630-644.

40.	Jenuwein, T.; Allis, C. D. *Science* **2001,** 293, 1074-80.

41.	Hayes, J. J.; Tullius, T. D.; Wolffe, A. P. *Proc. Natl. Acad. Sci. USA* **1990,** 87, 7405-7409.

42.	Bhalla, V.; Bajpai, R. P.; Bharadwaj, L. M. *Embo Rep.* **2003,** 4, 442-445.

43.	Bloomfield, V. A.; Crothers, D. M.; Tinoco, I., Jr., *Nucleic Acids: Structures, Properties and Functions*. ed.; University Science Books: Sausalito, California, 2000;

44.	Cao, H.; Schuster, G. B. *Bioconjugate Chem.* **2005,** 16, 820-826.

45.   Wagenknecht, H.-A.; Stemp, E. D. A.; Barton, J. K. *Biochemistry* **2000,** 39, (18), 5483-5491.

46.   Voityuk, A. A.; Jortner, J.; Bixon, M.; Rosch, N. *Chem. Phys. Lett.* **2000,** 324, (5,6), 430-434.

47.   Voityuk, A. A.; Michel-Beyerle, M. E.; Rosch, N. *Chem. Phys. Lett.* **2001,** 342, (1,2), 231-238.

48.   Barbara, P. F.; Meyer, T. J.; Ratner, M. A. *J. Phys. Chem.* **1996,** 100, 13148-13168.

49.   Giese, B. *Acc. Chem. Res.* **2000,** 33, 631-636.

50.   Olson, E. J. C.; Hu, D. H.; Hormann, A.; Barbara, P. F. *J. Phys. Chem. B* **1997,** 101, (3), 299-303.

51.   Luger, K.; Mader, A. W.; Richmond, R. K.; Sargent, D. F.; Richmond, T. J. *Nature* **1997,** 389, (6648), 251-260.

52.   Das, P.; Schuster, G. B. *Proc. Natl. Acad. Sci. USA* **2005,** 102, (40), 14227-14231.

53.   Li, G.; Levitus, M.; Bustamante, C.; Widom, J. *Nat. Struct. Mol. Biol.* **2005,** 12, (1), 46-53.

54.   Li, G.; Widom, J. *Nat. Struct. Mol. Biol.* **2004,** 11, (8), 763-769.

55.   Beard, B. C.; Wilson, S. H.; Smerdon, M. J. *Proc. Natl. Acad. Sci. USA* **2003,** 100, 7465-7470.

CHAPTER III

NUCLEOSOME CORE PARTICLE PACKAGING EFFECTS ON DNA CHARGE TRANSPORT IN THE 601 SEQUENCE

ABBREVIATIONS

AQ, anthraquinone; bp, base pairs; CT, charge transport; EMSA, electrophoretic mobility shift assay; ExoIII, Exonuclease III; G, guanine; $G^{\bullet+}$, guanine radical cation; 8OG, 8-oxoguanine; NCP, nucleosome core particle; $OH^{\bullet}$, hydroxyl radical; rNCP, reconstituted nucleosome core particle; Fpg, Formamido pyrimidino glycosylase; Tyr, tyrosine; Arg, arginine; Trp, tryptophan

SUMMARY

Long-range hole transport in DNA has been extensively studied in isolated DNA constructs. However, little is known about this phenomenon in the eukaryotic cell nucleus. The fundamental level of DNA compaction is the nucleosome core particle (NCP), consisting of ~147 base pairs of DNA wrapped one and a half turns around an octamer of histone proteins. In the studies reported here, we show that packaging DNA into a NCP perturbs the dynamics of DNA hole transport. To site-selectively inject an excess positive charge into DNA, we have utilized a covalent Anthraquinone photooxidant. We have shown that there are significant differences in piperidine-labile sites in contrast to Fpg-sensitive sites in lesions that are further packaged into the NCP. We also show that there may be significant contributions of the histone tails to the alteration of DNA CT dynamics in NCPs. Additionally, we have identified a unique protein-mediated DNA charge transport event facilitated by a tyrosine in histone H3.

INTRODUCTION

Oxidative stress affects many cellular components including the nucleic acids of the nucleus. In particular, the oxidation of Guanine (G) may result in a compromised genome due to the formation of stable G lesions that have mutagenic and potentially carcinogenic properties.[1-3] One-electron oxidation of G results in the formation of a Guanine radical cation ($G^{\bullet+}$). Further reaction with solvent (H_2O, O_2, $O_2^{\bullet-}$) results in chemical trapping to generate a G oxidative lesion (i.e. 8-oxoguanine (8OG)).[4-6] Another well known property of G oxidation is the propensity of the $G^{\bullet+}$ to undergo a nearly-isoenergetic electron exchange with another G within the DNA duplex.[7-10] This process mobilizes the $G^{\bullet+}$ into a region that is not the original site of oxidation via long-range DNA charge transport (CT). The transfer of the electron deficient hole can occur over long distances (>200 Å) before eventually becoming trapped through an irreversible reaction to form a stable G lesion.[2, 11]

The investigation of DNA CT has relied largely upon qualitative and quantitative studies utilizing short DNA duplexes in aqueous environments A lot of research has been dedicated to understanding the kinetics and the mechanisms of CT, yet minimal work has been done to understand these processes in a biological setting. In the eukaryotic cell, DNA does not inhabit the same type of environment, or display the prototypical B-form structure found in most short pieces of DNA. A human nucleus contains approximately 3 billion base pairs (bp) of DNA comprising 42 chromosomes, and when stretched end-to-end it is approximately 2 meters in length.[12] In order to fit all of this DNA into a nucleus with a diameter of ~10 μm, many levels of packaging are required. The first level of packing is around an octamer of histone proteins (2 each of

histones H2A, H2B, H3, and H4). There is approximately 147 bp of DNA wrapped 1.65 turns around this octamer to form the complex known as the nucleosome core particle (NCP).[12, 13] The NCP serves as an ideal biological model to study the dynamics of DNA CT in vivo.

Two previous reports have used the NCP to examine DNA CT and found differing results. Nunez et.al utilized a covalently attached Rh-metallointercalator onto a palindromic α-satellite DNA sequence to initiate DNA CT on the NCP.[14] Qualitatively, they observed minor changes in the G oxidation pattern of the DNA whether it was free in solution or packaged into NCPs. In a recent report from our lab, we found that there was a quantitative attenuation of DNA CT by packaging an NCP positioning element called the TG-motif into NCPs.[15] Our method of $G^{\bullet+}$ injection utilized the well characterized Anthraquinone (AQ) photooxidant (Figure 3.1a). Ultimately, we attributed the disparity of these two studies to the different types of photooxidant systems and the differences in NCP-DNA thermodynamic stabilities.

Here we report the results of DNA CT on NCPs utilizing another NCP positioning element, the 601 sequence (Figure 3.1b).[16] The findings reported here suggest that previous observations on the effects of NCPs to DNA CT are much more complex than the earlier studies might indicate. The 601 sequence represents a more complicated DNA CT model that has a full range of energetic $G^{\bullet+}$ traps (single, double, and triple G stacks). We report significant differences in G damage distribution at sites that are positioned ~40 bp away from the AQ photooxidant. Comparison of the G damage distribution using piperidine cleavage and enzymatic cleavage with formamido-pyrimidino glycosylase (Fpg) has also shown us that there are differences in the trapping reactions at distal G

sites when the DNA is packaged into NCPs. Additionally, we observe damage at sites

that are ~90 bp (~300 Å) from the AQ photooxidant, which is over 100 Å farther than

ever reported. Preliminary evidence indicates that this may be the result of protein-

mediated interduplex DNA CT.

MATERIALS AND METHODS

601 DNA constructs

Anthraquinone (AQ) modified and amino-capped (NH_2) DNA utilizing the 601^{16}

nucleosome core particle (NCP) positioning sequence were prepared by the method of

Bjorklund et.al.[15] A pGEM-3z (Promega) plasmid carrying the 282 bp high affinity NCP

sequence inserted into the HincII site (of the MCS) was obtained as a gift from Dr. Lisa

Gloss (Washington State University). Three forward primers, **FAQ-158** (**AQ-5'-*TA***

***TA*G CCG CCC TGG AGA ATC CC -3'), FAQ-162** (**AQ-5'-TAT ACG CGG CCG**

CCC TGG -3'), and **FAQ-168** (**AQ-5'-*TAT A*CC *CGG G*CG CGG CCG CCC -3'**)

were synthesized in-house on an ABI Applied Biosystems 380B DNA synthesizer**.** The

5'-ends were modified by an AQ-phosphoramidite during the solid phase synthesis as

previously described.[17] Italicized bases within primer sequences above indicate non-

homologous regions deliberately mutated to conserve the sequence that is most proximal

to the AQ in **AQ-162**. An additional forward primer **FNH₂-162 (NH_2-(CH_2)₆-5'-TAT**

ACG CGG CCG CCC TGG -3') was synthesized using a monomethoxytrityl-protected

amino linker phosphoramidite (Glen Research). A single reverse primer (**5'-CAC AGG**

ATG TAT ATA TCT GAC AC -3') was synthesized Trityl-on. All primers were

deprotected by incubation at 40 °C for 16 hours in concentrated ammonium hydroxide.

Primers were reverse-phase HPLC purified on a Waters 2690 system utilizing a

Photodiode Array Detector (monitored at A_{260}, A_{300}, and A_{330} for AQ-modified primers)

and a Nucleosil C18 RP column (Hichrom). The reverse and NH_2-linked primers were

de-tritylated in 80% acetic acid for 30 min at room temperature and all primers were

ethanol precipitated and washed with 70% ethanol. DNA concentrations were

determined by the measurement of A_{260} on a Cary Bio 100 (Varian). PCR reactions were

carried out in 50 μL reaction volumes in 0.5 mL thin-walled PCR reaction tubes utilizing

the standard protocol as suggested by the Elongase PCR kit (Invitrogen) on a Biometra

(Biotron) thermocycler. Individual PCR constructs utilized different forward primers (as

identified above) and the same reverse primer for each desired construct. PCR products

were purified on a preparative 3% agarose gel (Figure 3.2a) using Qiagen QiaQuick Gel

Extraction kits. DNA recovery was determined by A_{260} measurement. 601 PCR products

were ^{32}P-labeled on their 5'-reverse primer strand using T4 Polynucleotide Kinase (New

England Biolabs) and [γ-^{32}P]-ATP (Perkin Elmer; 5 mCi/mL, 3000 Ci/mmol specific

activity). These reactions were then extracted with equal volumes of phenol/chloroform,

and applied to Probe Quant G50 spin columns (Amersham), and ethanol precipitated.

Reconstituted Nucleosome Core Particles from Chicken Erythrocytes

Nucleosome Core Particles (NCPs) isolated from chicken erythrocytes (Lampire

Biologicals) were prepared and purified by a method described previously.[18]

Endogenous avian linker histones H1 and H5 were removed from the core histone

octamer and DNA complex. The purity of the isolated NCPs was determined by 18%

acrylamide (30:0.5) SDS-PAGE analysis. Reconstitution of ^{32}P-labeled 601 PCR

constructs onto NCPs was performed by a previously published method.[15] Briefly, ~100

nM ^{32}P-labeled DNA (10-100k cpm) was mixed with NCPs (0.6 mg/mL), 1 M NaCl, 10

mM sodium phosphate (pH 7.0) in a 60 μL volume at 4°C. These mixtures were then

placed in 3500 MWCO microdialysis units (Pierce) and dialyzed against 1 M NaCl, 10

mM sodium phosphate (pH 7.0) for 60 min, followed by successive dialysis against

sodium phosphate buffered 600 mM NaCl, 300 mM NaCl, and finally 10 mM sodium

phosphate. The efficiency of reconstitution was interrogated by 6% native gel

electrophoresis (Figure 3.2b). Briefly, 3k cpm of sample was suspended in formamide

loading buffer and electrophoresed for 75 min at 100 V. Gels were dried and analyzed by

autoradiography using a 445 SI Phosphorimager (Molecular Dynamics) and ImageQuant

software (Molecular Dynamics).

Footprinting of Reconstituted 601 Constructs

The translational setting of both free and reconstituted AQ-162 and NH$_2$-162 was

analyzed by ExoIII footprinting.[19] Both free and rNCPs were digested with one unit of

ExoIII for 3 min. at 37 ºC and immediately extracted with an equal volume of

phenol/chloroform. Samples were ethanol precipitated with glycogen, washed twice with

70% ethanol, and resuspended in formamide loading buffer. Rotational characterization

of all 601 constructs was achieved by hydroxyl radical footprinting.[20] Briefly, Fe-EDTA

(20 μM), 0.3% H$_2$O$_2$, and sodium L-ascorbate (1 mM) were mixed with either free AQ or

NH$_2$ 601 constructs or with reconstituted NCPs in 100 μL reactions and incubated at

room temperature. Reactions were stopped by the addition of 40 mM EDTA and 7 mM

thiourea, after 1 min. for free DNA or 10-12 min. for reconstituted DNA. The samples

were then phenol/chloroform extracted and ethanol precipitated in the presence of glycogen followed by resuspension in formamide loading buffer. All footprinting samples were run on 7 M urea 6% PAQE sequencing gels. Gels were dried and exposed to phosphor screens (Amersham Biosciences) and analyzed by autoradiography (ImageQuant).

UV-Irradiation and Cleavage Reactions

AQ-dependent photooxidation of DNA was initiated by irradiation of all samples in a Luzchem photoreactor (Luzchem Research) equipped with 10 UV-A lamps (~0.3 mW/cm^2 per lamp) centered at 350 nm. Samples were irradiated in 100 μL of 10 mM sodium phosphate (pH 7.0); in non-silanized 1.5 mL Eppendorf tubes at ambient temperature. Immediately following irradiation, samples were heated briefly at 90 ˚C and then extracted with phenol/chloroform before ethanol precipitation in the presence (or absence for the Fpg reactions) of glycogen. For piperidine cleavage reactions, DNA pellets were dissolved in 10% piperidine and incubated at 90 ˚C for 30 min. Samples were then dried in vacuo and washed twice with ddH$_2$O before suspension in formamide loading buffer. Enzymatic reactions involving Fpg were brought up in 50 μL reaction volumes and were incubated with 10 U of Fpg (Trevigen) for one hour at 37 ˚C. These reactions were stopped by immediate extraction with an equal volume of phenol/chloroform and ethanol precipitated in the presence of glycogen before resuspension in formamide buffer. All samples were electrophoresed on 6% acrylamide 7 M urea denaturing gels run at 60 W constant power for 2 hours. Gels were dried and analyzed by autoradiography.

84

Histone Tail Removal

Removal of histone tails from purified chicken erythrocyte NCPs was performed by a limited trypsin digestion procedure. NCPs (1.3 mg/mL) were mixed in a 100 µL reaction with fresh trypsin (60 µg/mL) (Sigma) and incubated at room temperature for 45 minutes. The reaction was stopped by addition of trypsin inhibitor (600 µg/mL) (Sigma) and the digested histones were analyzed by 18% SDS-PAGE. Following digestion, these tailless NCPs were used for reconstitutions and irradiation experiments as described above.

RESULTS

Production of AQ-Labeled 601 DNA Duplexes

The high affinity artificial NCP positioning sequence, 601, was originally identified to study the dynamics governing DNA and NCP interactions.[16, 21] This sequence has been shown to be one of the most thermodynamically stable NCP positioning sequences, displaying a single NCP-DNA structure.[21] Three AQ-modified 601 DNA constructs (Figure 3.1b) of varying lengths (158, 162, and 168 bp), and one NH_2-modified 601-DNA construct (162 bp) were generated through PCR reactions utilizing a 601-containing plasmid as the template. Each 601 construct contained the ~147 bp of the core NCP positioning element, a 1 bp overhang on the 3'-end of the sequence, and a varying overhang length (10, 14, and 20 bps) on the modified 5'-ends. The overhangs on the 5'-modifed ends were designed to possess a few essential characteristics: (1) they allow for the injection of a radical cation into a sequence that is

85

structurally similar to B-form DNA which is useful for, (i) comparison of DNA CT that initiates in unbound DNA and migrates into protein-bound DNA, and (ii) the resemblance of the DNA to the "linker" structure in between successive NCPs in vivo. (2) Placement of the AQ photooxidant away from the hydrophobic core of the histone octamer reduces undesired interactions of the hydrophobic AQ dye with the histones. Following PCR amplification, agarose gel purification, and quantification of all 601 constructs (Figure 3.2a), the duplexes were labeled with ^{32}P and utilized in both UV-irradiation and NCP reconstitution experiments.

Reconstitution and Footprinting:

Labeled 601-DNA was reconstituted onto purified chicken erythrocyte NCPs in a ~50:1 (NCPs:DNA) molar ratio by a stepwise salt gradient in microdialysis units.[15] Reconstitution efficiencies were analyzed by electrophoretic mobility shift assays (EMSA) which consistently found that >95% of the DNA was incorporated into NCPs (Figure 3.2b). Interrogation of the rotational and translational positioning of the 601-DNA was performed in order to structurally characterize the rNCPs. Hydroxyl radical footprinting experiments were employed to examine rotational settings of the constructs on the histone octamer core.[20] Free AQ-158, AQ-162, AQ-168, NH_2-162 and their NCP reconstituted counterparts were subjected to hydroxyl radical generation by in situ Fenton chemistry. The results indicate a single rotational position on the NCPs for each construct with the expected ten base pair periodicity associated with the helical twist of the DNA on the surface of the histone octamer (Figure 3.3a). Additionally, it was observed that neither the length of the AQ-modified 5'-end overhang (10 vs. 14 vs. 20

bp), nor the presence of the NH_2-linker (Data not shown) or AQ resulted in a different

hydroxyl radical footprint (Figure 3.3b). To clarify, the core 147 bp of the 601 was

always positioned the same on the NCP surface with no preference to the overall length

of the construct. The NCP translational setting was determined for both the reconstituted

AQ-162 (rAQ-162) (Figure 3.3a) and NH_2-162 (rNH_2-162) (Data not shown) via

Exonuclease III (ExoIII) footprinting. ExoIII is a 3'-5' exonuclease that rapidly chews

up free DNA but is inhibited by DNA protein contacts.[19] Figure 3.3a shows the results of

this reaction illustrating the approximate 14 bp overhang of the region that is most

proximal to the AQ photooxidant. This shows that the AQ is not within close proximity

with the histone core of the NCP and is most likely in an end-capped configuration on the

DNA duplex. Taken together, these footprinting experiments validate that these

macromolecular structures are very homogenous and that results can be properly

interpreted with confidence regarding the local DNA structure and environment. We

have taken this information and generated a model of the 601-NCP constructs utilizing

the crystal structure of Davey et.al[22] in Figure 3.4.

DNA CT and the Resultant Guanine Damage Distribution

The excitation of AQ at 350 nm results in an excited singlet state ($^1AQ^*$) that

rapidly undergoes intersystem crossing to form an excited triplet state ($^3AQ^*$) (Figure

3.1a).[23-25] This long lived triplet state is then energetically capable of oxidizing a nearby

guanine within the base stack. In the charge separated state ($AQ^{\bullet-}$ - $G^{\bullet+}$), oxygen removes

the excess electron from the $AQ^{\bullet-}$ resulting in the formation of a liberated $G^{\bullet+}$ (Figure

3.1a). This radical cation will either be trapped by an irreversible reaction (to form a G

lesion) with a reagent from the surrounding medium (H_2O, O_2, $O_2^{\bullet-}$) or the radical cation hole may migrate to other nearby guanines within the DNA duplex before trapping out as a G lesion.[7-10] The process is ultimately regulated by the relative rates of hopping (k_{hop}) and trapping (k_{trap}), and results in a steady state distribution of G oxidative products that can be detected by cleavage reactions with piperidine or a glycosylase like Fpg.

Following UV-A irradiation of both free DNA (AQ-158, AQ-162, AQ-168, and NH_2-162) and rNCPs (rAQ-158, rAQ-162, rAQ-168, and rNH_2-162), samples were heated to 90 °C in 10% piperidine for 30 min and analyzed by denaturing gel electrophoresis. Figure 3.5 shows a representative autoradiograph of the results from an AQ-158 irradiation experiment. The gel itself has been cut into two overlapping portions showing the 601 sequence most proximal to the AQ at the top and the sequence closest to the NCP dyad axis at the bottom (for a full explanation please see Figure legend). The G residues most proximal to the AQ photooxidant that have been revealed as G oxidative lesions due to their cleavage by piperidine have been labeled in Figure 3.1b (from GG_1 to G_7) with the resulting bands indicated in Figure 3.5. In the free AQ-158 lane, G damage occurs all the way out to G_7 (39bp/134Å away from AQ) indicating the migration of the injected $G^{\bullet+}$ to this distal bp under the conditions described. Direct comparison to rAQ-158 reveals that the distance of $G^{\bullet+}$ migration equally reaches out to the G_7 as in the unbound AQ-158. However, there are two important qualitative observations to be made here. 1) The presence of a new band in the rAQ-158 lane that does not correspond to any purine residue. This band has been assigned as PyB for pyrimidine band. Additional evidence has indicated that this band is the result of a novel DNA-protein crosslink (DPC) and has been thoroughly investigated and discussed in Chapter 4 of this thesis. 2)

The second major observation is the presence of piperidine labile bands on the lower section of the gel (G_{PENT} in Figures 3.1b and 3.5). These bands correspond to a pentad of G residues 86 bp (~300Å: ~320Å in AQ-162, ~334Å in AQ-168) away from the tethered AQ photooxidant. G_{PENT} lies near the dyad axis within the NCP as depicted in Figures 3.1b and 3.4. These two unique observations are isolated only to the UV-irradiated, piperidine-treated AQ-NCP complexes and not the naked AQ substrates. Additionally, the G_{PENT} oxidative lesion pattern is unique to only those 601 constructs modified by AQ and are not seen in either the irradiated, piperidine treated NH_2-capped construct (Chapter 4; Figure 4.5), nor the *non*-irradiated, piperidine treated AQ-601 constructs (Figure 3.5). This suggests that the G damage distribution is the direct result of DNA CT initiated by the AQ photooxidant and the resultant trapping reactions associated with those lesions. Variance of the 5'-overhang length (via 10, 14 or 20 bp) does not alter the distance of $G^{\bullet+}$ migration, nor does it change the appearance of the two unique damaged regions within their NCP complement.

Following UV-A irradiation and gel electrophoresis, quantitative analysis of the G damage distribution as depicted in the gel in Figure 3.5 was performed using reproducible measurements on the AQ-162 constructs (Figure 3.6). Relative damage ratios (i.e. GG_1/GGG_2) were calculated as a ratio of the total damage at each particular G site as compared to the damage at GG_1. Direct comparison of AQ-162 and rAQ-162 show that there are significant quantitative differences between the distribution of G damage (Figure 3.6). A precursory examination indicates that there is little to no difference between the ratios of the first few G steps out to the GG_4 site. However, at the more distal sites (especially G_6 and G_7) from the AQ photooxidant there is nearly 3-4 fold

differences in these damage ratios. These quantitative variations suggest that compaction into NCPs results in an increase in the amount damage at G_6 and G_7. In addition, we observe in the rNCPs that the amount of damage at the single G steps (G_6 and G_7), is nearly equal to that of the nearby GG_5, which should be a better $G^{\bullet+}$ trap. This is surprising since common wisdom indicates that GGs are better hole traps than single Gs in DNA duplexes, which is what is observed in the naked AQ-162.

Tailless NCPs and G Damage Distribution

While it is apparent that there are both qualitative and quantitative differences in DNA-mediated CT either in unbound DNA substrates or bound within DNA-NCP complexes, it is unclear what structural features give rise to these effects. The histone tails of the NCP octamer have been shown to be disordered into a random coil-like structure.[13, 22] The tails are thought to only minimally interact with the DNA wrapped around the core of the NCP and primarily with linker DNA between successive NCPs.[26] Nevertheless, some studies suggest at the low salt concentrations that we utilize, there may be more interaction with the core DNA than previously thought.[27] In the systems that we have employed for these studies, the AQ-modified overhang serves as a pseudo linker region. In order to probe any potential contribution of the tails to the observed perturbation of DNA CT by the histone octamer, we have removed the tails via a limited trypsin digestion. Following digestion, the NCPs were reconstituted via the same dialysis method used for native NCPs, and the reconstitution efficiency was analyzed by EMSA (Figure 3.2b). The duplicates in lanes 3 and 4 of Figure 3.2b show the gel shift into tailless rNCPs (trNCPs) which has a slightly higher mobility than the native rNCPs due to

the missing tails. These complexes were also examined for structural integrity by hydroxyl radical footprinting which showed the exact same rotational settings as that for native NCPs (data not shown).

UV-irradiation and piperidine treatment of AQ-162 on native and tailless NCPs reveal that there are minor differences between the damage distributions of rNCPs and trNCPs (Figure 3.6). As a general trend, all ratios increase slightly with a nearly 2-fold increase at the distal G_6 and G_7 sites in the trNCPs, but are still 2-fold less than that of the free AQ-162 damage ratios. This observed change at these most distal sites from the AQ indicate that there may be some potential contribution of the histone tails in altering the G damage distribution in NCPs, but that they do not account for all of the variation.

Fpg and G Damage Distributions

An additional consideration explored here is the potential for a difference in the trapping reactions associated with G lesion formation in both the NCPs and the free AQ constructs. This effect may arise from either an influence on the rates of reactions associated with the trapping chemistry or by favoring one type of trapping pathway over the other. We have employed an additional G lesion detection mechanism in the form of enzymatic cleavage of damaged substrates. Fpg is an endogenous *E.coli* glycosylase responsible for recognizing and excising many oxidized lesions within its genome.[28-30] While many of the Fpg substrates overlap with that of piperidine labile substrates, a G lesion like 8-oxoguanine is only cleaved by Fpg.[31]

Samples of AQ-162, rAQ-162, and trAQ-162 were subjected to UV-A radiation and the G lesions were cleaved with Fpg. These samples were then electrophoresed,

analyzed by autoradiography, and the relative damage ratios were quantified as previously described (Figure 3.7). In free AQ-162, the G damage distributions between piperidine cleavage reactions (Figure 3.6) and Fpg incubations (Figure 3.7) show virtually no difference in the G steps most proximal to the AQ. However, there is a significant difference in the distal G_6 and G_7 sites which show a 2-fold and 1.5-fold difference respectively. This suggests that the amount of piperidine labile lesions are in greater number than that of the Fpg labile lesions at these distal sites. Comparison of both piperidine (Figure 3.6) and Fpg cleavage reactions (Figure 3.7) on both native rAQ-162 and tailless trAQ-162 shows minor differences for both data sets suggesting that there is a similar distribution of Fpg-sensitive and piperidine-labile G lesions in both samples. In contrast to the observation of Fpg damage ratios for free AQ-162, this may indicate an increase in Fpg-labile substrates at these distal sites when the DNA is packaged into the NCP, regardless of the presence of the tails (Figure 3.7). Ultimately, this illustrates that the chemistry associated with $G^{\bullet+}$ trapping may differ depending upon the local DNA environment. Additional examination of the differences of the Fpg damage ratios between the free AQ-162 and the reconstituted substrates show that the same general trend was observed as that for the piperidine cleavage assays (Figure 3.6). The GG_1/G_6 and GG_1/G_7 ratios are 5-fold to 3.5 fold less than those in rAQ-162, and 3-fold to 2-fold less for the trAQ-162. These observations are consistent with the piperidine cleavage ratios that suggest either a change in the rates of hopping (k_{hop}) or the trapping reactions (k_{trap}) when the 601 construct is packaged into a NCP.

DISCUSSION

Oxidative damage to G has been predicted to be a key contributor to many disease states.[32-36] The one-electron oxidation of G results in the formation of a $G^{\bullet+}$ that can either deprotonate to form the neutral radical $G^{\bullet}(-H)$ and subsequently react with solvent to form an irreversible G lesion[6], or the $G^{\bullet+}$ may migrate along the DNA duplex until it is eventually trapped as a lesion[7-10]. The process of DNA CT has been shown to be a very complex event that is affected by many variables. Disruption of the base pair stacking, either by abasic sites, helix bulges, or DNA-binding proteins have all been shown to have varying effects on DNA CT efficiency.[37-39] The concept of this event occurring within eukaryotic cell systems is provocative for a number of reasons. On a global genomic scale, does DNA CT mobilize oxidative lesions into regions that may or may not be harder to repair (i.e. heterochromatin vs. euchromatin)? On lower chromatin structure like the NCP, does DNA CT mobilize oxidative lesions into areas of the nucleosome that may or may not be harder to repair (i.e. NCP entrance/exit vs. dyad axis)? These are just a few of the questions about in vivo DNA CT that remain poorly understood.

While short DNA duplexes in aqueous solution are useful models for investigating many of the fundamental processes of long-range DNA CT, they are poor models for biological systems. This is due in part to the complex arrangement of DNA in eukaryotic systems. DNA is packaged into many levels, beginning at the first level of compaction, the NCP.[13, 40-42] Characteristics of the double helical structure within NCPs are quite different from that of short pieces of DNA. The entrance and the exit of the NCP are overwound whereas the pseudo 2-fold dyad axis is underwound. Additionally, the NCP brings two tynes of DNA within a close proximity to each other as 147 bp are wrapped ~1.65 turns around the octamer of histones.[12, 13] The effects that these structural

changes and DNA-histone interactions might inflict upon DNA CT have only recently begun to be explored.[14, 15] We have chosen to use the NCP as a biological model to investigate the potential behavior of DNA CT within a cellular system. Additionally, we are utilizing an artificial NCP positioning sequence, named the 601, that forms extremely stable DNA-NCP complexes.[16, 43] The 601 sequence serves two important purposes, 1) it is more apt to form homogenous NCP structures, and 2) it is very G-rich with a variation in thermodynamic $G^{\bullet+}$ traps like the single (G), double (GG), and triple (GGG) steps that are proximal to the AQ photooxidant.

Characterization of the reconstituted 601-NCP complexes through footprinting experiments indicates homogenous and structurally sound substrates to study DNA CT. Interrogation of both rotational and translational positioning of the DNA constructs showed that there was consistently only one position of the 601 DNA on the NCPs.[15, 20] These experiments also indicate that the AQ photooxidant does not interact with the histone core of the NCP and it appears to be preferentially end-capped onto the DNA duplexes. Defining these characteristics is essential in order to interpret the data based on a few assumptions. 1) Injection of the $G^{\bullet+}$ occurs in a region that resembles both standard B-Form DNA and the linker regions between successive NCPs in vivo. 2) Any effects observed from the influence of the DNA-NCP interactions on DNA CT are unique and are not artifacts of spurious interactions of the proteins and the AQ.

The observed G damage distribution arising from DNA CT in both free AQ-158 and rAQ-158 is shown in Figure 3.5. The extent of $G^{\bullet+}$ migration appears to reach the G_7 in both samples, initially indicating that there is no qualitative disruption of DNA CT when this sequence is packaged into the NCP. However, several key points need to be

addressed here. There are two new significant features associated with irradiated, piperidine treated rAQ-158. First is the appearance of a new band directly below the GGG_2 stack. This band (PyB) does not correlate to any band associated with either the G or the G+A Maxam-Gilbert ladders, and actually corresponds to a pyrimidine tract within the sequence. In a separate report (Chapter 4), we attribute PyB to the formation of a novel DNA-protein crosslink with Tyr41 of histone H3 within the NCP. The second significant feature of the oxidative lesions associated with Figure 3.5 is the appearance of a pentad of G bands (G_{PENT}) that are 86 bp (~300 Å) away from the AQ. This observation is only seen in the irradiated, piperidine treated rAQ-158 lane. Historically, the maximum distance observed for DNA CT by DNA sequencing gels and autoradiography is 55 bps (~200 Å).[2, 11] Thus if the hole transport is wholly mediated by the DNA duplex, the observed distance is nearly 1.5 times greater than the previous record.

There are three hypotheses for the observation of G_{PENT} within the 601-NCP complexes. 1) Migration of a $G^{\bullet+}$ out to this distal site before becoming irreversibly trapped. This would mean that $G^{\bullet+}$ would migrate 86 bp into the 601 sequence, through the overwound entrance of the NCP, through the underwound dyad axis, and finally making a complete circle so that it traps out at the pentad of G residues. We rule out this scenario since there are at least 47 bps of DNA in between the G_7 and G_{PENT}, and none of them show piperidine lability above background. 2) Back intercalation of the AQ photooxidant near the dyad axis that would cause DNA CT to initiate in this region thus becoming trapped out at the G_{PENT}. However plausible this picture may seem, we reject this hypothesis as well. Molecular modeling[17] and NMR structures[44] of similar

95

hydrophobic dyes predict that the AQ will endcap onto the end of the DNA duplex, thereby making it inaccessible to back intercalate into the DNA strand elsewhere. Structural characterization of these 601-NCP complexes by hydroxyl radical and ExoIII footprinting suggest that the AQ-modified end is always associated away from the NCP core by its designated overhang length. Additionally, variation in the length of the overhang does not increase or decrease the yields of G_{PENT} formation on reconstituted NCPs. One would assume that by increasing or decreasing the length, and thus the flexibility of a linker that is involved in back intercalation of the AQ, would result in an alteration of the efficiency of $G^{\bullet+}$ injection in that region and thus alter the distribution of G_{PENT} damage, which is just observed. Also, there exists no observable damage in regions directly flanking the G_{PENT} site itself.

3) The last hypothesis explores the possibility of protein-mediated interduplex DNA CT. Using our footprinting experiments to generate a model of the 601 sequence on the NCP crystal structure, we have mapped out the local 3D environment of G_{PENT} (Figure 3.8). Immediately, it is noticed that even without back intercalation of the AQ, the true distance in between the G_{PENT} and the photooxidant is small depending upon the flexibility of the overhang. An additional observation is that G_{PENT} is in the second tyne of DNA making a complete circle around the histone octamer (Figure 3.4). The residues within this site are directly adjacent to the PyB proximal to the AQ (Figure 3.8). As previously mentioned, the PyB has been shown to potentially be the result of a DNA-protein crosslink (DPC) between the pyrimidine patch and Tyr41 on histone H3 of the NCP (Chapter 4). The proposed mechanism of DPC formation involves the oxidation of Tyr41 by a $G^{\bullet+}$ to form $Tyr-O^{\bullet} + H^{+}$. The Tyr radical then attacks either the sugar-

phosphate backbone or the nucleobases to form an array of covalent adducts in between the DNA and the protein. We now propose that the Tyr41 on histone H3 may also be involved in oxidizing the G_{PENT}. Thermodynamically, it is not clear if this reaction:

$$G^{\bullet +} + Tyr-OH + G_{PENT} \rightarrow G + Tyr-O^{\bullet} + G_{PENT} \rightarrow G + TyrOH + G_{PENT}^{\bullet +}$$
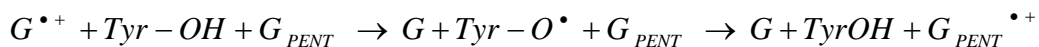
would be spontaneous. The oxidation potentials of Tyr ($E_{ox} = 0.94$ V vs. NHE)[45] and G ($E_{ox} = 1.3$ V vs. NHE)[46] make the initial step energetically favorable. Previous studies have identified this initial reaction step using small DNA-binding peptides that contain either Tyr or Trp.[47] However, it is not known what the oxidation potential of a G pentad would be, especially within this macromolecular environment. It is well documented that the preferential sites of $G^{\bullet +}$ trapping during DNA CT are at GGG > GG > G[48, 49] due to lower ionization potentials that stabilize the $G^{\bullet +}$ within these stacks[50], allowing the rates of chemical trapping to be faster than the migration. Conversely, not much has been demonstrated or measured for a G stretch beyond a triple G. Assumedly, the G pentad would have an even lower ionization potential, low enough that oxidation by the tyrosine radical would be energetically favorable. An additional consideration is that of the electrostatic contribution of the DNA-NCP interactions that may also alter the oxidation potentials enough to drive this proposed reaction forward. The concept of a protein-mediated interduplex DNA CT event is a reasonable interpretation of these results for a couple of reasons. Studies involving other higher-order DNA structures like three-way and four-way junctions found no such interduplex transfer[51, 52] of the $G^{\bullet +}$, which indicates that even in closely associated DNA duplexes, interduplex CT is not observed. Additionally, the concept of CT across two tynes of DNA would completely disregard

everything accepted about the mode of radical cation migration, i.e., via the base pair stack.

Irradiation of the 601 constructs and subsequent piperidine treatment show several significant differences between unbound DNA and reconstituted DNA. Quantitative analysis of G damage distributions showed significant differences between the free and NCP-bound DNA. Relative damage ratios were consistently observed higher for the free AQ-162 as compared to rAQ-162, indicating less damage at the distal sites as compared to the proximal GG_1 site (Figure 3.6). The difference in damage ratios between AQ-162 and rAQ-162 at the sites most proximal to the AQ were small and typically within error. These results should be expected for a couple of reasons. According to the footprinting experiments the AQ-modified overhang in the NCPs should resemble the B-Form DNA structure of the unbound DNA so that the efficiency of $G^{\bullet+}$ injection is similar in both systems. Therefore the rates of k_{hop} and k_{trap} should be similar with both free and reconstituted complexes resulting in similar damage distributions. When AQ-162 is wrapped around the NCP, the entrance should be in close proximity to GGG_2 (Figure 3.1b). The extent of the $G^{\bullet+}$ migration into the NCP is then three helical turns to the G_7 damage site. It is at these most distal sites (G_6 and G_7) into the NCP that the major differences in relative damage ratios are observed. Recent FRET measurements have shown that there is an inherent flexibility of DNA on a mononucleosome at both the entrance and the exit of the NCP.[53] These motions have been measured to be on the millisecond timescale. In contrast, the further into the NCP the DNA goes, the more restricted this breathing motion is. Considering the time scales of hundreds of microseconds for hole transfer in DNA[54, 55], it is conceivable that the effect that NCPs

may have on DNA CT might not be dramatic in regions that are closest to the entrance or exit. Taken together, this would indicate that the predominant differences in relative damage ratios should be expected in regions that are further into the NCP, which is what is observed here at the distal G_6 and G_7 sites.

The decrease in damage ratios across all of the G positions in the rAQ-162 indicates an increase in DNA CT efficiency. In a previous report from our lab we found an attenuation of DNA CT using a different NCP positioning sequence called the TG-motif[15]. The attenuation was small but significant and we attributed those effects to a contribution of an energetic shift due to an arginine residue inserted into the minor groove at the site of a specific G doublet. In order to investigate the potential for a global trend of this observation, we employed the 601 sequence in the same types of studies as reported previously. The differences between both studies might be explained by a few different courses of thought. The TG-motif utilized a simple model that only had three distinct G damage sites. The first site was within a 10 bp AQ-modified overhang, the second was near the NCP entrance, and the third was two helical turns into the NCP (Chapter 1). In contrast, the 601 sequence has 7 sites of G damage that stretch all the way into the third helical turn, making this sequence a more complex DNA CT model. The 601 sequence also has single, double, and triple G stacks that additionally complicate the energetics of hole transfer and the rates of hopping and trapping. There is also an inherent difference in the thermodynamic stabilities of the DNA-NCP complexes. The 601 sequence has nearly a two-fold greater affinity for the NCP complex than does the TG-motif.[16] It should be apparent that the physical differences between the two types of NCP positioning elements complicate the direct comparison of G damage distributions.

However, the observation that DNA CT can be affected differently on NCPs utilizing distinct sequences further complicates the predictability of this behavior in vivo.

Determining the potential causes for the variation between AQ-601 dependent DNA CT in unbound and reconstituted NCPs, is an extremely difficult task. A simple question that can be explored however is the influence of histone tails. The histone proteins that make up the NCP core are folded into a combination of α-helices and random coils.[40] The majority of the random coils are in their N-terminal (and to some extent C-terminal) tails. These tails have been shown to be important for gene regulation, DNA replication, and DNA repair.[42] The actual interaction of these tails with the 147 bp core DNA that wraps around the octamer is believed to minimal.[13, 27] However, some studies suggest that this interaction may be dependent upon local salt concentrations and whether or not linker regions are present.[13, 27] In order to determine if any of the DNA CT effects observed from compaction into NCPs were influenced by these histone tails, we removed them by limited trypsin digestion. Slight differences were measured between rAQ-162 and trAQ-162 at the sites most proximal to the AQ, while nearly a 2-fold difference was seen at the distal G_6 and G_7 sites (Figure 3.6). However, the increase in the damage ratios for trAQ-162 as compared to the rAQ-162 doesn't result in the same ratios as that for the free AQ-162. Nonetheless, the 2-fold change at the two distal sites indicates that there may be at least some interactions of the tails with the DNA and they may contribute at least partially to the observed differences. These interactions may be influencing either k_{trap}, k_{hop}, or both, but the limitations of this experimental setup do not allow us to determine the exact effect or to what extent. Additionally, it cannot be determined which tails are responsible for these interactions.

There are many pathways for formation of stable G lesions due an initial one electron oxidation. In order to react with a molecule from solvent (H_2O, O_2, $O_2^{\bullet-}$), the $G^{\bullet+}$ deprotonates to the $G^{\bullet}(-H)$ which is the species thought to be required for the trapping chemistry. The trapping chemistry, which is described by k_{trap}, can thus form a variety of G lesions (i.e. 8-oxoguanine (8OG), oxazolone (Oz) imidazolone (Iz), formamidopyrimidine (FAPY), or cyanuric acid (Ca)).[6] Most of these can be formed directly from a one-electron oxidation event while others are products of secondary oxidations. Piperidine cleavage of oxidized lesions is the most common and effective method for detecting an oxidized G product. The range of piperidine-labile substrates is extensive and most G lesions can be cleaved under hot 10% piperidine conditions.[56] However, the most extensively studied G lesion, 8OG, is not cleaved under these conditions. Fpg is an alternative to piperidine to detect oxidative G lesions. The range of Fpg-labile substrates is quite extensive and includes 8OG. While Fpg will detect and excise 8OG from a DNA duplex, it has varying degrees of cleavage efficiencies on other substrates like Oz (less efficient) and Ca (won't cut).[31] Comparison of piperidine-labile, and Fpg labile lesions within irradiated AQ-162, rAQ-162, and trAQ-162 has shown that there are some observable distinctions between them. The most curious result is that in the free AQ-162. In the more distal lesions of G_6 and G_7, there is an increase in the amount of piperidine-labile lesions than Fpg-labile ones (Figure 3.7). Therefore the distribution of G lesions at these distal sites is not equal and that perhaps a different chemical trapping pathway is predominant. Comparison of the unbound AQ-162 Fpg-labile sites to the rAQ-162 and the trAQ-162 shows large discrepancies, especially out at the G_6 and G_7 sites (Figure 3.7). These results indicate that there are similar distributions

of piperidine-labile and Fpg-labile G lesions, and that one trapping pathway is not favored over another. Studies by Angelov et.al have shown that there may be sequence and local helical structure dependence on the formation of certain types of G lesions.[57] They showed that the local helical structure will give variations in Fpg-sensitive and piperidine-labile G lesions after treatment with ionizing radiation. It is also assumed that the local helical structure between the AQ-162 and the rAQ-162 are going to be inherently different, especially the further into the NCP the DNA winds.[12, 13] Additionally, an increase in 8OG formation at these distal sites, are in NCP regions that may complicate DNA repair. There is experimental evidence that indicates a decrease in the efficient removal of DNA lesions that are associated with a mononucleosome.[58] Therefore, DNA repair machinery may have more difficult access to DNA lesions that are more intimately associated with the core of the NCP.

The experiments reported here present a complicated picture of DNA CT dynamics in NCPs. The most alarming observation is the potential for protein-mediated interduplex DNA CT. Structural evidence indicates that Tyr41 of histone H3 may be facilitating this unique event. From a biological standpoint, the consequences of this behavior are uncertain. However, taking into account the role of H3Tyr41 in DPC formation, this dual functionality may result in extremely damaged genomic regions, depending upon sequence and NCP positioning. Additionally, these results support our previous findings that DNA CT is altered when DNA is packaged into NCPs. Even though the results do not confirm an original hypothesis that the NCP may serve as the first line of oxidative defense. In this case we observed significant differences in G damage distributions, especially at the sites most distal from the photooxidant. Whether

or not these differences are facilitated by the structural or electrostatic contributions of the NCP to influence either k_{trap} or k_{hop} is unclear. One potential contribution of the observed changes in G damage distribution in NCPs is the histone tails. The tails are primarily composed of positively charged amino acids (Lys and Arg), and may be interacting with the DNA and altering energetic potentials of some of the G sites. In addition to these observations, we have also determined that there may be more preference for the formation of Fpg sensitive lesions like 8OG, within the NCP. In all, we feel that the results of the experiments reported here will have a significant impact in not only the field of DNA CT but also in the molecular understanding of DNA oxidative damage at the fundamental level of chromatin compaction.

Figure 3.1

a

Anthraquinone (AQ)

b

AQ	AQ	AQ	NCP
168	162	158	Entrance

AQ-5'-GGA CCC TAT ACG CGG CCG CCC TGG AGA ATC CCG GTG CCG AGG
3'- CCT GGG ATA TGC GCC _GG₁_C _GGG₂_ ACC TCT TA_G GG₃_C CAC _GG₄_C TCC

CC G C T C AAT TGG TCG TAG CAA GCT CTA GCA CCG CTT AAA CGC ACG
_GG₅_C _G₆_A_G₇_ TTA ACC AGC ATC GTT CGA GAT CGA GGC GAA TTT GCG TGC

Dyad Axis

TAC GCG CTG TCC CCC   GCG TTT TAA CCG CCA AGG GGA TTA CTC CCT
ATG CGC GAC A_GG GGG__{PENT} CGC AAA ATT GGC GGT TCC CCT AAT GAG GGA

AGT CTC CAG GCA CGT GTC AGA TAT ATA CAT CCT GTG-3'
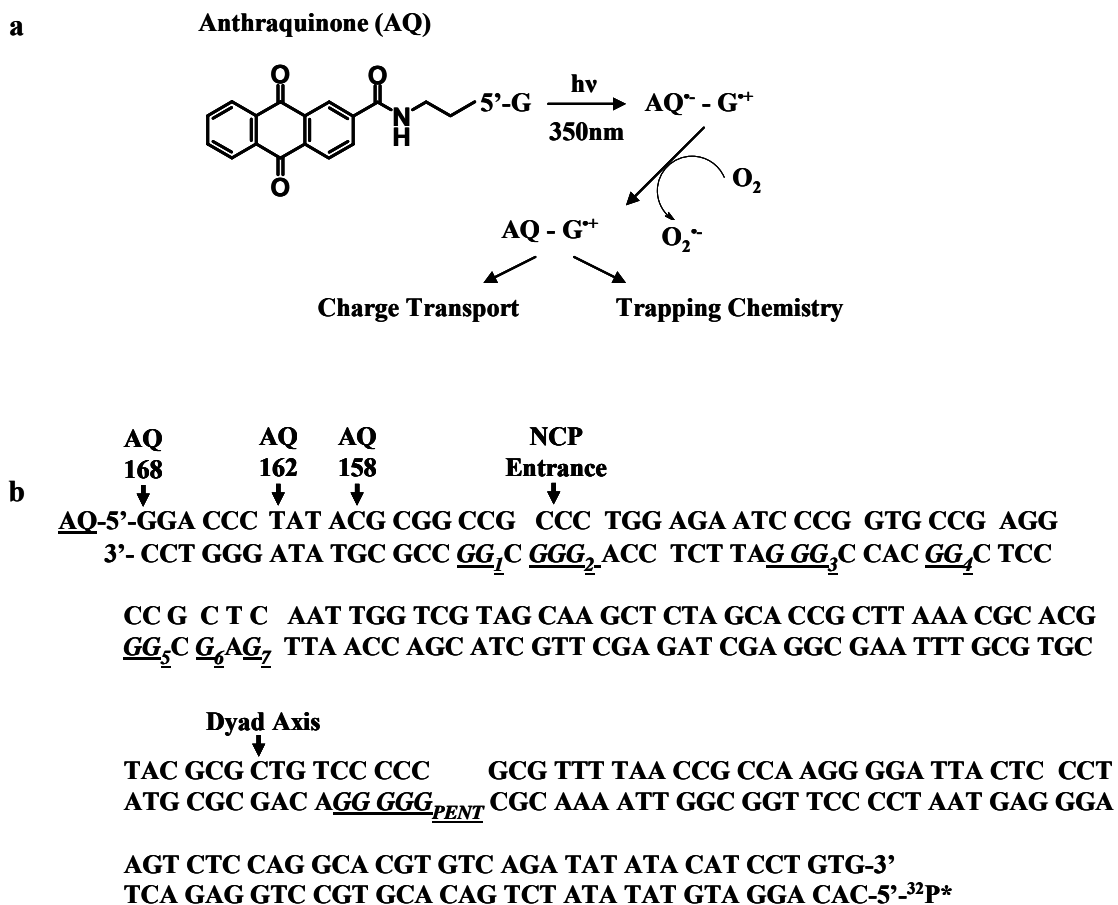TCA GAG GTC CGT GCA CAG TCT ATA TAT GTA GGA CAC-5'-³²P*

Figure 3.1: (a) Structure of Anthraquinone (AQ) photooxidant and scheme of photoinduced oxidation of G. (b) 601 sequence showing the 147 bp core and the various overhang lengths indicated by AQ-168, AQ-162, and AQ-158.
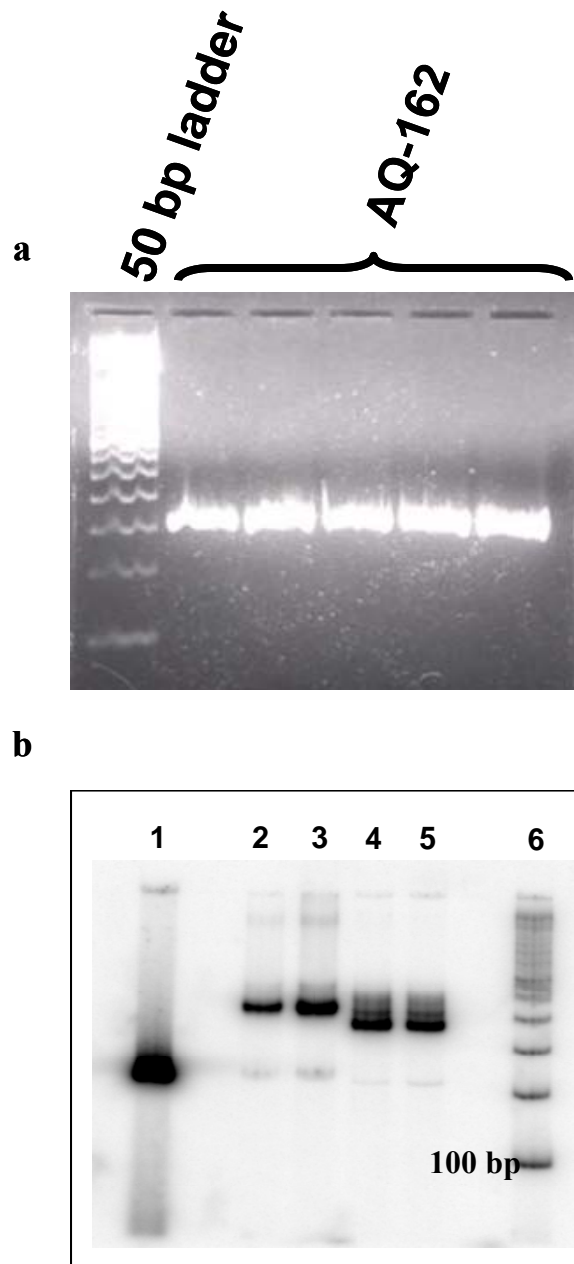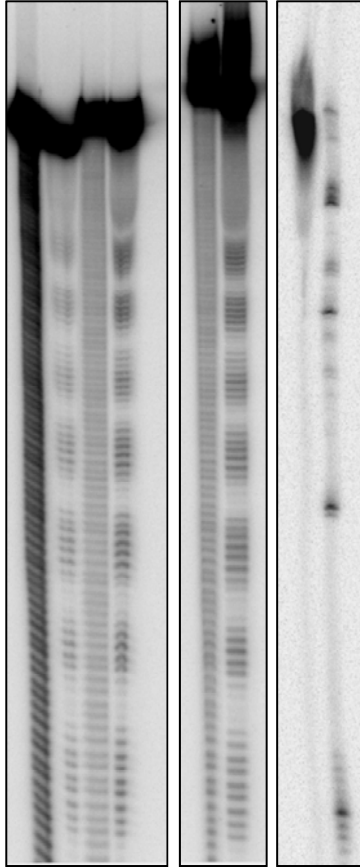
Figure 3.2

Figure 3.2: (a) 3% agarose gel showing PCR products for AQ-162. (b) Electrophoretic mobility shift assay (EMSA) showing the relative reconstitution efficiencies of both regular NCPs (rNCPs) and partially trypsin digested NCPs (trNCPs) using AQ-158. Lane 1 is free AQ-158. Lanes 2 and 3 are duplicate rNCPs. Lanes 4 and 5 are duplicate trNCPs. Lane 6 is a 50 bp ladder. Analysis of autoradiographs consistently shows greater than 95% reconstitution efficiency.
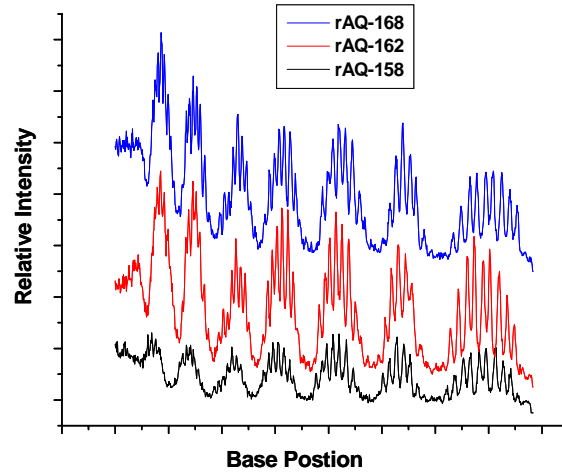
Figure 3.3

a)

b)

Figure 3.3 (a) Hydroxyl radical and ExoIII footprinting autoradiographs. The hydroxyl radical lanes show both free DNA and reconstituted NCPs. In the rNCP lanes there is the expected 10 base pair periodicity showing the contacts of the sugar phosphate backbone with the histone octamer. The ExoIII gel shows nearly complete digestion of the free DNA and only digestion of the14 bp overhang for AQ-162 rNCPs. (b) Scan of the hydroxyl radical footprints for NCP reconstituted AQ-158, AQ-162, and AQ-168 showing the exact rotational positioning. These scans indicate that the length of the AQ overhang doesn't effect the rotational positioning and that all constructs sit on the NCP the same.
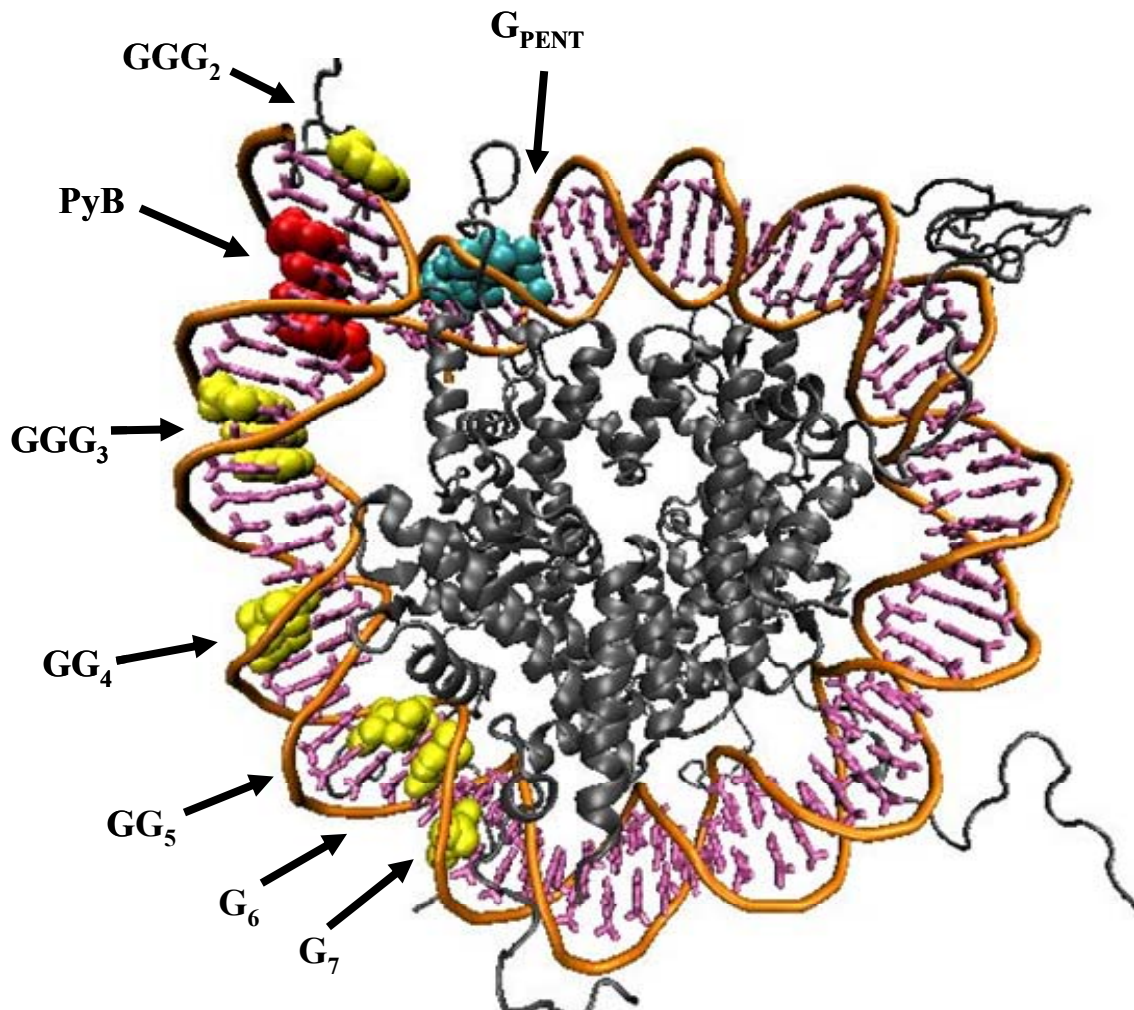
Figure 3.4

Figure 3.4: Crystal structure of the nucleosome core particle (Protein Data Bank Accession # 1KX5) with 147 base pairs of DNA (nucleobases = purple, sugar-phosphate backbone = orange). The histone octamer is in dark grey. The relative positions of the guanine oxidation sites of AQ-601 are highlighted in yellow, minus the AQ-5'-modifed overhang including the GG_1 step. The PyB region is highlighted in red and the G_{PENT} is colored cyan.
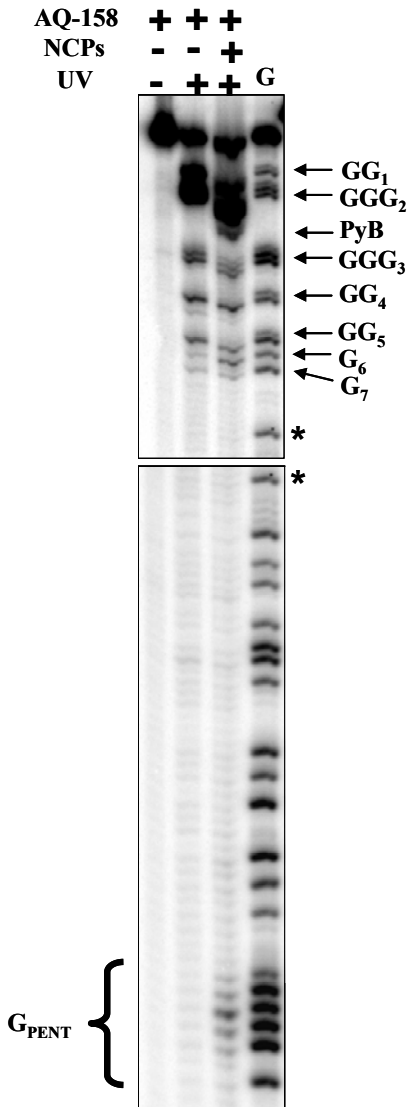
Figure 3.5

Figure 3.5: Autoradiograph of both AQ-157 and rAQ-157 after UV Irradiation (except Lane 1) and piperidine treatment (90°C for 30 min.) and Maxam-Gilbert G ladder Lane 4. Lanes 2 and 3 show the extent of G oxidative damage following photooxidation of the DNA strand by the AQ. Individual G bands are labeled GG_1 through G_7 (38 bp/130 Å from AQ). PyB band represents a potential DNA-protein crosslink thoroughly investigated and discussed in a previous publication (ref.) The bands identified at the bottom of the gel (86 bp/ ~300Å from AQ) as LB (lower bands) appear in the reconstituted AQ-157 and not the free AQ-157. This figure is the product of two separate autoradiographs of the same DNA sequencing gel. In each case, the top or the bottom was not exposed, so two different exposures were combined from the same gel to visualize the entire gel. The asterisks (*) indicate the same G band from the G ladder on both exposures that serve as the overlapping reference point.

Figure 3.6
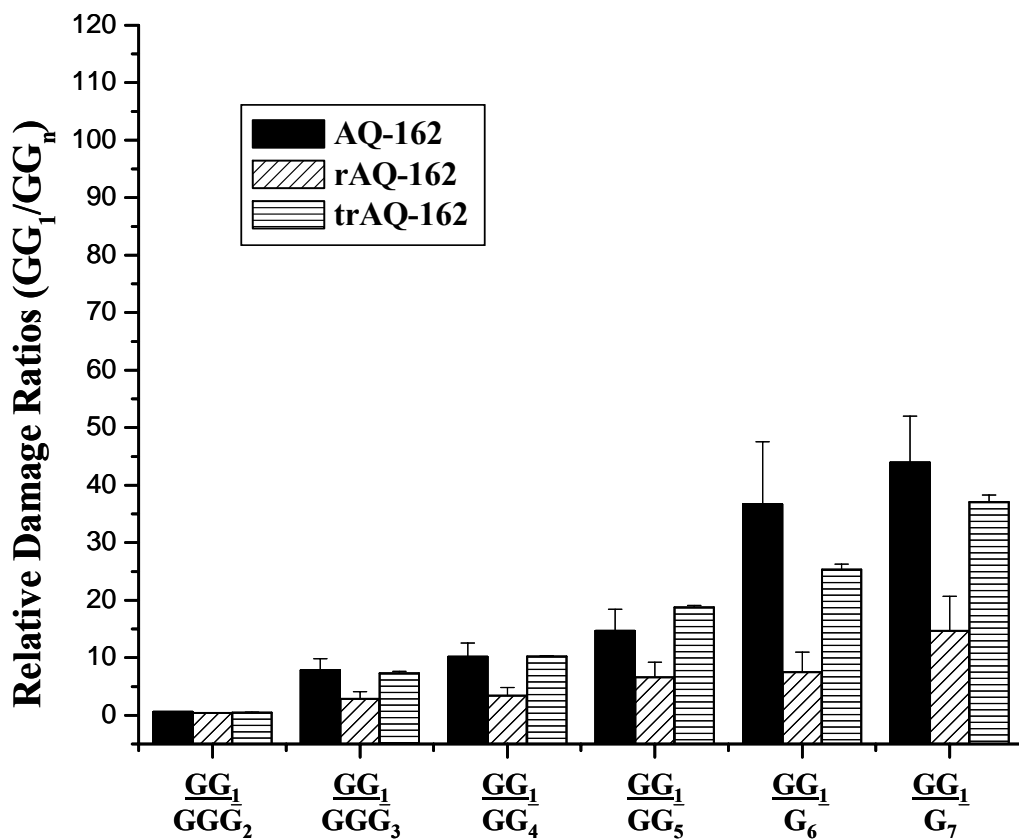
Figure 3.6: Quantification of relative damage ratios (GG_1/GG_n) from autoradiography of UV irradiated and piperidine treated AQ-162, rAQ-162, and trAQ-162.

Figure 3.7
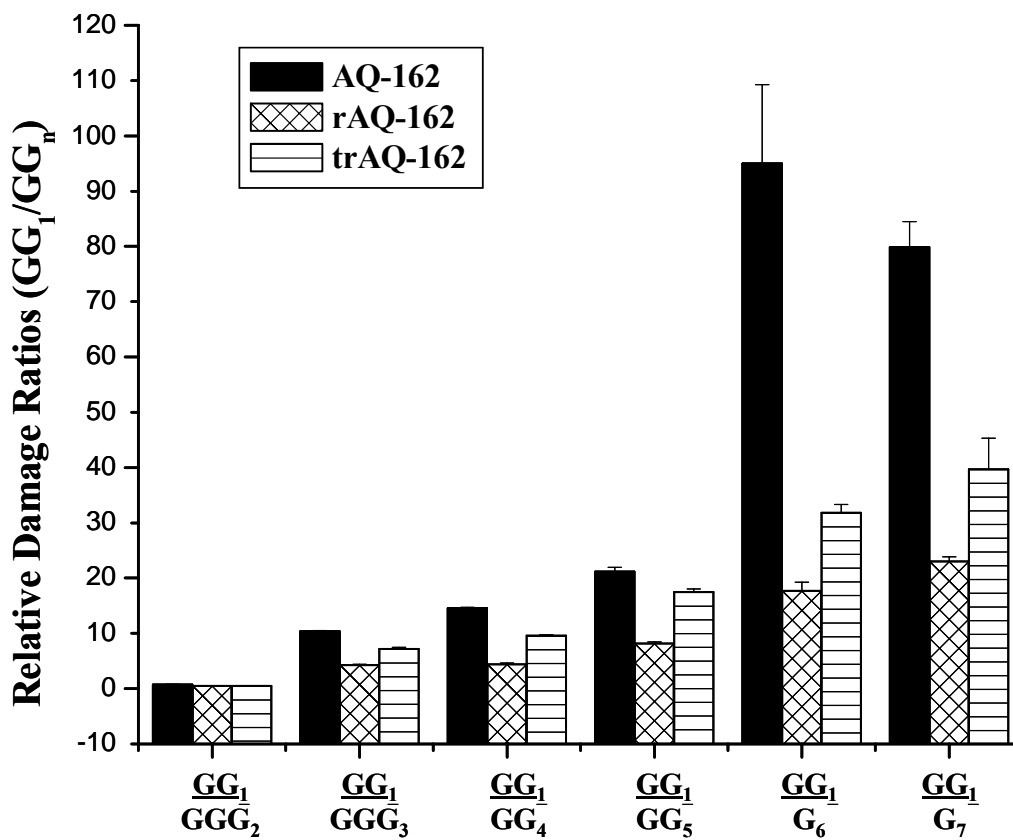
Figure 3.7: Quantification of relative damage ratios (GG_1/GG_n) from autoradiography of UV irradiated and Fpg treated AQ-162, rAQ-162, and trAQ-162.

Figure 3.8
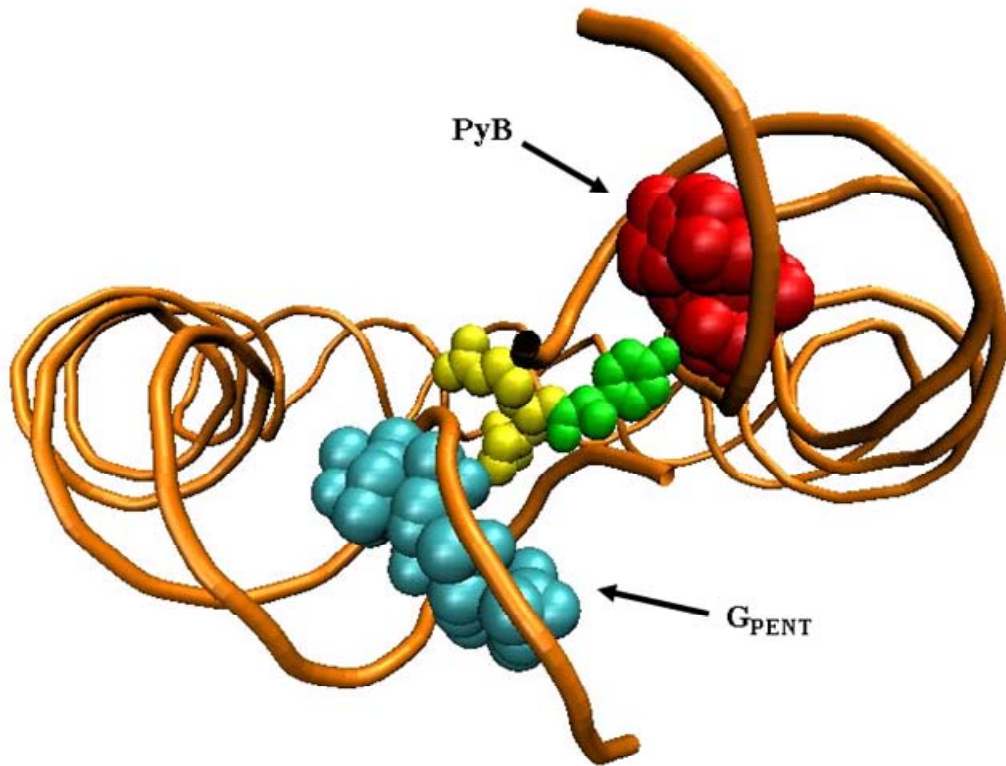
Figure 3.8: 601 DNA-H3 interface around PyB (red) and G_{PENT} (cyan). The sugar-phosphate backbone is colored orange. In between PyB and G_{PENT} is the H3Tyr41 (green), H3Leu42 (yellow), and H3Pro43 (yellow). This is the proposed structural model of interduplex DNA CT through the PyB region to the G_{PENT} via H3Tyr41.

References:

1.   Avkin, S.; Livneh, Z. *Mut. Res.* **2002,** 510, 81-90.

2.   Henderson, P. T.; Jones, D.; Hampikian, G.; Kan, Y.; Schuster, G. B. *Proc. Natl. Acad. Sci. USA* **1999,** 96, 8353-8.

3.   Hsu, G. W.; Ober, M.; Carell, T.; Beese, L. S. *Nature* **2004,** 431, 217-221.

4.   Cullis, P. M.; Malone, M. E.; Merson-Davies, L. A. *J. Am. Chem. Soc.* **1996,** 118, 2775-81.

5.   Kennedy, L. J.; Moore, K., Jr.; Caulfield, J. L.; Tannenbaum, S. R.; Dedon, P. C. *Chem. Res. Toxicol.* **1997,** 10, 386-92.

6.   Neeley, W. L.; Essigmann, J. M. *Chem. Res. Toxicol.* **2006,** 19, 491-505.

7.   Boon, E. M.; Barton, J. K. *Curr. Opin. Struc. Biol.* **2002,** 12, 320-329.

8.   Giese, B. *Ann. Rev. Biochem.* **2002,** 71, 51-70.

9.   Joy, A.; Schuster, G. B. *Chem. Comm.* **2005**, 2778-2784.

10.   Lewis, F. D.; Letsinger, R. L.; Wasielewski, M. R. *Acc. Chem. Res.* **2001,** 34, 159-170.

11.   Nunez, M. E.; Hall, D. B.; Barton, J. K. *Chem. Biol.* **1999,** 6, 85-97.

12.   Wolffe, A. P., *Chromatin Structure and Function*. ed.; Academic Press: San Diego, 1992;

13.   Hayes, J. J.; Tullius, T. D.; Wolffe, A. P. *Proc. Natl. Acad. Sci. USA* **1990,** 87, 7405-9.

14.   Nunez, M. E.; Noyes, K. T.; Barton, J. K. *Chem. Biol.* **2002,** 9, 403-415.

15.   Bjorklund, C. C.; Davis, W. B. *Nucleic Acids Res.* **2006,** 34, 1836-1846.

16.   Lowary, P. T.; Widom, J. *J. Mol. Biol.* **1998,** 276, 19-42.

17.   Gasper, S. M.; Schuster, G. B. *J. Am. Chem. Soc.* **1997,** 119, 12762-12771.

18.   Moyer, R.; Marien, K.; Van Holde, K.; Bailey, G. *J. Biol. Chem.* **1989,** 264, 12226-31.

19.   Prunell, A. *Biochemistry* **1983,** 22, 4887-94.

20.   Tullius, T. D.; Dombroski, B. A.; Churchill, M. E.; Kam, L. *Methods Enzym.* **1987,** 155, 537-58.

21.   Thastrom, A.; Lowary, P. T.; Widom, J. *Methods (San Diego, CA, United States)* **2004,** 33, 33-44.

22.   Davey, C. A.; Sargent, D. F.; Luger, K.; Maeder, A. W.; Richmond, T. J. *J. Mol. Biol.* **2002,** 319, 1097-1113.

23.   Armitage, B.; Schuster, G. B. *Photochem. Photobiol.* **1997,** 66, 164-170.

24.   Breslin, D. T.; Schuster, G. B. *J. Am. Chem. Soc.* **1996,** 118, 2311-19.

25.   Santhosh, U.; Schuster, G. B. *J. Am. Chem. Soc.* **2002,** 124, 10986-10987.

26.   Angelov, D.; Vitolo, J. M.; Mutskov, V.; Dimitrov, S.; Hayes, J. J. *Proc. Natl. Acad. Sci. USA* **2001,** 98, 6599-604.

27.   Bertin, A.; Leforestier, A.; Durand, D.; Livolant, F. *Biochemistry* **2004,** 43, 4773-4780.

28.   Fromme, J. C.; Verdine, G. L. *J. Biol. Chem.* **2003,** 278, 51543-51548.

29.   Morland, I.; Rolseth, V.; Luna, L.; Rognes, T.; Bjoras, M.; Seeberg, E. *Nucleic Acids Res.* **2002,** 30, 4926-4936.

30.   Pereira de Jesus, K.; Serre, L.; Zelwer, C.; Castaing, B. *Nucleic Acids Res.* **2005,** 33, 5936-44.

31.   Coste, F.; Ober, M.; Carell, T.; Boiteux, S.; Zelwer, C.; Castaing, B. *J. Biol. Chem.* **2004,** 279, 44074-83.

32.   Ames, B. N.; Shigenaga, M. K.; Hagen, T. M. *Proc. Natl. Acad. Sci. USA* **1993,** 90, 7915-22.

33.   Loh, K. P.; Huang, S. H.; De Silva, R.; Tan, B. K. H.; Zhu, Y. Z. *Curr. Alz. Res.* **2006,** 3, 327-337.

34.   Simmons, R. A. *Free Rad. Biol. Med.* **2006,** 40, 917-922.

35.   Singh, U.; Jialal, I. *Pathophysiology* **2006,** 13, 129-142.

36.   Wang, J.; Xiong, S.; Xie, C.; Markesbery, W. R.; Lovell, M. A. *J. Neurochem.* **2005,** 93, 953-962.

37.   Delaney, S.; Barton, J. K. *J. Org. Chem.* **2003,** 68, 6475-6483.

38.   Rajski, S. R.; Barton, J. K. *Biochemistry* **2001,** 40, 5556-5564.

39.   Williams, T. T.; Odom, D. T.; Barton, J. K. *J. Am. Chem. Soc.* **2000,** 122, 9048-9049.

40.   Arents, G.; Moudrianakis, E. N. *Proc. Natl. Acad. Sci. USA* **1993,** 90, 10489-93.

41.   Ausio, J.; Dong, F.; Van Holde, K. E. *J. Mol. Biol.* **1989,** 206, 451-63.

42.   Kornberg, R. D.; Lorch, Y. *Cell* **1999,** 98, 285-294.

43.   Widom, J. *Proc. Natl. Acad. Sci. USA* **1992,** 89,1095-9.

44.   Norman, D. G.; Grainger, R. J.; Uhrin, D.; Lilley, D. M. *Biochemistry* **2000,** 39, 6317-24.

45.   DeFelippis, M. R.; Murthy, C. P.; Broitman, F.; Weinraub, D.; Faraggi, M.; Klapper, M. H. *J. Phys. Chem.* **1991,** 95, 3416-19.

46.   Steenken, S.; Jovanovic, S. V. *J. Am. Chem. Soc.* **1997,** 119, 617-618.

47.   Wagenknecht, H.-A.; Stemp, E. D. A.; Barton, J. K. *Biochemistry* **2000,** 39, 5483-5491.

48.   Davis, W. B.; Naydenova, I.; Haselsberger, R.; Ogrodnik, A.; Giese, B.; Michel-Beyerle, M. E. *Angew. Chemie Int. Ed.* **2000,** 39, 3649-3652.

49.   Saito, I.; Nakamura, T.; Nakatani, K.; Yoshioka, Y.; Yamaguchi, K.; Sugiyama, H. *J. Am. Chem. Soc.* **1998,** 120, 12686-12687.

50.   Voityuk, A. A.; Jortner, J.; Bixon, M.; Rosch, N. *Chem. Phys. Lett.* **2000,** 324, 430-434.

51.   Odom, D. T.; Dill, E. A.; Barton, J. K. *Nucleic Acids Res.* **2001,** 29, 2026-2033.

52.   Santhosh, U.; Schuster, G. B. *Nucleic Acids Res.* **2003,** 31, 5692-5699.

53.   Li, G.; Widom, J. *Nat. Struc. Mol. Biol.* **2004,** 11, 763-769.

54.   Giese, B. *Acc. Chem. Res.* **2000,** 33, 631-6.

55.   Lewis, F. D.; Liu, X.; Liu, J.; Miller, S. E.; Hayes, R. T.; Wasielewski, M. R. *Nature* **2000,** 406, 51-53.

56.   Burrows, C. J.; Muller, J. G. *Chem. Rev.* **1998,** 98, 1109-1151.

57.   Spassky, A.; Angelov, D. *Biochemistry* **1997,** 36, 6571-6576.

58.   Beard, B. C.; Wilson, S. H.; Smerdon, M. J. *Proc. Natl. Acad. Sci. USA* **2003,** 100, 7465-7470.

CHAPTER IV

STABLE DNA-PROTEIN CROSS-LINKS ARE PRODUCTS OF DNA CHARGE

TRANSPORT IN THE NUCLEOSOME CORE PARTICLE

ABBREVIATIONS

AQ, anthraquinone; bp, base pairs; CT, charge transport; DPC, DNA-protein cross-link; EMSA, electrophoretic mobility shift assay; ExoIII, Exonuclease III; $G^{\bullet+}$, guanine radical cation; NCP, nucleosome core particle; $OH^{\bullet}$, hydroxyl radical; PyB, pyrimidine band; rNCP, reconstituted nucleosome core particle; H3Tyr41, histone H3 tyrosine 41

SUMMARY

DNA-protein cross-links (DPCs) in chromatin are expected to impair processes like chromatin remodeling, transcription, DNA replication and epigenetic marking. In this manuscript we establish that long-range DNA charge transport (CT) reactions can lead to DPC formation in the nucleosome core particle (NCP), the fundamental building block of chromatin. Our model substrates are NCPs reconstituted with DNA containing the 601 NCP positioning sequence, and DNA CT is initiated by irradiation of a covalently-attached Anthraquinone photooxidant. Using a combination of experimental techniques we establish that Histone H3, but not Histones H2A, H2B, and H4, is involved in these DPCs, and present evidence that H3Tyr41 is a key residue in DPC formation. Since the majority of these DPCs possess a half life >48 hours at 37°C, cells may be forced to deal with stable DNA-histone cross-links buried in chromatin arising from oxidative stress.

INTRODUCTION

Aberrant intracellular oxidation is a ubiquitous problem for aerobic organisms. While oxidative stress is a recognized contributor to human disorders like diabetes[1], atherosclerosis[2], and cancer[3], its effects are manifested at the cellular level as damage to macromolecular assemblies. The attack of oxidizing agents on DNA leads to a vast spectrum of mutagenic products including oxidized nucleobase lesions, sugar damage, single and double strand breaks, and DNA-DNA cross-links.[4] In addition to these lesions, the oxidation of proteins and/or DNA can lead to the formation of DNA-protein cross-links (DPCs). A wide variety of nuclear proteins have been identified in DPCs, including actin and other nuclear scaffolding proteins, heat shock proteins, and transcription factors.[5] Intuitively, DPCs in eukaryotic cells commonly involve the proteins bound to DNA in chromatin structures.[5-9] The most abundant of these proteins are the histones H2A, H2B, H3, and H4 which form the octameric protein core of the nucleosome core particle (NCP). Given i) the importance of the histone proteins in cellular processes like chromatin packaging, transcriptional regulation, and DNA repair, and ii) the propensity of histones to cross-link to DNA, it is surprising that there exist very few reports which describe the oxidation chemistry leading to DNA-histone cross-links[10, 11] and no reports of the exact molecular sites of DPC formation within oxidized chromatin structures.

A recently recognized source of cross-links between DNA and amino acids in either bound peptides[12, 13] or randomly associated proteins[14] are reactions initiated by the generation of a guanine radical cation ($G^{\bullet+}$). Unlike other radicals formed in DNA, the reaction of a $G^{\bullet+}$ with protein residues does not require an oxidant to attack the DNA

proximal to the DNA-protein binding site. In fact, the initial oxidation can occur up to 200 Å away[15, 16] from the DNA-protein interface and still potentially lead to DPC formation. This expectation arises from one of the best studied properties of $G^{\bullet+}$–the propensity for oxidized guanines to lead to long-range DNA charge transport (CT) in naked duplex DNA structures[17-20], and DNA-protein complexes[17, 21, 22]. DNA CT is initiated by the removal of an electron from DNA and usually leads to the formation of a $G^{\bullet+}$ since G is the site of lowest oxidation potential in DNA.[23] The initially formed $G^{\bullet+}$ can next undergo an electron transfer reaction with a neighboring G residue to move the electron deficient site along the DNA chain. DNA CT doesn't continue indefinitely because of direct competition between the rates of inter-guanine electron transfer and the rates of reactions between $G^{\bullet+}$ and H_2O or O_2. These latter reactions halt DNA CT and lead to the formation of guanine oxidative lesions like 8-oxguanine. In summary, DNA CT typically leads to a steady state distribution of guanine oxidative lesions radiating outward from the site of initial oxidation.

To date, the involvement of DNA CT reactions in DPC formation in chromatin substrates has not been established. Given i) the propensity of the histone proteins in NCPs to form DPCs in vivo and in vitro, and ii) the ability of DNA CT to progress through the DNA-protein contact regions of the core histone octamer[21, 24], we decided to look for evidence of DPC formation during DNA CT in reconstituted NCPs (rNCPs). To initiate DNA CT we chose to use a well-characterized[19] Anthraquinone (AQ) photooxidant (Figure 4.1a). AQ was covalently attached to the 5'-terminus of a DNA duplex incorporating the 601 NCP positioning sequence, a DNA sequence known for forming thermodynamically stable NCPs[25], and occupying one well-defined position on

the surface of a NCP[26]. In this manuscript we present evidence that DNA CT in rNCPs

containing the 601 sequence does indeed lead to DNA-histone cross-linking.

Furthermore, our data provide a molecular understanding of where and how DPCs arise

in chromatin structures because of DNA oxidative damage.

MATERIALS AND METHODS:

601 DNA Construction

The 161 bp DNA duplexes **AQ-601** and **NH$_2$-601** (Figure 4.1c) were prepared

using PCR reactions on a pGEM-3z (Promega) plasmid containing the 601 nucleosome

binding sequence (Dr. Lisa Gloss, WSU). The two forward primers **AQ-F** (**AQ-5'-TAT**

ACG CGG CCG CCC TGG -3') and **NH$_2$-F (NH$_2$-(CH$_2$)$_6$-5'-TAT ACG CGG CCG**

CCC TGG -3') and one reverse primer **601-R (5'-CAC AGG ATG TAT ATA TCT**

GAC AC -3') were synthesized at WSU on an ABI Applied Biosystems 380B DNA

synthesizer. **NH$_2$-F** was synthesized using a monomethoxytrityl-protected amino linker

phosphoramidite (Glen Research), while **AQ-F** was modified at the 5'-terminus by a

previously described anthraquinone phosphoramidite[27]. After synthesis, the primers were

deprotected in NH$_4$OH (55°C overnight), purified by RP-HPLC on a Waters 2690 system

equipped with a 996 photodiode array detector and a C18 RP column (Hichrom), and

lyophilized. Primer **AQ-F** was resuspended in water and subjected to ethanol

precipitation, while primers **601-R** and **NH$_2$-F** were detritylated in 80% acetic acid for 30

minutes and ethanol precipitated.

PCR reactions were performed using the Elongase Enzyme PCR mix (Invitrogen)

on a Biometra personal PCR cycler (Biotron). Primers **AQ-F** and **601-R** were used for

AQ-601, and primers **NH₂-F** and **601-R** were used for **NH₂-601**. The desired 161 bp PCR products were purified using preparative scale 3% agarose gels. **AQ-601** and **NH₂-601** were ^{32}P-labeled at their free 5'-termini by incubation with T4 Polynucleotide Kinase (New England Biolabs) and [α-^{32}P]-ATP (Perkin Elmer; 5 mCi/mL, 3000 Ci/mmol specific activity) for 1 hour at 37°C. After chloroform/phenol extraction, the radiolabeled 601 constructs were purified using Probe Quant G50 spin columns (Amersham) followed by ethanol precipitation.

Nucleosome Core Particle Reconstitution.

Chicken Erythrocyte Nucleosome Core Particles (NCPs), devoid of avian linker histones H1 and H5, were isolated from chicken erythrocytes (Lampire Biologicals) using a previously reported protocol[28]. The integrity of the histones was confirmed by 18% (30:0.5 acrylamide:bis) SDS-PAGE analysis before the NCPs were utilized. Individual reconstitutions of ^{32}P-labeled **AQ-601** and **NH₂-601** into NCPs (**rAQ-601** and **rNH₂-601** respectively) were performed as described[21]. Briefly, native NCPs and ^{32}P-labeled DNA were mixed in 1M NaCl at a 50:1 ratio. Several dialysis steps at decreasing salt concentrations (600 mM, 200 mM, 10 mM) were carried out. NCP reconstitution efficiency was assessed by running 6% native PAGE EMSAs. Dried gels were placed into phosphorimaging cassettes (Amersham), and the EMSAs analyzed by autoradiography using a 445 SI Phosphorimager (Molecular Dynamics) and ImageQuant software (Molecular Dynamics).

ExoIII and Hydroxyl Radical Footprinting.

ExoIII and OH$^\bullet$ footprinting reactions were used to assess the DNA translational and DNA rotational setting, respectively, in **rNH$_2$-601** and **rAQ-601**. For ExoIII footprinting, either free DNA or rNCPs were incubated with one unit of ExoIII at 37 °C for 3 minutes. The reaction was stopped by the addition of an equal volume of phenol/chloroform, and the DNA ethanol precipitated using glycogen as a carrier. In the case of OH$^\bullet$ footprinting, Fe-EDTA (20 µM), 0.3% H$_2$O$_2$, and sodium L-ascorbate (1 mM) were mixed with either free DNA or rNCPs in 100 µL total volume, and the reactions incubated at room temperature for 1 min for free DNA or 10-12 min for the rNCPs. The reactions were stopped by the addition of 40 mM EDTA and 7 mM thiourea. The samples were next subjected to phenol/chloroform extraction followed by ethanol precipitation in the presence of glycogen. The reaction products were run on 7 M urea, 6% PAGE sequencing gels, and analyzed using autoradiography.

UV-Irradiation and Assessment of DNA Oxidative Damage

100 µL DNA or rNCP samples (10 mM sodium phosphate; pH 7.0) were irradiated for 60 minutes at room temperature using a Luzchem photoreactor (Luzchem Research) equipped with 10 UV-A lamps (0.3 mW/cm^2 each; 300-390 nm emission). Next, the samples were briefly heated to 90˚C, extracted with phenol/chloroform, and ethanol precipitated in the presence of glycogen. Both irradiated and non-irradiated samples were then dissolved in 10% piperidine and incubated at 90˚C for 30 min. The treated DNA was dried under reduced pressure, washed and dried twice with ddH$_2$O, followed by suspension in formamide loading buffer and electrophoresis on 6%

acrylamide, 7 M urea sequencing gels. After drying, the gels were analyzed by autoradiography.

Phenol Partitioning

Samples of **rNH2-601** and **rAQ-601** were irradiated for varying lengths of time (0, 15, 30, 45, or 60 minutes). After irradiation, each sample was immediately mixed with an equal volume of phenol/chloroform, vortexed for 15-30 seconds, and centrifuged for 3 min at 14,000 RPM on a microcentrifuge. The aqueous layer was carefully removed and the organic layer was extracted two more times using equal volumes of 10mM sodium phosphate (pH 7.0). The amount of DNA in the organic and combined aqueous phases was quantified by Cerenkov counting. The yield of DPCs (Y_{DPC}) was determined by calculating the percentage of Cerenkov counts in the organic phase of each reaction, i.e., Y_{DPC} = (organic cpm)/(organic cpm + aqueous cpm). Finally, each Y_{DPC} value was normalized by subtracting the value calculated for a non-irradiated, but otherwise identical rNCP sample.

SDS-PAGE EMSAs

Irradiated and non-irradiated rNCP samples were lyophilized using a speed vac. The dried pellets were then resuspended in 6 μL of 2% SDS and incubated at 50ºC for 1-2 hours. The samples were mixed with a glycerol-based SDS loading buffer and electrophoresed on 18% acrylamide (30:0.5) SDS-PAGE gels. The resulting wet gels were analyzed by autoradiography.

Western Blot Analysis

Wet SDS-PAGE EMSA gels were transferred to a nitrocellulose membrane by electrophoresing the gel sandwich at 200 mA constant current in western transfer buffer (12.5mM Tris, 125 mM Glycine, 0.1% SDS, 20% methanol pH 8.3). After blocking the membrane with 10% milk-phosphate buffered saline-0.05% Tween-20 (milk-PBST) for one hour at room temperature, the membrane was incubated with primary (rabbit serum) anti-histone antibody (Upstate; 1:5000 dilution) in milk-PBST overnight at 4ºC with slight agitation. The membrane was next washed with PBST (5x, 10 min, each), followed by incubation with HRP conjugated goat-anti-rabbit secondary antibody (Upstate; 1:25000 dilution) for 1 hr at room temperature with agitation. After washing the membrane with PBST, chemiluminescent detection of the histone proteins was carried out using an ECL-kit (Pierce) and Omat X-Blue autoradiography film (Kodak).

Determination of DNA-Protein Cross-link Lifetime

rAQ-601 samples were irradiated for 60 min at room temperature and immediately placed in a 37°C dry heating block. After 0, 1, 3, 24, and 48 hours, an aliquot was removed from the NCP sample and mixed with an equal volume of phenol/chloroform. The aqueous and organic layers were separated, the organic layer washed twice with 10mM sodium phosphate (pH 7.0), and the washes combined with the initial aqueous extraction. The organic and aqueous fractions were subjected to scintillation counting (Cerenkov) and Y_{DPC} was calculated at each time point as described in the phenol portioning assay. The percent of cross-links remaining at each time point

was calculated using the equation % DPC remaining = $Y_{DPC}(t = x\ hr) / Y_{DPC}(t = 0\ hr) \times$ 100%, where $Y_{DPC}(t = x\ hr)$ is the Y_{DPC} value observed at x hours of incubation at 37°C.

RESULTS

Preparation and NCP Reconstitution of AQ-601 and NH₂-601 duplexes

The 162 base pair (bp) duplexes **AQ-601** and **NH₂-601** (Figure 4.1c) were PCR amplified from a pGEM-3z plasmid harboring the 601 sequence[25] using forward primers 5'-modified by an AQ photooxidant and a NH_2-$(CH_2)_6$ linker, respectively. **NH₂-601** serves as a control duplex in these studies since the amino link is similar in size to AQ but will not undergo any UV-A induced photochemical reactions with DNA. **AQ-601** and **NH₂-601** include the 147 bp 601 NCP binding sequence[29], a 14 bp DNA overhang proximal to the 5'-modifications, and a one bp overhang at the unmodified end. We designed the 14 bp overhang to i) initiate photooxidation in a region that models B-form linker DNA, and ii) to minimize unwanted hydrophobic interactions between AQ and the histone octamer. After PCR and gel purification (Figure 4.2a), the reverse primer strand in each duplex was 5'-labeled with ^{32}P.

^{32}P-labeled **AQ-601** and **NH₂-601** were individually reconstituted onto purified chicken erythrocyte NCPs using a previously published salt-dependent dialysis protocol.[21] The reconstitution efficiencies of **AQ-601** and **NH₂-601** were assessed using electrophoretic mobility shift assays (EMSA; Figure 4.2b) which consistently showed that >95% of the free DNA was incorporated into NCPs to form **rAQ-601** (reconstituted **AQ-601**) and **rNH₂-601**. Next, we structurally characterized **rAQ-601** and **rNH₂-601** by performing ExoIII and OH• footprinting assays.[30, 31] The footprinting results for **AQ-601**

126

and **rAQ-601** are shown in Figure 4.2c, and data not shown for **NH$_2$-601** and **rNH$_2$-601** is identical to that in Figure 4.2c. The net conclusion we draw from these footprinting experiments is that the structures of **rAQ-601** and **rNH$_2$-601** are indistinguishable from one another because 1) in both **rAQ-601** and **rNH$_2$-601** we observe that the 147 bp 601 NCP positioning sequence is in contact with the histone octamer and the 14 bp proximal to AQ and the amino link are not associated with protein, and 2) there is an identical ~10 bp periodicity of OH$^\bullet$ cleavage in both **rAQ-601** and **rNH$_2$-601**, indicating that the DNA rotational position is the same in both rNCPs. Furthermore, the AQ photooxidant must interact with the DNA through end capping[27] since its presence does not lead to changes in the DNA footprinting. By combining the results of our footprinting reactions with the NCP crystal structure of Davey et al.[32] (PDB# 1KX5) we have produced the structural model of our rNCPs shown in Figure 4.3a. Not shown in this structural model are the 14 bp overhang and AQ photooxidant.

DNA Oxidative Damage in UV-Irradiated AQ-601 and rAQ-601

UV-A irradiation of AQ-modified DNA duplexes typically results in the formation of a steady state distribution of guanine oxidative lesions arising from the interplay of i) DNA hole hopping reactions leading to the migration of the guanine radical cation (G$^{\bullet+}$), and ii) reactions of G$^{\bullet+}$ with H$_2$O or other trapping reagents to form irreversible lesions (Figure 4.1b). Treatment of these guanine lesions with agents like piperidine leads to a strand break at each oxidized site. Irradiation of **AQ-601**, followed by treatment with hot piperidine results in the guanine oxidation spectrum shown in Figure 4.4. Transfer occurs over 42 bp (~150 Å) in naked 601 DNA to site G7 (our

127

nomenclature for the guanine oxidation sites is in Figure 4.1c). As controls, neither unirradiated, piperidine treated **AQ-601** (Figure 4.4) nor irradiated, piperidine-treated **NH₂-601** (Figure 4.5) show any piperidine-induced strand breaks. Therefore we conclude that DNA oxidation in **AQ-601** arises solely from the photoexcitation of AQ and the ensuing DNA CT.

After the irradiation and subsequent piperidine treatment of **rAQ-601** (Figure 4.4), we observe a similar spectrum of guanine oxidation sites as in **AQ-601**. There is a slight increase in the mobility of the **rAQ-601** piperidine cleavage products on this denaturing PAGE gel, however this effect is not reproducible between replicate gels. Therefore, we assign this difference in mobility to a gel artifact which has been observed before in previous studies utilizing chicken erythrocyte rNCPs[21]. After accounting for the gel shift, it can be observed that the same guanine residues are oxidized in both **AQ-601** and **rAQ-601**, and DNA CT extends from AQ to G7 in both systems. We will report a full analysis of the differences in the yields of guanine oxidative lesions between **AQ-601** and **rAQ-601** in a forthcoming manuscript.

We now turn our focus in this report to the major difference between the naked DNA and rNCPs—the presence of a unique piperidine-labile band in irradiated **rAQ-601** (PyB, Figure 4.4). This band is named PyB for Pyrimidine Band, since it does not correlate with any of the bands arising from Maxam-Gilbert G or G+A sequencing. In particular, it arises somewhere in the pyrimidine tract of **AQ-601** indicated in Figure 4.1c and it lies between 5-8 bp into the nucleosome according to Figure 4.3a. Since PyB always appears diffuse on our DNA sequencing gels, we suspect that this damage is inhomogeneous and arises from DNA lesions at several neighboring pyrimidine sites.

The appearance of PyB is completely correlated with the formation of guanine oxidation products in **rAQ-601**, and does not appear in piperidine treated, UV irradiated **rNH₂-601** samples (Figure 4.5). In contrast to the guanine oxidation lesions normally observed during DNA CT, PyB is not strictly a piperidine-labile lesion since it also appears in samples heated to 90°C in the absence of piperidine (data not shown). The trapping of radical cations at pyrimidines during DNA CT is not normally observed since the oxidation potential of C and T are much higher than G.[23] Even though C (and by inference T) has been shown to be transiently oxidized during DNA CT[33], irreversible, piperidine-sensitive pyrimidine oxidation products are only observed in the absence of guanines.[34] Since the formation of an oxidized pyrimidine lesion seemed an unlikely origin for PyB, we were forced to consider the possibility that DNA damage other than oxidized nucleobases is being generated in irradiated **rAQ-601**. Due to the intimate contact between the DNA and histones in **rAQ-601**, we decided to investigate the possibility that PyB might correspond to DPCs arising from long-range DNA CT.

Our first interrogation was through phenol partioning experiments on irradiated **rNH₂-601** and **rAQ-601** samples. The time course of DPC yields (Y_{DPC}) measured in these experiments are shown in Figure 4.6. In **rAQ-601**, Y_{DPC} increases from background levels to plateau around 35% after 30 minutes of irradiation. The results of control reactions with irradiated **rNH₂-601** indicate that even after 60 minutes Y_{DPC} stays near background levels in these samples. We conclude from these experiments that covalent cross-linking between the DNA and one or more histone proteins occurs during the course of DNA CT in **rAQ-601**.

Visualization of DPCs through SDS-EMSAs and Western Blotting

Although the phenol partitioning experiments are consistent with the formation of DNA-protein cross-links in irradiated **rAQ-601**, the identity of the histones involved cannot be determined using this methodology. Therefore, we turned to denaturing EMSAs (SDS-EMSA) coupled with Western Blotting to further interrogate the nature of the DNA-histone cross-linking reactions. In SDS-EMSAs, any DNA-histone cross-linked complexes are expected to give rise to ^{32}P-containing bands which migrate slower through the gel than the native 601 DNA. We found it necessary to utilize protein denaturing EMSAs in these experiments because of the strong non-covalent interactions between DNA and the histone proteins. Also, we took care to make sure that samples were maintained at temperatures less than 50°C during all manipulations since PyB appears after heating irradiated **rAQ-601** samples to 90 °C. Figure 4.7a shows autoradiographs of SDS-EMSAs for **NH₂-601**, **AQ-601**, **rNH₂-601**, and **rAQ-601** in the absence and presence of UV irradiation. Only in the case of irradiated **rAQ-601** are there higher molecular weight ^{32}P-labeled products observed by autoradiography.

To identify the histone proteins involved in these DNA-protein cross-links, we performed Western Blotting on replicate **rAQ-601** SDS-EMSA gels using anti-H2A, anti-H2B, anti-H3, and anti-H4 polyclonal antibodies (Figure 4.7b). In the Westerns of all four histones, there is a band which appears at a location separate from any ^{32}P-labeled DNA (Figure 4.7a) in the non-irradiated **rAQ-601** samples. We assign this band to the non-covalently bound histone monomers. In the blot of Histone H3 for non-irradiated **rAQ-601** samples, there is an additional, slower migrating band which does not overlap with ^{32}P-labeled DNA in the non-irradiated **rAQ-601** SDS-EMSA. Since H3 is the only

histone containing a Cys residue (Cys110) we assign this second band to a histone dimer arising from the formation of disulfide linkages. In the irradiated **rAQ-601** sample we observe a novel histone band corresponding to Histone H3, along with a slight increase in intensity near the H3 dimer band. Both of these new H3 bands overlap with the higher migrating ^{32}P-containing bands in Figure 4.7a. From these results, we conclude that DNA CT in a NCP can directly result in the formation of DNA-H3 cross-links.

Lifetime of H3-DNA cross-links at 37°C

Having established the presence of H3-DNA cross-links in irradiated **rAQ-601** samples, we next turned our attention to the stability of these lesions. Previous reports on DPC stability have placed their in vivo lifetime from hours[35] to days[36]. To see how the DNA-H3 lesions in this study compare, we took duplicate **rAQ-601** samples and incubated them at physiological temperature for varying lengths of time. After incubation, the samples were subjected to the phenol partitioning assay and the percentage of DPCs remaining as a function of time was determined. Figure 4.8 shows the stability of the H3-DNA lesions over a 48 hour time window. During the first hour we observe a decrease in the amount of DPCs remaining, followed by little, if any decrease over the next 48 hours. The apparent biphasic nature of the curve indicates the existence of multiple types of cross-linking, consistent with the SDS-EMSA and Western Blot analyses. Since the majority of these DNA-H3 cross-links are stable for days at 37 °C, we hypothesize that during oxidative stress most eukaryotic cells will have to contend with extremely stable DNA-protein cross-links buried in chromatin arising from DNA CT.

DISCUSSION

The studies reported here demonstrate that the one-electron oxidation of DNA can lead to the formation of DNA-histone cross-links within chromatin structures. In particular, we have found evidence for histone H3-pyrimidine cross-links using several different experimental techniques including SDS-EMSA, Western Blotting, Phenol Partitioning, and the visualization of DNA damage products on sequencing gels. Because of the phenomenon of long-range charge transport in DNA, the initial oxidation event leading to DNA-histone cross-linking does not have to take place within a NCP but can be initiated within the more accessible linker DNA regions. There are many reactions which could lead to the formation of oxidized DNA nucleobases in chromatin. As one example, Giese and coworkers[37] have shown that C4' radicals, which can be formed by reagents such as $OH^\bullet$ and bleomycin[38], are capable of oxidizing neighboring nucleobases. However, the drawback to using typical DNA oxidants like $OH^\bullet$ in studies of DNA oxidation is their multiple reaction pathways. Therefore, we have utilized the simpler, and better understood, DNA oxidation chemistry initiated by an AQ photooxidant covalently appended to the DNA in our model NCP substrates.

To ensure that the chemistry we are observing arises from DNA oxidation and not direct protein oxidation, we have designed DNA constructs which possess three structural elements. The first is the utilization of the 601 NCP binding sequence, the second is the use of a DNA end-capping AQ photooxidant, and the third is the placement of a 14 bp DNA linker between AQ and the 601 NCP start site. $OH^\bullet$ and ExoIII footprinting reactions show that the histone octamer is indeed positioned on the 601 sequence in **rAQ-**

132

601, and that AQ lies at the end of a 14 bp overhang which has minimal, if any, contact with the histones. As further evidence for the lack of random AQ-histone or AQ-DNA association, we have manipulated the DNA linker length between AQ and the entrance to the NCP from 10-20 bp and not observed any difference in the relative yields of G oxidation products and PyB (data not shown). Therefore DNA-H3 cross-linking does not arise from spurious interactions between the AQ photooxidant and either the DNA or the histone proteins comprising the core particle.

There are several pieces of evidence in our data which point towards a 1:1 correspondence between PyB and the DNA-H3 cross-links in irradiated **rAQ-601**. By comparing the location of PyB in the **AQ-601** sequence (Figure 4.1c) and the structural model of Figure 4.3a we predict that PyB lies in a region 5-8 bp into the NCP. Immediately striking is that the PyB sequence is therefore in contact with histone H3, the only histone found cross-linked in the Western blots. Additionally, PyB is in contact with the H3 core domain and not the H3 tail, consistent with our observation that the removal of the H3 N-terminal tail by trypsin did not affect the formation of PyB (data not shown). One unique feature of the DNA-H3 contacts in the PyB region of **rAQ-601** is that the phenol side chain of H3Tyr41 is in close contact with the DNA minor groove surface (Figure 4.3b). This expectation comes from i) our model of **rAQ-601** (Figure 4.3), and ii) a previous study[39] showing that H3Tyr41 does not react with *p*-nitrobenzenesulfonyl fluoride in calf thymus NCPs at our salt concentration. The recognition that H3Tyr41 is so arranged allows us to formulate the proposed model for the origin of DNA-Histone H3 cross-linking shown in Figure 4.9.

In Step 1, photoexcitation of AQ initiates DNA CT. The observation that there are no photoproducts in **rNH$_2$-601** indicates that the AQ photooxidant, and by default the accompanying DNA CT reactions, are absolutely required for DNA-H3 cross-linking. Once initiated DNA CT in the 601 sequence leads to the formation of a G$^{\bullet+}$ neighboring H3Tyr41. From Figure 4.1c sites GG$_{1*}$ and G$_{2*}$ on the AQ-modified strand are located at or near the location of PyB. Their oxidation during DNA CT is almost certain since we observe guanine oxidation products out to site G7 in the rNCPs. Step 2 involves the oxidation of H3Tyr41 by a neighboring G$^{\bullet+}$. Several lines of evidence support this proposed reaction. First, the oxidation potentials of Tyr (E_{ox} = 0.94 V vs. NHE)[40] and G (E_{ox} = 1.3 V vs. NHE)[41] make the redox reaction G$^{\bullet+}$ + Tyr-OH $\rightarrow$ G + Tyr-O$^{\bullet}$ + H^{+} spontaneous. Second, electron transfer reactions between G$^{\bullet+}$ and bound amino acids have been observed in small peptides containing Trp[13] (E_{ox} = 1.0 V vs. NHE)[40] and Tyr[13] providing precedence for the proposed oxidation of H3Tyr41. Finally, during Step 3 the H3Tyr41 radical attacks the neighboring DNA to form H3-DNA cross-links. Previous investigations of DNA oxidation in short oligomers bound to tripeptides[13], and chromatin[42] have found that tyrosine radicals formed in proximity to DNA can form covalent adducts with T and C. Using GC-MS, these adducts were characterized as having a carbon-carbon bond arising from attack of the tyrosyl radical on the pyrimidine 5-6 double bond[10, 11]. These Tyr-pyrimidine lesions are extremely stable at physiological temperatures *in vivo* since it takes 19 days for their levels to return to background in the renal cells of ferric nitrilotriacetate-treated Wistar rats[36]. This stability is consistent with the long half life of the majority of the DNA-H3 adducts at 37°C in Figure 4.6. This much said, the SDS-EMSAs, Western Blots, and the biphasic kinetics of cross-link

stability at 37°C all indicate that there is at least one more type of DNA-protein cross-link present in irradiated **rAQ-601**. Histone H3 makes contact with the first 1.5 turns of the 601 sequence on the surface of the NCP according to Figure 4.3, and cross-linking at other DNA or protein sites could also contribute. For instance, there is the potential that cross-linking reactions between oxidized pyrimidines[10] and/or oxidized purines[12] and the Lysine residues in H3 are also present.

There are three significant impacts of this research on the study of DNA-protein cross-linking during times of cellular oxidative stress. First, this study bridges two previously disparate literature observations; i) treatment of cells by low dose IR leads to the cross-linking of the core histones to DNA[5, 8], and ii) a common cross-linking chemistry involves the covalent attachment of Tyr to C or T residues in chromatin[10, 11]. Our observation of DNA-H3 cross-linking in response to DNA CT is one missing link needed to round out the picture of DPC formation in chromatin structures. Second, since H3Tyr41 appears to be involved in the histone-DNA cross-links observed in 601 DNA, many known genomic NCP binding sequences are also expected to be susceptible to DPC formation. In a recent study Segal et al.[43] report a genomic code for NCP positioning which is consistent with a majority of the currently known NCP binding sequences in eukaryotic organisms. If one maps their DNA positioning code onto the NCP crystal structure[32], their data predict that the base pairs around H3Tyr41 are not expected to be relatively G-poor as compared to the rest of the generic NCP positioning sequence. Therefore the vast majority of human NCPs are predicted to be susceptible to DNA-H3 cross-linking arising from DNA CT and other forms of oxidative stress. Furthermore, this raises the possibility for i) the existence of genomic hot-spots for DNA-histone cross-

linking, and ii) a dynamic nature to these hot-spots arising from chromatin remodeling events accompanying, e.g., cell cycle progression and transcriptional regulation. The third and final impact of this study is that the consequences of these chromatin lesions to the eukaryotic cell, and even the full repair mechanisms for DNA-histone cross-links[44, 45], are currently uncertain and remain to be delineated. We feel that the cross-links in **rAQ-601** can be optimized to generate model substrates for studying the effects of chromatin-based DPCs on nuclear events.
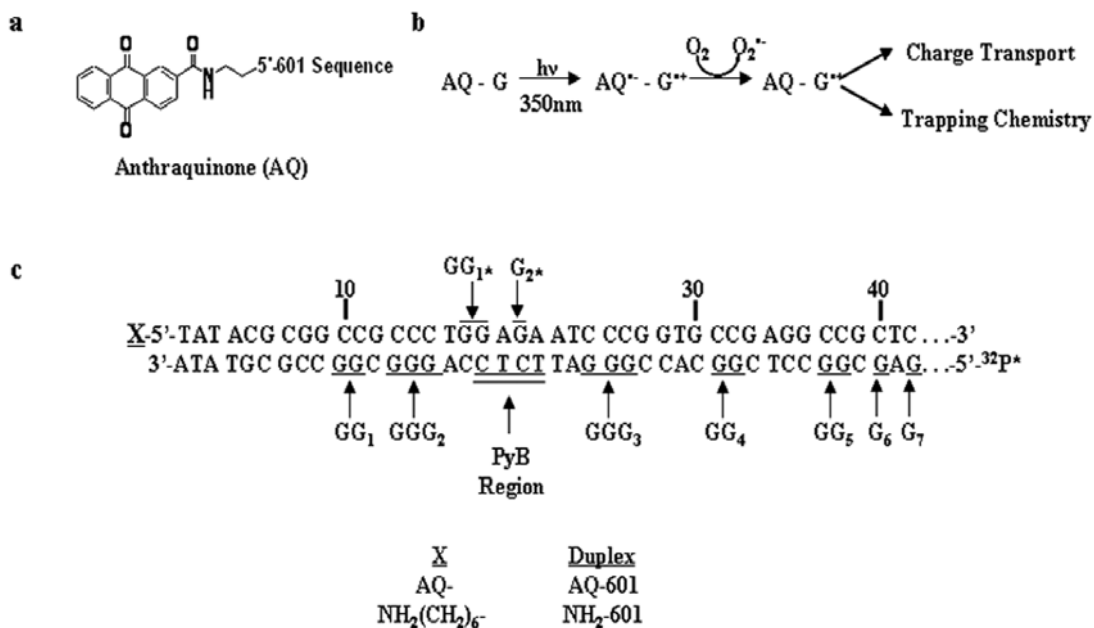
Figure 4.1

Figure 4.1: Overview of the AQ photooxidant, UV-A induced DNA CT, and the 601 DNA duplexes used in this study. (a) Structure of AQ and its covalent attachment to DNA. (b) The normal dynamics of DNA CT in AQ-modified DNA. Selective excitation of AQ with UV-A light leads to photoinduced electron transfer from a neighboring nucleobase. Next, charge liberation occurs via oxidation of $AQ^{\bullet-}$ by O_2. At this point $G^{\bullet+}$ can either be trapped to yield guanine lesions, or initiate charge transport. (c) Sequence of the 601 DNA duplex oxidized in these studies. The observed G oxidation sites ($GG_1 - G_7$) and PyB region on the ^{32}P-labeled strand are indicated, as are the G residues (GG_{1*} and G_{2*}) near PyB on the AQ-modified strand.
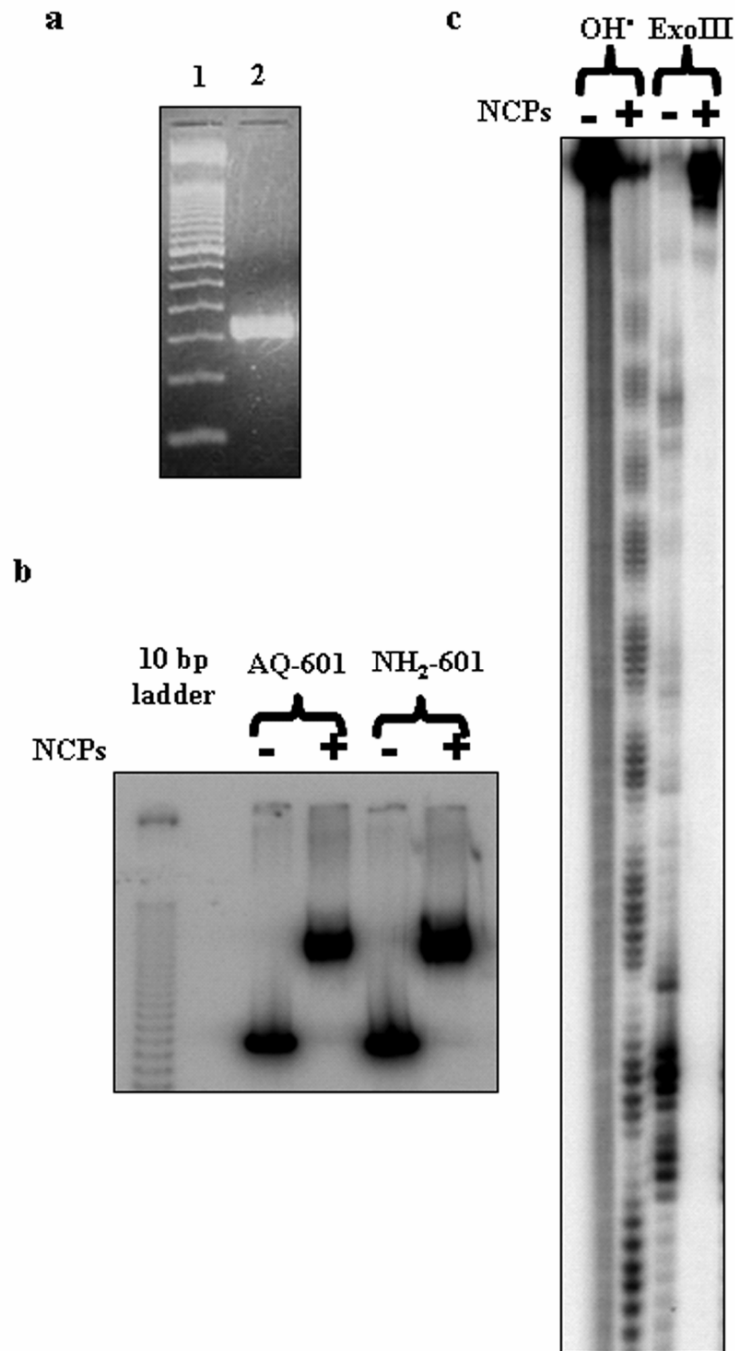
Figure 4.2

Figure 4.2: (a) 3% agarose gel showing the result of a PCR reaction of the pGEM-3z clone to generate the AQ-601 construct. (b) EMSA showing the reconstitution efficiencies of AQ-601 and NH2-601 constructs. (c) Exo III and hydroxyl radical (OH$^{\bullet}$) footprinting of AQ-601.
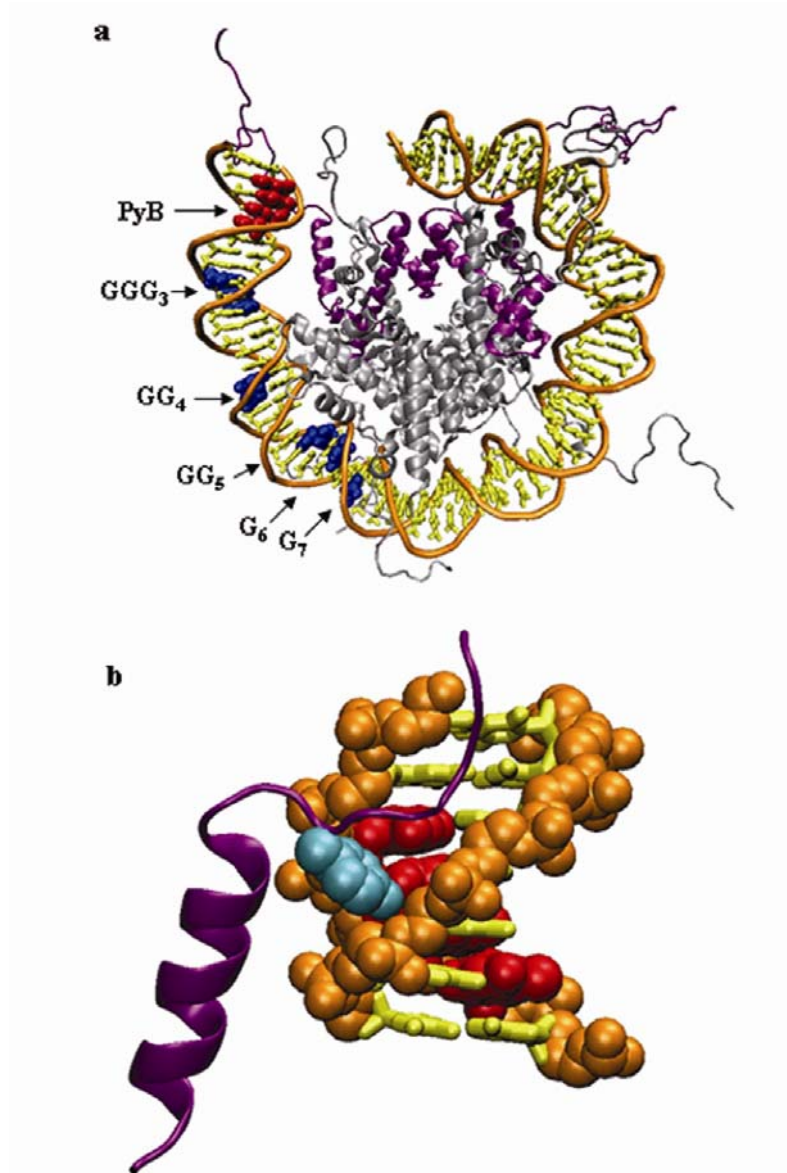
Figure 4.3

Figure 4.3: Model structure of **AQ-601** rNCPs. (a) Position of the 601 DNA on the histone octamer surface as deduced from a comparison of the results of DNA footprinting on **rAQ-601** (Supporting Figure 1) and a high resolution NCP crystal structure (PDB #1KX5). The position of the oxidized G residues (blue) within the NCP, PyB (red), and Histone H3 (purple) are indicated. (b) DNA-H3 interface around PyB. The insertion of residue H3Tyr41 (cyan) into the DNA minor groove is illustrated. Both images were rendered using the program VMD (www.ks.uiuc.edu/Research/vmd).

139

Figure 4.4

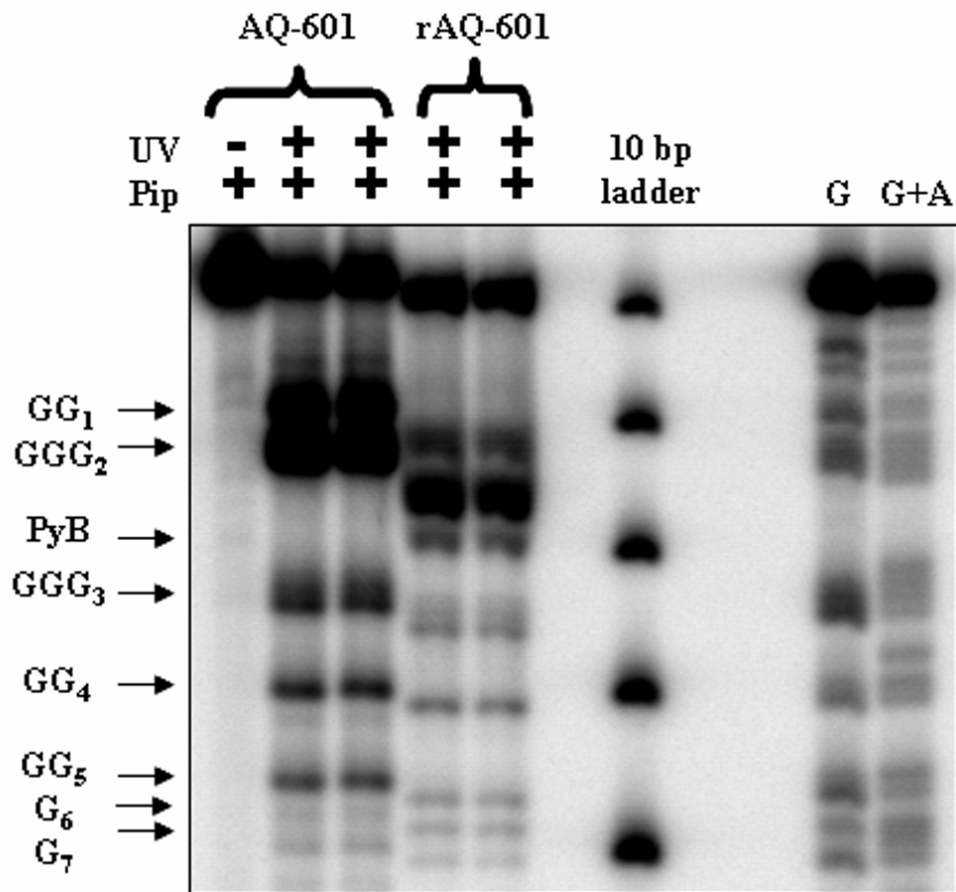**Figure 4.4:** The products of DNA CT reactions in **AQ-601** and **rAQ-601**. The positions of piperidine-sensitive oxidation products at sites $GG_1 - G_7$ (**Figure 4.1**) were determined by comparisons with the Maxam-Gilbert G and G+A ladders, and the 10 bp DNA ladder. The G oxidation bands in the **AQ-601** and **rAQ-601** samples are slightly uneven since the latter bands migrate a bit faster because of an unsystematic gel shift (see text). Also indicated is the position of the PyB lesion which is only observed in UV-A irradiated **rAQ-601**.
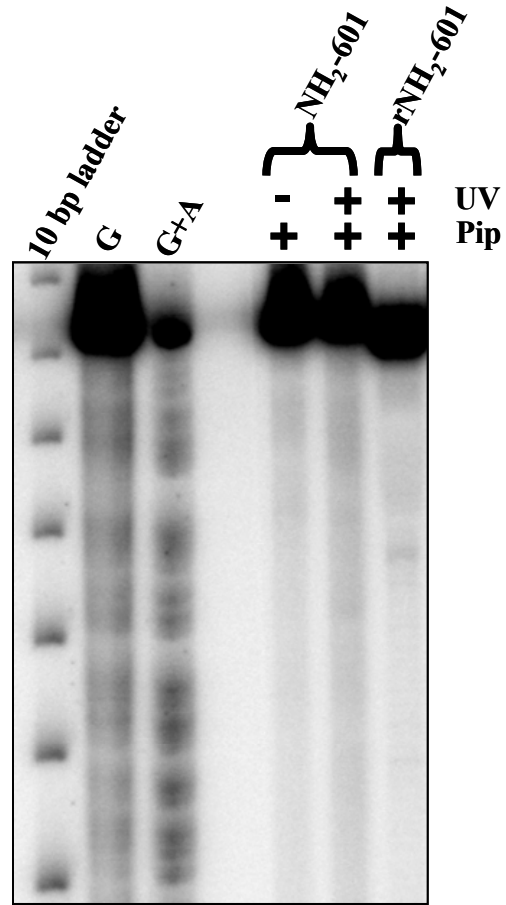
Figure 4.5

Figure 4.5: The products of DNA CT reactions in **rNH₂-601** and **r NH₂-601** following UV-irradiation and piperidine treatment.
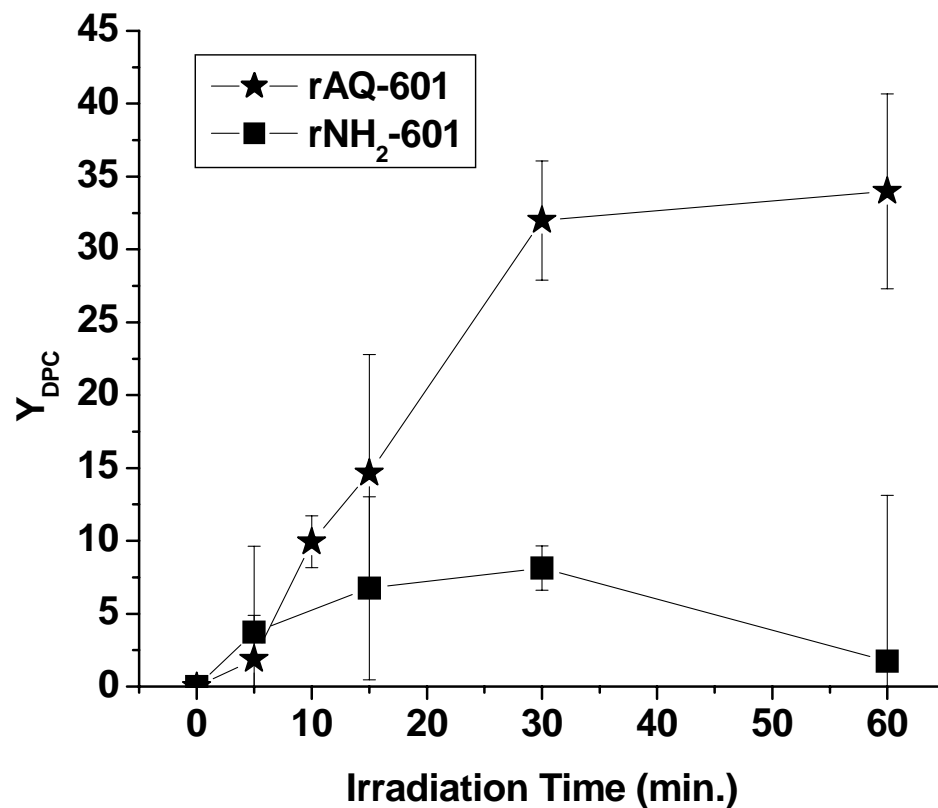
Figure 4.6

Figure 4.6: Phenol partitioning of irradiated rAQ-601 (stars) and rNH$_2$-601 (squares). Following irradiations, samples were extracted with an equal volume of phenol/chloroform and washed twice with sodium phosphate (pH 7.0). Aqueous layers were combined and both the aqueous and organic layers were counted by Cerenkov counting. The yield of DPCs (Y$_{DPC}$) were calculated as: 100*(organic counts)/(organic counts + aqueous counts). Over a 60 minute time course, the Y$_{DPC}$ increases and plateaus around 30%, while the control NH$_2$-link samples stayed close to background.
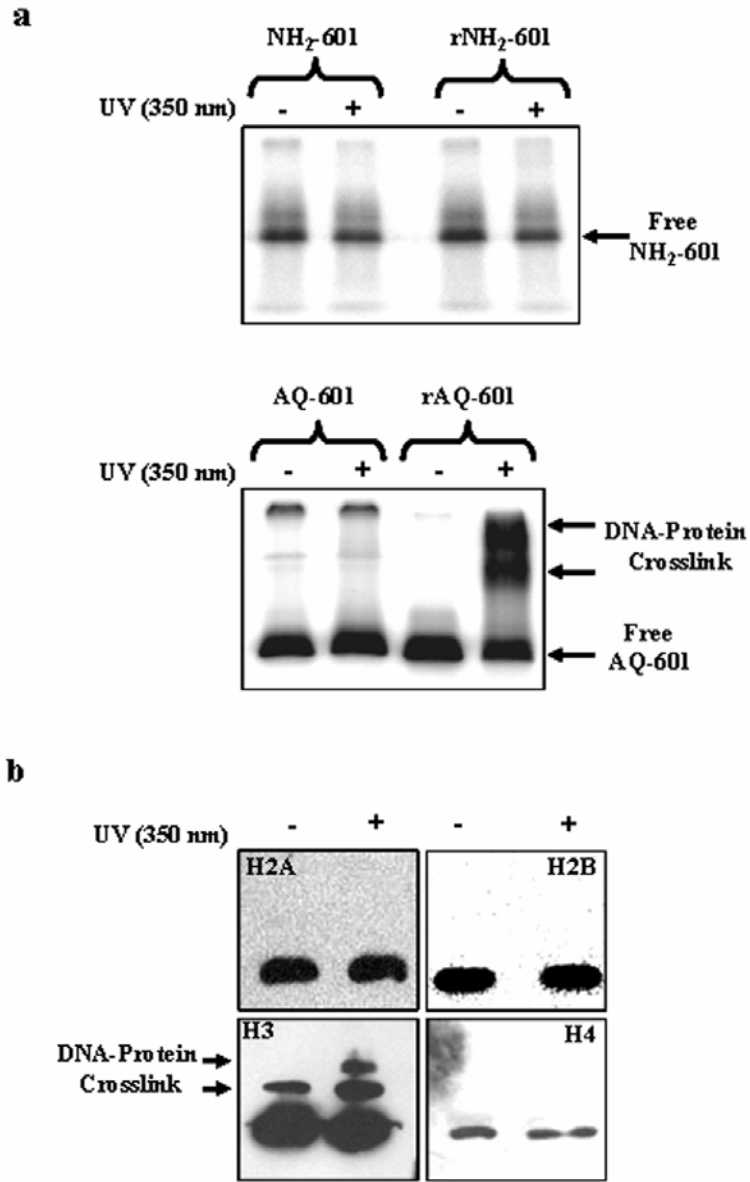
Figure 4.7

Figure 4.7: DNA-H3 cross-links are generated by DNA CT in **AQ-601** rNCPs. (a) Autoradiographs of SDS-EMSAs performed on **rNH$_2$-601** and **rAQ-601** samples. Only in the UV-A irradiated (1 hr.) **rAQ-601** samples are new, higher migrating ^{32}P-containing bands observed. (b) Western blots carried out on **rAQ-601** SDS-EMSA gels. Only with anti-H3 antibodies are higher migrating bands observed on the Western blot. There is complete co-localization of the higher migrating ^{32}P-bands (a) and H3 bands (b) in the irradiated **rAQ-601** samples.
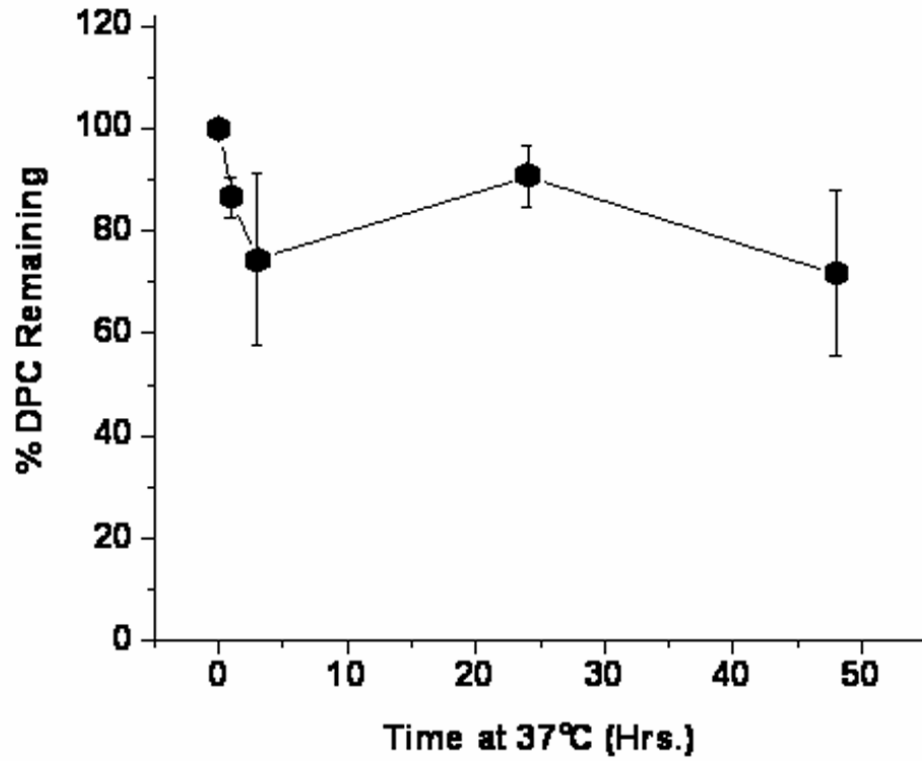
Figure 4.8

Figure 4.8: Stability at 37°C of the DNA-H3 cross-links arising from DNA CT in **rAQ-601**. Each point is the average of three independent experiments, and the error bars represent the standard deviation. The solid line has been drawn as a guide.
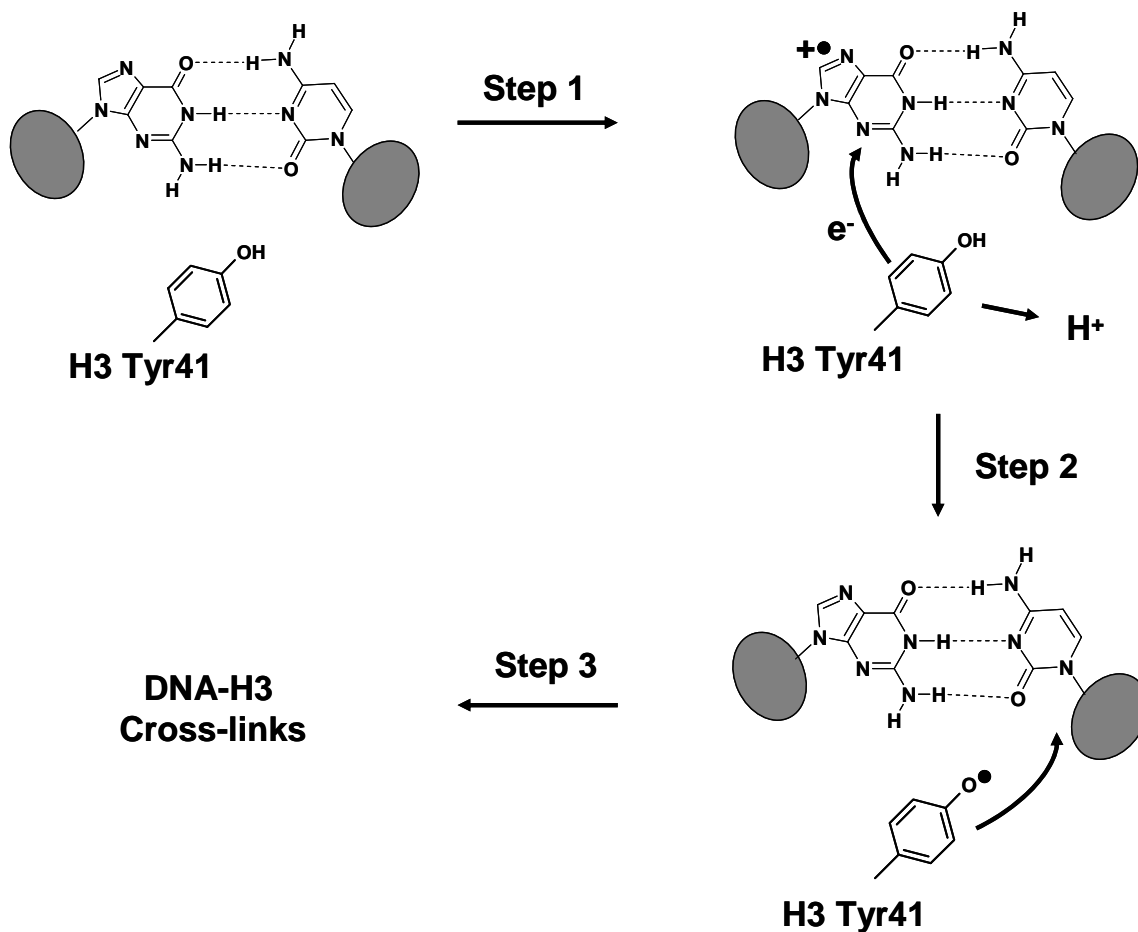
Figure 4.9:

Figure 4.9: Proposed mechanism involving residue H3Tyr41 (Figure 4.3b) which accounts for the presence of both PyB (Figure 4.4) and DNA-H3 cross-linking (Figure 4.7) in irradiated **rAQ-601**. The ovals represent the generic phosphodeoxyribose backbone of DNA, and e⁻ represents an electron transferred from H3Tyr41 to a neighboring $G^{\bullet+}$.

References:

1.   Houstis, N.; Rosen Evan, D.; Lander Eric, S. *Nature* **2006,** 440, 944-8.

2.   Kojda, G.; Harrison, D. *Cardiovasc. Res.* **1999,** 43, 562-571.

3.   Feig, D. I.; Reid, T. M.; Loeb, L. A. *Cancer Res. Suppl.* **1994,** 54, 1890-1894.

4.   Halliwell, B.; Gutteridge, J. M. C., In *Free Radicals in Biology and Medicine*, 3rd
        ed.; Oxford University Press: Oxford, 1999; 'pp 86-95.

5.   Barker, S.; Weinfeld, M.; Murray, D. *Mut. Res.* **2005,** 589, 111-135.

6.   Cao, T. M.; Sung, M. T. *Biochemistry* **1982,** 21, 3419-27.

7.   Matsumoto, A.; Hanawalt, P. C. *Cancer Res.* **2000,** 60, 3921-3926.

8.   Mee, L. K.; Adelstein, S. J. *Proc. Natl. Acad. Sci. USA* **1981,** 78, 2194-8.

9.   Miller, C. A., 3rd; Costa, M. *Mol. Toxicol.* **1989,** 2, 11-26.

10.   Dizdaroglu, M.; Gajewski, E.; Reddy, P.; Margolis, S. A. *Biochemistry* **1989,** 28,
        3625-8.

11.   Gajewski, E.; Dizdaroglu, M. *Biochemistry* **1990,** 29, 977-80.

12.   Perrier, S.; Hau, J.; Gasparutto, D.; Cadet, J.; Favier, A.; Ravanat, J.-L. *J. Am.
        Chem. Soc.* **2006,** 128, 5703-5710.

13.   Wagenknecht, H.-A.; Stemp, E. D. A.; Barton, J. K. *Biochemistry* **2000,** 39, 5483-
        5491.

14.   Kurbanyan, K.; Nguyen, K. L.; To, P.; Rivas, E. V.; Lueras, A. M. K.; Kosinski,
        C.; Steryo, M.; Gonzalez, A.; Mah, D. A.; Stemp, E. D. A. *Biochemistry* **2003,** 42,
        10269-10281.

15.   Henderson, P. T.; Jones, D.; Hampikian, G.; Kan, Y.; Schuster, G. B. *Proc. Natl.
        Acad. Sci. USA* **1999,** 96, 8353-8358.

16.   Nunez, M. E.; Hall, D. B.; Barton, J. K. *Chem. Biol.* **1999,** 6, 85-97.

17.   Boon, E. M.; Barton, J. K. *Curr. Opin. Struc. Biol.* **2002,** 12, 320-329.

18.   Giese, B. *Annu. Rev. Biochem.* **2002,** 71, 51-70.

19.   Joy, A.; Schuster, G. B. *Chem. Comm.* **2005**, 2778-2784.

20.   Lewis, F. D.; Letsinger, R. L.; Wasielewski, M. R. *Acc. Chem. Res.* **2001,** 34, 159-170.

21.   Bjorklund, C. C.; Davis, W. B. *Nucleic Acids Res.* **2006,** 34, 1836-1846.

22.   Rajski, S. R.; Barton, J. K. *Biochemistry* **2001,** 40, 5556-5564.

23.   Seidel, C. A. M.; Schulz, A.; Sauer, M. H. M. *J. Phys. Chem.* **1996,** 100, 5541-5553.

24.   Nunez, M. E.; Noyes, K. T.; Barton, J. K. *Chem. Biol.* **2002,** 9, 403-415.

25.   Lowary, P. T.; Widom, J. *J. Mol. Biol.* **1998,** 276, 19-42.

26.   Smith Corey, L.; Peterson Craig, L. *Mol. Cell. Biol.* **2005,** 25, 5880-92.

27.   Gasper, S. M.; Schuster, G. B. *J. Am. Chem. Soc.* **1997,** 119, 12762-12771.

28.   Libertini, L. J.; Small, E. W. *Nucleic Acids Res.* **1980,** 8, 3517-3534.

29.   Anderson, J. D.; Widom, J. *J. Mol. Biol.* **2000,** 296, 979-987.

30.   Prunell, A. *Biochemistry* **1983,** 22, 4887-94.

31.   Tullius, T. D.; Dombroski, B. A.; Churchill, M. E.; Kam, L. *Methods Enzymol.* **1987,** 155, 537-558.

32.   Davey, C. A.; Sargent, D. F.; Luger, K.; Maeder, A. W.; Richmond, T. J. *J. Mol. Biol.* **2002,** 319, 1097.

33.   Shao, F. W.; Augustyn, K.; Barton, J. K. *J. Am. Chem. Soc.* **2005,** 127, 17445-17452.

34. Joy, A.; Ghosh, A. K.; Schuster, G. B. *J. Am. Chem. Soc.* **2006,** 128, 5346-5347.

35. Quievryn, G.; Zhitkovich, A. *Carcinogenesis* **2000,** 21, 1573-1580.

36. Toyokuni, S.; Mori, T.; Hiai, H.; Dizdaroglu, M. *Int. J. Cancer* **1995,** 62, 309-13.

37. Giese, B. *Acc. Chem. Res.* **2000,** 33, 631-636.

38. Pogozelski, W. K.; Tullius, T. D. *Chem. Rev.* **1998,** 98, 1089-1107.

39. Zweidler, A. *Biochemistry* **1992,** 31, 9205-11.

40. DeFelippis, M. R.; Murthy, C. P.; Broitman, F.; Weinraub, D.; Faraggi, M.;

    Klapper, M. H. *J. Phys. Chem.* **1991,** 95, 3416-19.

41. Steenken, S.; Jovanovic, S. V. *J. Am. Chem. Soc.* **1997,** 119, 617-618.

42. Olinski, R.; Gackowski, D.; Foksinski, M.; Rozalski, R.; Roszkowski, K.; Jaruga,

    P. *Free Radic. Biol. Med.* **2002,** 33, 192-200.

43. Segal, E.; Fondufe-Mittendorf, Y.; Chen, L.; Thastroem, A.; Field, Y.; Moore, I.

    K.; Wang, J.-P. Z.; Widom, J. *Nature* **2006,** 442, 772-778.

44. Minko, I. G.; Zou, Y.; Lloyd, R. S. *Proc. Natl. Acad. Sci. USA* **2002,** 99, 1905-

    1909.

45. Reardon, J. T.; Sancar, A. *Proc. Natl. Acad. Sci. USA* **2006,** 103, 4056-4061.

CHAPTER V

CONCLUSIONS AND FUTURE DIRECTIONS

NCPs as Biological Model to Study DNA Charge Transport

The concept of DNA charge transport (CT) first surfaced over 40 years ago when Eley and Spivey predicted that DNA may act as an electrical conductor due to its unique structural properties.[1] Since then, DNA CT has been observed over distances greater than 200 Å.[2] The excitement over this DNA property has driven many areas of research including the potential to be used in molecular electronics and biosensors.[3-6] However, from a biological standpoint there is still a fundamental lack of understanding of the impact of DNA CT on cell systems. Much of our comprehension of DNA CT comes from studies that have solely focused upon short pieces of B-form DNA. While these studies have generated a wealth of valuable information regarding many of the fundamental dynamics of DNA CT, these studies do not necessarily reflect how these phenomena will behave in vivo.

Certainly, DNA in a living cell does not display the same structural features as DNA free in solution. DNA is bundled into multiple levels of compaction beginning with the fundamental building block of chromatin, the nucleosome core particle (NCP).[7] Beyond the NCP, DNA is wound into a 30 nm core fiber, followed by additional levels of coiling that also involve a variety of DNA-binding proteins (Figure 5.1). While it is apparent that DNA does not look the same inside a cell nucleus as it would free in solution, the question of interest is whether or not DNA CT might occur under physiological conditions, and if so how does it compare to the CT dynamics of naked DNA. Ultimately, we want to understand the potential consequences of DNA CT in vivo. The experiments, results, and discussions reported in Chapters 2-4 of this thesis describe the first extensive studies of DNA CT in a biological system. In particular, this

thesis has utilized the fundamental building block of eukaryotic chromatin, the NCP, as a biological model to examine DNA CT.

Examination of DNA CT on NCPs was facilitated by UV-A induced Anthraquinone (AQ) photooxidation of DNA duplexes that contained previously defined NCP positioning elements. Two NCP positioning sequences, the TG-motif[8] and the 601 sequence[9] were both utilized to observe the differences in G damage as a result of DNA CT in both unbound DNA and NCP-DNA complexes. Structural characterization of the TG-motif (Chapter 2) and the 601 constructs (Chapters 3 and 4) by both hydroxyl radical[10] and ExoIII[11] footprinting techniques showed us that i) the AQ did not perturb the efficiency of NCP reconstitution, ii) the AQ did not interact with the histone core and was in contact with only DNA in solution, and iii) the initiation of DNA CT occurred in a region that resembled B-Form, NCP linker DNA. Utilizing this structural information, we were able to generate three dimensional models of our reconstituted NCPs (rNCPs) based upon the crystal structure of the NCP.[12]

UV irradiation and piperidine treatment of the TG-157 both free in solution and compacted onto a NCP resulted in observed damage at three distinct G sites (GG_1, G_1, and GG_2; Chapter 2).[13] Closer examination of quantitative damage ratios revealed that there was a significant difference in the amount of damage at the GG_2 site when the DNA was packaged into NCPs. Determination of whether or not this was due to an effect on either of the kinetic pathways (k_{trap} or k_{hop}) that determine the amount of observable damage at any one site was unclear. Ultimately, we attributed the differences in G damage at GG_2 to an Arg residue of histone H2A that is inserted into the minor groove at the exact site of GG_2. We argued that since the major groove was accessible to bulk

solvent, that k_{trap} should not be affected and that the electrostatic contribution of the positively charged Arg most likely affected k_{hop}. This argument is supported by the observation of Saito et.al that saw an attenuation of charge transfer though DNA that is bound to the restriction endonuclease *BamHI* .[14]. That particular DNA-protein complex causes no structural distortion of the DNA base stack as a result of the *BamHI* binding.[15] In addition, a positively charged Arg residue sits in the major groove. The authors attributed the attenuation of DNA CT to an energetic alteration due to the bound protein and more specifically the Arg residue.[14] Nonetheless, our studies with the TG-motif clearly indicated that protein environment of the NCP altered the DNA CT dynamics. Initially, we believed that this observation indicated that the NCP may serve as the first line of defense for DNA oxidation. In pursuit of more evidence to support that hypothesis, we carried out similar experiments utilizing the 601 NCP positioning sequence.

Successful irradiation and piperidine treatment of the AQ-601 complexes revealed that the initial hypothesis developed from the TG-motif data would not serve as a global trend. Even before the quantitation of G damage distributions, qualitative observations showed significant disparities between the free DNA and the NCP-DNA complexes (Chapters 3 and 4). The appearance of a band (PyB) directly beneath the GGG_2 band in the rNCP lanes (Chapter 4; Figure 4.4) corresponded to a pyrimidine tract on the ^{32}P-labeled strand. After ruling out the possibility of an oxidized pyrimidine lesion at this site, we speculated that the strand cleavage may have resulted from a DNA-protein crosslink (DPC). Confirmation of DPC formation resulted from experiments that included phenol partitioning, EMSAs, and western blot identification of the crosslinked

protein. It was determined that histone H3 was the primary histone involved in the formation of DPCs. According to our model of the 601 sequence on the crystal structure, we identified Tyr41 of histone H3 as a potential source of the DPC. Energetically, the oxidation potential of Tyr is lower than that of G, indicating a spontaneous reaction that would generate a Tyr-O$^{\bullet}$. According to our model, the Tyr radical would then attack either the sugar-phosphate backbone or the nucleobases themselves to form a covalent adduct. Additionally, it was shown that there were at least two types of DPCs being formed, with at least one form having a half-life greater than 48 hours.

The hypothesis that DNA CT is initiating DPC formation facilitated by Tyr 41 of histone H3 is a unique explanation that bridges previously unconnected observations. These observations include i) DNA CT to a Tyr on DNA-binding peptides[16, 17], ii) DPC formation involving histone proteins under both ionizing radiation (IR) and UV photosensitized reactions[18, 19], and iii) identification of Tyr-pyrimidine covalent adducts isolated from IR-treated chromatin[19-21]. The results reported here are the first identification of a bona fide DPC formed under DNA CT conditions. In addition, histone H3 Tyr41 is highly conserved, stretching across all higher eukaryotic organisms except some plants (i.e. *Arabidopsis thaliana* has histone H3 Phe41). While the evidence that we have presented cannot definitely determine what the chemical structure of these crosslinks are, the data serves as both a unique model for further investigations of DPC formation, and as a potential in vitro substrate for DNA repair of DPCs. Further studies should include the identification of the crosslink structures by mass spectrometry, positive identification of the tyrosine radical intermediate by electron paramagnetic

153

resonance (EPR), and site-directed mutagenesis of the Tyr41 in a recombinant histone system to eliminate the DPC.

The second significant observation of G damage in the 601 rNCPs was cleavage of a pentad of G residues (G_{PENT}) over 300 Å away from the AQ photooxidant. This observation extended the current record of DNA CT by over a 100 Å.[2] A closer look at the three-dimensional configuration of this damaged region revealed that the G_{PENT} resided on the second tyne of DNA that wrapped around the NCP (Chapter 3; Figure 3.8). Not only was the G_{PENT} in the second tyne of DNA, it sat directly adjacent to the site of the PyB, which was originally attributed to formation of a DPC. According to our crystal structure model, Tyr41 of histone H3 sits directly in between these two unique observations on the irradiated, piperidine treated 601 rNCP. The observation of the G_{PENT} resulted in an even more complicated hypothesis involving Tyr41 of histone H3. If Tyr41 was being oxidized by a $G^{\bullet+}$, thus forming the Tyr-O$^{\bullet}$, then we reasoned that the G_{PENT} must be low enough in oxidation potential to be oxidized by the tyrosyl radical, thus generating oxidized lesions at G_{PENT} when treated with piperidine. If our hypothesis holds up, this would be the first report of a protein-mediated interduplex DNA CT event. The impact of this finding has yet to be determined; however the excitement of the DNA CT field will probably be noteworthy. Additional manipulations of this research should be to mutate the 601 sequence at the G_{PENT} in order to change the energetic environment and reduce the amount of interduplex CT. This in turn should increase the yields of DPC formation since there will be an elimination of the interduplex CT pathway. An additional consideration should be to mutate the Tyr41 on recombinant histones to i)

154

eliminate interduplex DNA CT, and ii) eliminate DPC formation. This would be definitive evidence to support both of our hypotheses involving H3Tyr41 and DNA CT.

Experiments with the 601 also revealed significant differences in G damage distributions associated with DNA CT in the NCPs. Most of the differences occurred at regions that were deep into the NCP (G_6 and G_7; Chapter 3). We also observed differences in piperidine and Formamidopyrmidino glycosylase (Fpg) cleavage at these distal sites (G_6 and G_7; Chapter 3) when comparing free DNA and rNCPs. This indicated that the overall distribution G lesions formed in the NCP are different, depending on the location of the damaged site. To clarify, there was a nearly equal distribution of piperidine-labile and Fpg-sensitive G lesions in the 601 sequence at the most proximal sites to the AQ, whether the construct was naked or NCP-bound. At the distal G sites, these distributions of these lesions were different between free and NCP DNA, indicating a preference for the type of trapping reactions at these sites. Overall, there appeared to be some contribution of the histone tails to the observed effects of the NCPs on DNA CT in the 601 sequence. All of these observations were unique in the fact that the results differed from that of TG-motif data (Chapter 2) and from previous work by Nunez et.al[22] that utilized a palindromic α-satellite sequence. Consideration of all of these results indicates that there is not a global trend concerning the effects of NCP packaging on DNA CT. Additionally, there appears not to be an overall protection from oxidative damage as originally proposed.[13] In fact, these observations may indicate that DNA CT will behave differently on different DNA sequences with varying degrees of NCP-DNA thermodynamic stabilities. Taken together, this might indicate that different regions of the genome are going to be affected by DNA CT asymmetrically. That is to say that

there may in fact be genomic "hot spots" vulnerable to oxidative attack that may result in the formation of specific oxidative lesions, DPC formation, or an overall increase of oxidative damage.

Additional studies should include using other DNA sequences of varying degrees of NCP-DNA thermodynamic stabilities, placement of the AQ at internal NCP positions, and studies using recombinant histones. Since it has already been observed that at least two different NCP binding sequences show differing effects on DNA CT when packaged into NCPs, further studies should be pursued with other NCP positional elements. Specifically, examination of NCP influenced DNA CT on natural sequences, like promoter elements or portions of active/inactive genes. Altering the position of the AQ may also provide insight about the importance of the original sites of oxidation. Perhaps DNA CT is affected differently, depending upon where it originates from (i.e. the dyad axis vs. the linker region). And lastly, examination of DNA CT on recombinant NCPs should be pursued. The NCPs utilized in all previous studies were isolated from chicken erythrocytes. These NCPs may have a heterogeneous mixture of histones with posttranslational modifications. The extent of these modifications is unknown, and is not taken into account during the studies reported here, although it is assumed that they played a minimal role these studies.

In all, the NCP is an excellent model to examine DNA CT in a biological setting. It has provided us with a vast amount of intriguing observations that have opened up the door for many exciting new research topics for the DNA CT scientific community.

The Chromatosome and Beyond

156

A next logical step in understanding DNA CT in chromatin might include the investigation of higher order chromatin structure. The chromatosome consists of the NCP with DNA that is extended on both ends to form linker regions that are bound by an additional linker histone (i.e. histone H1 or H5) (Figure 5.1).[23] The chromatosome could serve as a model for higher level of chromatin compaction to study DNA CT. Research using other forms of DNA compaction might also include using oligonucleosome arrays to examine DNA CT. The downside of using these types of arrays is the lack of structural homogeneity between the reconstituted macromolecules; however the upside is that it might be a better model for in vivo conditions. Another reasonable direction might be the use of cell culture models to investigate DNA CT. However, these types of experiments would be extremely difficult and would require a well designed system with excellent controls. In any case, the experiments and results reported within this thesis should serve as the foundation for future aspirations in determining the role of DNA CT in vivo, and the pathological consequences associated with these phenomena.
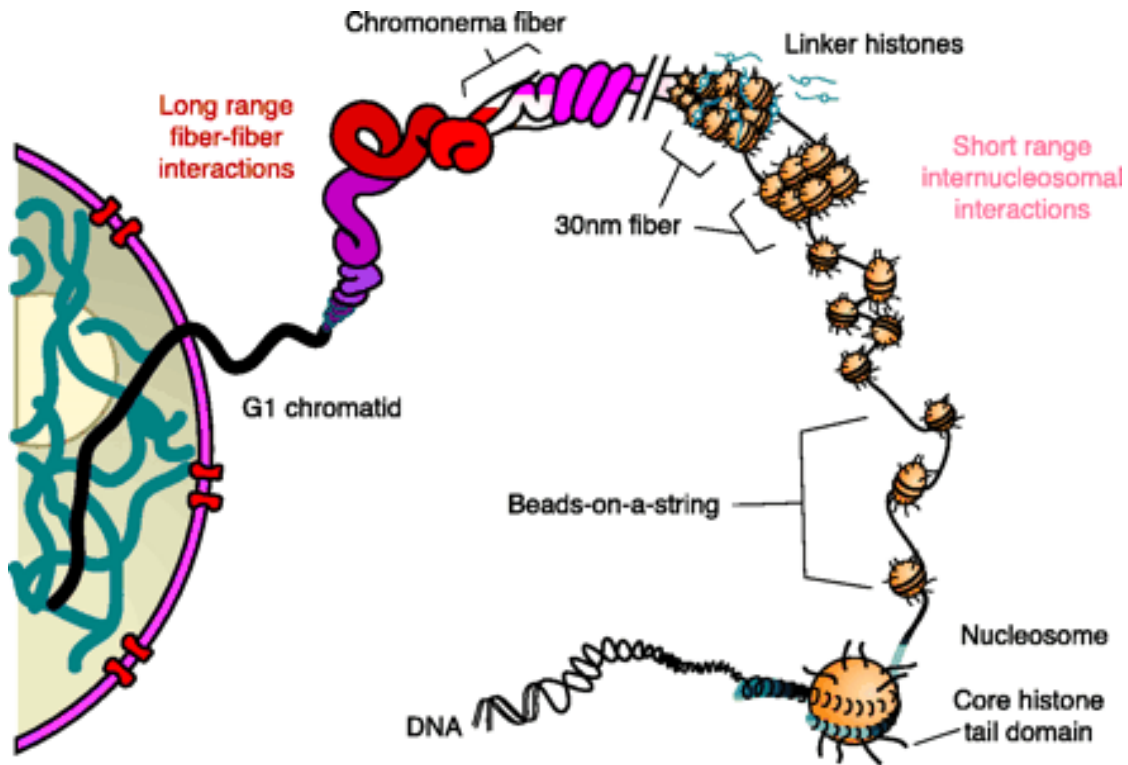
Figure 5.1

Figure 5.1: DNA compaction in a eukaryotic cell nucleus. The DNA duplex is first packaged into the nucleosome core particle to generate the "beads on a string" structure. Next is the formation of the 30 nm fiber facilitated by linker histones. Further compaction is facilitated by extensive coiling of the 30 nm fiber to eventually form the basis of the chromosomal structure. (Picture from Horn, P.J.; Peterson, C.L. (**2002**) *Science*, **297**, 1824-1827.)

References:

1.   Eley, D. D.; Spivey, D. I. *Trans. Faraday Soc.* **1962,** 58, 411-15.

2.   Nunez, M. E.; Hall, D. B.; Barton, J. K. *Chem. Biol.* **1999,** 6, 85-97.

3.   Boon, E. M.; Barton, J. K. *Curr. Opin. Struc. Biol.* **2002,** 12, 320-329.

4.   Giese, B. *Ann. Rev. Biochem.* **2002,** 71, 51-70.

5.   Joy, A.; Schuster, G. B. *Chem. Comm.* **2005**, 2778-2784.

6.   Lewis, F. D.; Letsinger, R. L.; Wasielewski, M. R. *Acc. Chem. Res.* **2001,** 34, 159-170.

7.   Wolffe, A. P., *Chromatin Structure and Function*. ed.; Academic Press: San Diego, 1992;

8.   Shrader, T. E.; Crothers, D. M. *Proc. Natl. Acad. Sci. USA* **1989,** 86, 7418-22.

9.   Lowary, P. T.; Widom, J. *J. Mol. Biol.* **1998,** 276, 19-42.

10.   Tullius, T. D.; Dombroski, B. A.; Churchill, M. E.; Kam, L. *Methods Enzym.* **1987,** 155, 537-58.

11.   Prunell, A. *Biochemistry* **1983,** 22, 4887-94.

12.   Davey, C. A.; Sargent, D. F.; Luger, K.; Maeder, A. W.; Richmond, T. J. *J. Mol. Biol.* **2002,** 319, 1097-1113.

13.   Bjorklund, C. C.; Davis, W. B. *Nucleic Acids Res.* **2006,** 34, 1836-1846.

14.   Nakatani, K.; Dohno, C.; Ogawa, A.; Saito, I. *Chem. Biol.* **2002,** 9, 361-366.

15.   Newman, M.; Strzelecka, T.; Dorner, L. F.; Schildkraut, I.; Aggarwal, A. K. *Science* **1995,** 269, 656-63.

16.   Mayer-Enthart, E.; Kaden, P.; Wagenknecht, H.-A. *Biochemistry* **2005,** 44, 11749-11757.

17.   Wagenknecht, H.-A.; Stemp, E. D. A.; Barton, J. K. *Biochemistry* **2000,** 39, (18), 5483-5491.

18.   Kurbanyan, K.; Nguyen, K. L.; To, P.; Rivas, E. V.; Lueras, A. M. K.; Kosinski, C.; Steryo, M.; Gonzalez, A.; Mah, D. A.; Stemp, E. D. A. *Biochemistry* **2003,** 42, (34), 10269-10281.

19.   Olinski, R.; Nackerdien, Z.; Dizdaroglu, M. *Arch. Biochem. Biophys.* **1992,** 297, (1), 139-43.

20.   Nackerdien, Z.; Rao, G.; Cacciuttolo, M. A.; Gajewski, E.; Dizdaroglu, M. *Biochemistry* **1991,** 30, (20), 4873-9.

21.   Simic, M. G.; Dizdaroglu, M. *Biochemistry* **1985,** 24, (1), 233-6.

22.   Nunez, M. E.; Noyes, K. T.; Barton, J. K. *Chem. Biol.* **2002,** 9, (4), 403-415.

23.   An, W.; van Holde, K.; Zlatanova, J. *Nucleic Acids Res.* **1998,** 26, (17), 4042-6.